ABSTRACT

Title of Document: DESIGN OF CLICK HYDROGELS FOR CELL ENCAPSULATION

Joyce Catherine Breger, Ph. D., 2011

Directed By: Dr. Nam Sun Wang, Department of Chemical and Biomolecular Engineering

The long-term stability of ionically crosslinked alginate hinders the development of a bioartificial pancreas for the treatment of Type I Diabetes. Ionically crosslinked alginate with divalent cations is traditionally utilized to encapsulate islets of Langerhans serving as a protective barrier between the host's immune system and the donor islets of Langerhans. However, due to ion exchange with monovalent ions from the surrounding serum, alginate degrades exposing donor tissue to the host's immune system. The overall goal of this dissertation was to explore the possibility of utilizing 'click' chemistry to introduce covalent crosslinking in alginate for therapeutic cell encapsulation. 'Click' chemistry is customarily defined as the Cu (I) catalyzed reaction between an azide and alkyne to form a 1,2,3 triazole ring. To achieve the goal of covalently crosslinked polysaccharides, the following aims were determined: (1) synthesis and characterization of functionalized polysaccharides (alginate and/or hyaluronic acid) with alkyne or azide end groups; (2) measurement and comparison of the stability and transport properties of covalently crosslinked alginate hydrogels to

that of ionically crosslinked alginate hydrogels; (3) determination of the inflammatory potential and cytotoxicity of these functionalized polysaccharides and 'click' reagents by employing RAW264.7, a murine macrophage cell line under various simulated inflammatory states (with or without endotoxin, with or with out the inflammatory cytokine γ-interferon); (4) optimization of the 'click' reaction for therapeutic cell encapsulation utilizing RIN-5F, a rat insulinoma cell line, while minimizing cytotoxicity and maintaining insulin production; (5) encapsulation of primary porcine islets of Langerhans in either ionically and/or covalently crosslinked alginate capsulation and comparing insulin response to a glucose challenge. The results of these experiments demonstrate the utility of employing 'click' chemistry to increase the overall stability of alginate hydrogels while maintaining therapeutic cell function.

DESIGN OF CLICK HYDROGELS FOR CELL ENCAPSULATION

By

Joyce Catherine Breger

Dissertation submitted to the Faculty of the Graduate School of the
University of Maryland, College Park, in partial fulfillment
of the requirements for the degree of
Doctorate of Philosophy
2011

Advisory Committee:
Professor Nam Sun Wang, Chair
Dr. John Fisher
Dr. Srinivasa Raghavan
Dr. Ganesh Sriram
Dr. Adam Hsieh
Dr. Irada Isayeva
Dr. Benjamin Fisher

Acknowledgements

I would like to especially acknowledge my parents, Alice and James Breger, for their unwavering support and encouragement.

I would like to thank Dr. Nam Sun Wang my advisor at UMCP for his interest and support of my project.

Dr. Dan Lyle, my first advisor at FDA, for his advice and mentorship at the beginning of my research project.

Dr. John Langone, my supervisor at FDA, for his advice and leadership.

Thanks to Dr. Steven Pollack for the numerous discussions and advice regarding 'click' chemistry.

For guidance on the characterization and material properties work, I thank Dr. Irada Isayeva.

For patiently teaching me NMR and all the numerous experiments that can be performed I thank Dr. Darón Freedberg.

Thanks to Dr. Samy Raghu for performing some of the NMR experiments at the FDA.

For help with the ELISA assays, I thank Larissa Baeva.

I especially thank Drs. Ben Fisher and Marilyn Lightfoote for their editorial comments, guidance, and moral support; especially towards the end of my work.

I would also like to thank all the wonderful staff at the FDA who make it a truly nice, comfortable place to work and perform research.

Oak Ridge Institute for Science and Education (ORISE) are thanked for the financial support.

Table of Contents

List of Tables

List of Figures

List of Abbreviations

Name	Abbreviation
11-azido-3,6,9-trioxaudecan-1-amine	AA
2-(N-Morpholino)ethanesulfonic Acid Sodium Salt	MES
2,3-Diaminonaphthalene	DAN
Alginate	Aln
Alginate Functionalized with Alkyne End Groups	Aln-Alk
Alginate Functionalized with Azide End Groups	Aln-Az
α-L-guluronate	G
Alkyne Functional End group	Alk
Average Diffusion Coefficient	D
Average Molecular Weight	M_W
Azide Functional End group	Az
β-D-mannuronate	M
Boltzmann Constant	k_B
Branched Intrinsic Viscosity	η_b
Calcein-AM	CalAM
Complete Media	CM
Copper Sulfate	$CuSO_4$
Dalton	Da
Degree of Polymerization	DPn
Deuterium Oxide	D_2O
D-Glucuronic Acid	GlcUA
Dithizone	DTZ
D-N-acetylglucosamine	GlcNAc
Dry Diameter	D_d
Endotoxin Unit	EU
Ethidium Homodimer	EthD-1
Ethylenediaminetetraacetic Acid	EDTA
Fourier Transform Infrared Spectroscopy	FTIR
Fourier Transform Infrared-Attenuated Total Reflectance	FTIR-ATR
Fraction GGM Triads	F_{GGM}
Fraction MGM Triads	F_{MGM}
Fraction of G Monads	F_G
Fraction of GGG Triads	F_{GGG}

Fraction of M Monads	F_M
Fraction of MGG Triads	FMGG
Gel Permeation Chromatography	GPC
γ-Interferon	γ-IFN
High Molecular Weight	HMW
Hyaluronic Acid	HA
Hydrodynamic Radius	R_h
Hydrolyzed Alginate	HAln
Hydrolyzed Alginate-Alkyne	HAln-Alk
Hydrolyzed Alginate-Azide	HAln-Az
Infinite Diffusion Coefficient	Do
Intrinsic Viscosity	[η]
Ion Selective Electrode	ISE
Ion Strength Adjuster	ISA
Linear Intrinsic Viscosity	η_l
Lipopolysaccharide	LPS
Low Molecular Weight	LMW
Lowest Observable Effect Level	LOEL
Mass Fraction of Dye at Time Infinity	M_∞
Mass Fraction of Dye at Time t	M_t
Molecular Weight	MW
Molecular Weight Cutoff	MWCO
N-Ethyl-N′-(3-dimethylaminopropyl) Carbodiimide Hydrochloride	EDC·HCl
N-Hydroxy Succimide	NHS
Nitric Oxide	NO
Nitrite	NO_2
No Observable Effect Level	NOEL
Nuclear Magnetic Resonance	NMR
Number Average Block Length of G	N_G
Number Average Block Length of M	N_M
Number Average Molecular Weight	M_n
Number of Average Block Length Greater Than 1	$N_{G>1}$
Overall Branching Index	g'
Peak Molecular Weight	M_P
Phosphate Buffered Saline	PBS
Polydispersity	M_w/M_n
Polyethylene Glycol	PEG
Propargylamine	PA

Radius	a
Radius of Gyration of The Branched Polymer	s_b
Radius of Gyration of The Linear Polymer	s_l
Sodium Ascorbate	NaAsc
Solvent Viscosity	η
Swollen Diameter	D_{sw}
Temperature	T
Time	t
Volumetric Swelling Ratio	VSR
Water Content	WC
Weight in Dry State	W_d
Weight in Swollen State	W_{sw}

Chapter 1: Introduction

1.1 Objectives

This dissertation accomplished four main objectives. The first objective was to functionalize alginate (Aln) and hyaluronic acid (HA) with reactive end groups such that they could undergo covalent ('click') crosslinking. 'Click' chemistry is based on a 1,3-dipolar cycloaddition Huisgen reaction between an azide and an alkyne to form 1,2,3-triazole catalyzed by Cu (I) salts. The functionalization of HA and/or Aln with appropriate reactive end groups were confirmed with Fourier transform infrared spectroscopy (FTIR), nuclear magnetic resonance spectroscopy (NMR), and gel permeation chromatography (GPC). The second objective was to determine the inflammatory potential of a wide range of defined average molecular weights (M_W) of HA, functionalized Aln, or functionalized HA using a fluorescent based assay. Experiments were conducted to determine a range of M_W of HA that did not instigate a significant inflammatory response. Also, to confirm that the presence of functional groups did not instigate a significant inflammatory response suitable for accomplishing the creation a novel 'click' gel of varying HA and Aln composition. The third objective was to compare some key material properties (volumetric swelling ratio (VSR), water content (WC), and absorption/desorption of dextran dyes of known molecular weight (MW)) between ionic and covalently ('click') crosslinked Aln hydrogels. The fourth objective was to use the 'click' gels as a novel tissue engineering construct for encapsulation of therapeutic cells. Cell death, insulin

production, and other biomarkers were used to determine the success of the gels as a biocompatible construct.

1.2 Background

1.2.1 Problem Statement

This project was designed to develop a cell-friendly, adaptable modular framework for constructing future tissue engineered bioartificial organs. These bioartificial organs can be used in a number of applications and will help alleviate the current shortage of available donor tissue. Depending on the application, the biomaterial should either degrade over time as the donor tissue becomes incorporated with the native tissue or be permanent and provide continued protection against the host's immune system.

One application receiving considerable interest by the medical community is the development of a bioartificial pancreas using donor pancreatic islets and the biomaterial Aln[1, 2]. Current Aln preparations are not optimal as they may be unstable over extended periods of time[3], may be incompatible with desired cell types[4], or may instigate an immunogenic response[4, 5]. To address the instability of Aln, a novel biomaterial construct was proposed that employed 'click' chemistry that could be utilized in tissue engineering for a number of applications, specifically for encapsulating islets of Langerhans. The 'click' hydrogels composed of Aln and/or HA might provide a matrix for cellular encapsulation thus improving long-term stability, providing a "cell friendly" matrix, and evoke a low to no immunogenic response.

1.2.2 Description of Type I Diabetes

Diabetes mellitus type 1 is an autoimmune disease of unknown origin that results in the destruction of islets of Langerhans, the cell type responsible for producing insulin and maintaining glucose homeostasis. There are approximately 20.8 million children and adults in the U.S. that have diabetes of which roughly one third are undiagnosed[2, 6]. Unfortunately, the disease is often only diagnosed once the majority of the islets have been irrevocably destroyed. This particular version of the disease is commonly referred to as juvenile diabetes as historically the majority of the cases are diagnosed in children and young adults.

If the disease is left untreated, the quality of life for a diabetic individual is greatly diminished and can lead to premature death. The symptoms of diabetes include: polyuria (excess urination), hyperglycemia (high blood sugar), blurred vision, polydisperia (excess thirst), and tiredness. Even with the best treatments presently available, the long-term side effects of Type I diabetes often include: blindness, poor vascular circulation leading to sores and possible amputation, cardiovascular disease, chronic renal failure, and in extreme cases coma leading to death[1].

Diabetes treatment requires tight dietary monitoring, blood sugar monitoring, and insulin injections. The problem with insulin injections are that they provide a burst of insulin at a moment in time and if inappropriately administered may lead to hypoglycemia or extremely low blood sugar, which can cause seizures and coma. Insulin pumps have been developed to help provide a more continuous supply of insulin. There is progress in attempting to couple insulin pumps with blood glucose

monitors so that insulin will be injected once a threshold level of glucose is reached. However, the downside of such an "artificial pancreas" implant is that the monitor could become faulty providing either too much or too little insulin. Also, an inherent disadvantage of an insulin pump is that it cannot respond to moment-to-moment changes in blood sugar like native islets. In general, implantable glucose sensors are unreliable and must be replaced after only a few days use.

1.2.3 Development of a Bioartificial Pancreas

A more promising research area is the development of the bioartificial pancreas, a device containing donor islets that is implanted in the body[1]. These islets would be able to respond to changes in blood glucose levels immediately, providing insulin in response to hormone signals similar to native islets. A bioartificial pancreas will also provide permanent patient freedom from painful insulin injections. Traditionally, the idea is to take donor islet cells and encapsulate them in a biomaterial, usually Aln (Figure 1). Aln forms a gel around the islets creating a barrier between the donor tissue and the immune system while allowing the diffusion of nutrients, waste, hormone signals, and insulin through the capsule. The immune system is extremely sensitive to donor tissue and these capsules serve as a shield to block the immune system from recognizing the presence of donor islets, effectively eliminating the need for toxic immunosuppressive drugs[1]. This also opens up the possibility of using xenogeneic donor islets (i.e. porcine) alleviating the scarcity of current available human donor islets.

Figure 1. Encapsulated islet of Langerhans in Ca^{+2}-crosslinked alginate capsule.
A single Ca^{+2}-crosslinked capsule containing one islet of Langerhans in the center (orange cell cluster). The capsule is clear in appearance and approximately 500 μm in diameter.

Utilizing primary porcine islets is an appropriate and applicable islet source for encapsulation because porcine insulin differs from human insulin by only one amino acid. Any encapsulation therapy for the treatment of Type I diabetes is going to require a large source of islet cells. Projected numbers of encapsulated islets required to restore euglycemia ranges on order of magnitude 10^6 islets/transplant[7]. The availability of islets from human cadavers is scare and usually the tissue is only used in organ transplants. A bioartificial pancreas that incorporates porcine islets could restore euglycemia in a patient by providing enough islets to produce effective quantities of insulin on demand.

1.2.4 The Chemistry of Alginate

Aln is a linear polysaccharide made of β-D-mannuronate (M) and α-L-guluronate (G) units (Figure 2) that forms common block patterns such as GG, MM, GM, MG through the formation of 1→4 glycosidic bonds[8]. There is a unique cavity structure that is formed when two G monomers come together causing divalent cations (most commonly used is Ca^{+2}) to preferentially bind over other block patterns (Figure 2).

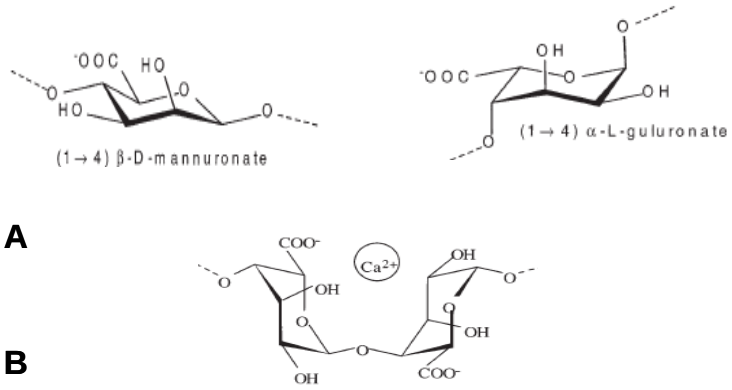

Figure 2. Alginate monomers and ionic crosslinking.
Alginate is composed of α-L-guluronate (G) and β-D-mannuronate (M) subunits that form random block patterns via 1→4 glycosidic bonds. The cavity formed by adjacent G units creates a cavity for divalent ions, such as Ca^{+2}, to bind and form crosslinks with other G units to create a hydrogel.

When many GG blocks are strung together and are in the presence of a divalent cation, an "egg-box model" structure appears creating a mesh network that is suitable for immunoisolation or other tissue engineering projects[9]. Unfortunately, the crosslinks that form between Aln strands are not permanent and Aln beads have been shown to burst or to degrade away in animal studies due to Ca^{+2} leaching out over time[2] or mechanical forces within the body. Other divalent ions or biomaterials have been added to Aln to increase its strength, durability, and modulate its porosity[10-13]. However, these materials also tend to be toxic or more immunogenic requiring additional coatings of Aln for implantation[12].

1.2.5 The Chemistry of Hyaluronic Acid

Hyaluronic acid (HA) is another popular biomaterial applied in tissue engineering. It is found naturally in the body in the lubrication fluid in between joints, vitreous humor, skin, and in cartilage[14]. Several HA products are FDA approved and are used in ocular protection[15], dermatological treatments, adhesion prevention, and osteoarthritis therapy[14]. HA is critical in some tissue engineered constructs that

employ adherent cell types such as hepatocytes[16, 17] or chrondrocytes[18, 19] where attachment is required for proliferation and function or as a poragen in biogel preparations when not chemically modified[20]. Over time, however, the HA will leach out[21], providing space for capillaries to grow into the gel. As a naturally occurring substance in the body whose sequence is evolutionarily conserved, HA should elicit low to no immune response whether the source is bacterial or animal[22].

Hyaluronan is the simplest glycosaminoglycan and is an unbranched polysaccharide consisting of alternating glucuronic acid (GlcUA) and N-acetylglucosamine (GlcNAc)[14] (Figure 3). The biomaterial HA does not form crosslinks with divalent cations the way that Aln does. Instead, HA is usually chemically modified so that it is reactive in UV light to form a gel[23-25]. This is disadvantageous as UV light is very toxic to cells, especially sensitive islets. Besides crosslinking with UV light, gels can be created utilizing high molecular weight HA mixed with another biomaterial such as Aln[18, 20, 21]. While the Aln crosslinks in the presence of a divalent cation, the HA becomes entangled and entrapped within the Aln. High viscosity liquid gels from high MW HA and Aln, however, are hard to use in a microencapsulator, a device utilized to form micrometer-sized capsules.

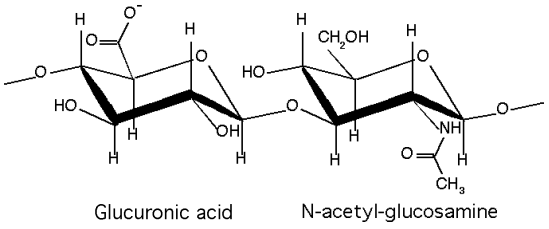

Figure 3. Structure of hyaluronic acid.
An unbranched polysaccharide composed of a repeat unit composed of glucuronic acid and N-acetyl-glucosamine.

1.2.6 Attempts at Increasing Alginate Stability

Multiple efforts by researches have focused on increasing the long term stability of Aln. Researchers have tried various solutions, including coating Aln with chitosan[12, 13] or poly-L-lysine[11] or by chemically modifying Aln to undergo covalent crosslinking via UV radiation[26, 27]. The presence of an additional coating improves gel stability but, generally, reduces hydrogel pore size[28] and compromises gel biocompatibility. Crosslinking by UV methods utilize photoinitiator solutions that generate free radicals for bond formation which can be toxic to the cells and also reduces the overall pore size. The reduction in pore size can adversely affect the ability of encapsulated therapeutic cells to produce catabolic products and receive the optimal amount of oxygen and nutrients as the overall diffusion into and out of the capsule decreases[13, 26]. This current research project proposes to improve the stability of Aln hydrogel capsules by employing covalent 'click' crosslinking instead of a transient, ionic-type of crosslink.

Others have tried to functionalize Aln such that it can undergo covalent crosslinking via chemical means. Gattas-Asfura et al.[29] tried to exploit the Staudinger reaction to covalently crosslink Aln for cell encapsulation. The benefit of employing the Staudinger reaction is that it is non-toxic to cells, however the reaction is slow taking up to 6 hrs to completely react[29]. This amount of time is too long to create a stable hydrogel network without employing a secondary ionic crosslinker in alginate. The 'click' reaction is much quicker. In most applications that employ 'click' chemistry, the reaction time is usually kept at 10 min to ensure reaction completion[30-33].

1.2.7 Nitric Oxide Hinders Development of Bioartificial Pancreas

A combination device combines a therapeutic component (i.e. drugs, biological molecules, or cells) and a polymeric structural component to treat pathological conditions. A source of concern when employing biomaterials in combination devices, such as the bioartificial pancreas, is if they induce an adverse inflammatory response because this can harm the patient or adversely affect the encapsulated cells. An inflammatory response may be triggered by contaminates in natural biomaterials, drugs, foreign biological molecules, and/or reactive chemical sites[34-39]. Inflammatory responses to either natural or functionalized biomaterials need to be assessed to determine any safety concerns. A significant inflammatory response to a combination device due to one these factors may harm surrounding patient tissue and/or hinder the proper function of the device[39-41].

Pervious studies have shown the usefulness of employing RAW264.7 cells in the presence of simulated inflammatory states to asses the inflammatory potential of biomaterials[35, 42]. When exposed to proinflammatory agents, RAW264.7 is a murine monocyte cell line which produces large quantities of nitric oxide (NO) and cytokines[43, 44]. The NO can easily diffuse through a porous biomaterial due to its low MW and kill the encapsulated cells while the cytokines can trigger other inflammatory cascades (Figure 4). NO production can be determined in a variety of ways including quantification of nitrates and/or nitrites present in CM. The nitrite concentration found in RAW264.7 culture supernatant has been shown to directly correlate to NO production[43, 45-48].

In this thesis, the production of NO was used as an indicator of inflammation and immune response since NO is a significant hurdle in the development of a bioartificial pancreas[40, 41, 45, 46, 49-51] (Figure 4). The concern is that since NO is such a small compound it can easily diffuse through Aln and stop insulin production by the islets of Langerhans due to cell death[41]. The biomaterial used in any encapsulation technique must allow the diffusion of oxygen, nutrients, chemical signals, etc. into the construct while also allowing diffusion of waste and cellular products out of the construct[1, 51]. It is impossible to create a biomaterial with a small enough pore size to prevent the NO diffusion without impeding the diffusion of nutrients, oxygen, waste products, and hormone signals. Therefore, a concerted effort is underway to better understand the immune response to biomaterials and how to better manage the effect on any surgical grafts.

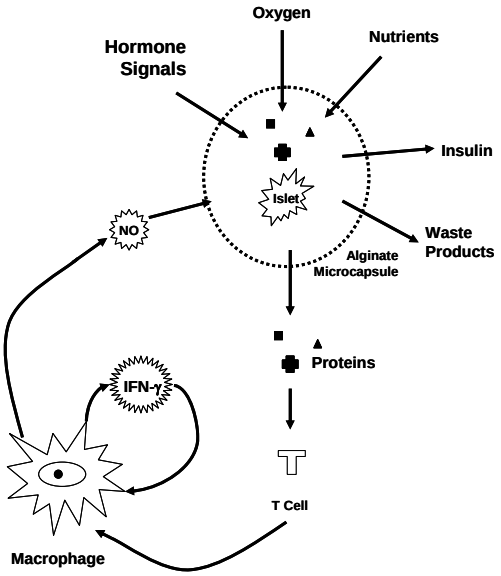

Figure 4. How macrophages can affect the development of the bioartificial pancreas. Macrophages produce a number of cytotoxic products including NO. NO can easily diffuse through alginate as a soluble gas. NO will kill islets limiting the effectiveness of the graft. Figure adapted from Thu, 1996.

1.2.8 'Click' Chemistry

'Click' chemistry has recently gained a tremendous amount of attention due to a landmark review paper by Sharpless et al[52, 53]. A 'click' reaction is characterized by occurring rapidly (within a few minutes), under physiological conditions, in the presence of benign solvents (like water), generating inoffensive byproducts, and producing high, quantitative yields[52]. Therefore, the starting materials seem to just 'click' into place. Traditionally, 'click' chemistry has been employed in the development of drug libraries[53, 54] but given that the reaction is fast and nontoxic it has also been applied in creating dendronized linear polymers[55, 56], bio-labeling[57, 58], immobilization of proteins on solid surfaces[33], novel hydrogels[30], and many other applications[59-62].

The classic ‘click’ reaction is the 1,3-dipolar cycloaddition Huisgen reaction between an azide and an alkyne to form 1,2,3-triazole catalyzed by Cu (I) salts (Figure 5)[52]. A major advantage of the triazole ‘click’ reaction is that it is irreversible and not responsive to hydrolytic enzymes[52]. Therefore, there is the potential for forming a hydrogel that combines the biocompatible properties like those found in Aln or HA, with the stability and strength of a crosslinked network that can be formed by the ‘click’ reaction. This research project used HA as a model “secondary” biomaterial to determine the feasibility of using ‘click’ chemistry to create tailored hydrogels of great strength, durability, and biocompatibility for application in future tissue-engineered implantable combination products.

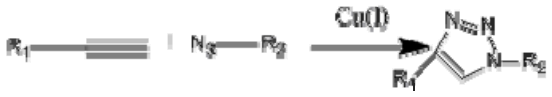

Figure 5. 'Click' reaction scheme.
The most common type of ‘click’ reaction is the Cu (I) catalyzed 1,3-dipolar cycloaddition Huisgen reaction between an azide and an alkyne to form 1,2,3-triazole.

1.3 Summary of Previous Work

1.3.1 Introduction

The Master’s Thesis was approved by the Department of Chemical and Bimolecular Engineering (September, 2007) entitled: “Defining Critical Parameters for Producing and Modulating Inflammation Caused by Cell Encapsulating Alginate Microspheres”. The aim of the Master’s thesis was to define conditions under which cell-encapsulating Aln microspheres may trigger hazardous NO production by macrophages. Pursuant of that goal, the *in vitro* RAW264.7/DAN assay was used to detect inflammatory LPS contamination under a variety of defined circumstances. These experiments assessed different factors that could affect the production of NO

by RAW264.7 cells in response to Aln microspheres. These factors included: 1) the contamination of ubiquitous LPS present in the biomaterial; 2) bead diameter and bead delivery volume; and 3) the presence of anti-inflammatory drugs in the biomaterial (bisphosphonates or parthenolide).

1.3.2 Summary of Conclusions

The conclusions of the Master's Thesis were: 1) the RAW264.7/DAN assay was efficient in detecting the inflammatory consequences of LPS contamination at extremely low levels; 2) NOEL and LOEL concentrations for endotoxin, also known as lipopolysaccharide (LPS), contamination in pharmaceutical grade Aln were much lower than previously thought, particularly when γ-interferon is present; 3) adverse reactions in patients implanted with biomaterial containing devices may be dependent upon the preexisting inflammatory state of the patient, both systematically and at the site of implantation; 4) the bioavailability of LPS when contained within Aln microcapsules, in the presence or absence of a T-cell mediator IFN-γ was decreased versus free LPS, suggesting that an implanted device could safely contain more LPS than suggested by free LPS results; 5) the inflammatory effect of LPS-contaminated biomaterials was related to the amount of surface area exposed to tissues; though a strong pre-existing immune response may swamp any surface area-mitigating effects; and 6) possible modulating physical agents, like anti-phagocytic drugs such as parthenolide, may be directly incorporated into biomaterial to diminish impurity-stimulated inflammatory responses.

Chapter 2: Synthesis and Characterization of Functionalized Polysaccharides

2.1 Introduction

The overall aim of this dissertation is to explore the possibility of employing 'click' chemistry to covalently crosslink functionalized polysaccharides (either Aln or HA) for therapeutic cell encapsulation. This chapter describes (1) functionalization of Aln or HA such that it is able to undergo covalent crosslinking via 'click' chemistry and to (2) FTIR, NMR, and GPC studies to confirm polymer functionalization. The material properties of the resulting hydrogels and the affects on cell function will be discussed in proceeding chapters.

2.2 Methods

2.2.1 Materials

The following were purchased from Sigma-Aldrich: low viscosity Alginate (Aln), 11-azido-3,6,9-trioxaudecan-1-amine (AA), propargylamine (PA), N-Ethyl-N′-(3-dimethylaminopropyl) carbodiimide hydrochloride (EDC·HCl), N-hydroxysuccinimide (NHS), D_2O (99.9% purity), and 2-(N-Morpholino) ethanesulfonic acid sodium salt (MES).

2.2.2 Synthesis of Functionalized Polysaccharide-Azide

The method described by Crescenzi et al.[30] was adapted for functionalization of Aln. Briefly, approximately 500 mg Aln was dissolved in to 50 mL of MES buffer (50

mM, pH= 4). To this solution, 0.1954 g of EDC·HCl, 0.8108 g of NHS, and 1.8 mL of AA was added. Approximately 0.400 g of HA (starting M_W 35 kDa) was dissolved in MES to a final concentration of 1% w/v. To this solution, 0.4802 g of EDC·HCl, 0.3094 g NHS and 0.8 mL of AA was added. Both reactions proceeded overnight; under constant stirring, inert atmosphere (i.e. N_2), and at room temperature. An excess of regents was used with respect to Aln or HA given the limited yield of the amidation process in aqueous solutions. The reaction solutions were dialyzed (cutoff = 10 kDa) against saturated NaCl solution for 1 day and against d.i.H_2O for 5 days. To further remove any impurities or unreacted regents, the Aln-Az or HA-Az solutions were precipitated in cold acetone (-70^oC), filtered, and dried. Finally, Aln-Az or HA-Az were dissolved in d.i.H_2O, filtered, and lyophilized to recover the final product.

2.2.3 Synthesis of Functionalized Polysaccharide-Alkyne

To a 1 % w/v solution of Aln (approximately 500 mg) in MES buffer (50 mM, pH=4) the following was added: 0.4980 g EDC·HCl, 0.2831 g NHS, and 0.25 mL (0.223 g) of PA. To a 1% w/v solution of HA in MES buffer, 1.2791 g EDC·HCl, 0.7576 g NHS, and 0.7 mL (0.652 g) of PA was added. The reactions proceeded under the same conditions as stated above. The products were purified and isolated also in the same manner as described in section 2.2.2.

2.2.4 Fourier Transform Infrared-Attenuated Total Reflectance Spectroscopy

FTIR attenuated total reflectance (FTIR-ATR) spectra for Aln, Aln-Az, and Aln-Alk were recorded with a Nicolet FTIR spectrometer with a single bounce Ge ATR attachment. A spectrum was collected after 128 scans, at 4 cm^{-1} resolution, and ATR correction was performed.

2.2.5 Nuclear Magnetic Resonance Spectroscopy

Aln was first hydrolyzed according to ASTM standard F2259[63] and lyophilized to recover the final product. This hydrolyzed alginate (HAln) was split into three groups. Two of the groups were functionalized with either PA or AA and recovered as described in sections 2.2.2 and 2.2.3 to obtain hydrolyzed alginate-azide (HAln-Az) and hydrolyzed alginate-alkyne (HAln-Alk). The third group consisted of HAln and was used without further modification for NMR analysis.

All samples were analyzed utilizing a Varian 400 MHz NMR. AA was dissolved in D_2O and PA dissolved in deuterated chloroform ($CDCl_3$) at 10 mg/mL. ^1H data were acquired using 32 scans per experiment with 65 k data points in F1. Spectra of the starting materials were taken at 25^oC. Functionalized polysaccharides were dissolved in D_2O, lyophilized, and redissolved in D_2O at 10 mg/mL twice in order to increase the deuterium signal. NMR analysis of Aln and functionalized Aln samples were performed at 80^oC as recommend by ASTM F2064-00(2006)e1 Standard[63] and referenced to the water peak at 4.19 ppm. HA samples were performed at 25^oC and referenced to the water peak at 4.80 ppm.

2.2.6 Gel Permeation Chromatography

The number average molecular weights (M_n), the weight average molecular weight ($M_{w)}$, polydispersity (M_n/M_w), and peak molecular weight (M_P) of Aln, Aln-Az, Aln-Alk, HA-Az, HA-Alk, HAln, HAln-Az, and HAln-Alk were determined by Waters Alliance GCPV 2000 system containing a chromatography pumps, two mixed bed PLaqua gel-OH 8μm columns in series (Polymer Laboratories, 300 x 7.5 μm, 100-10,000,000 M_W), in-line capillary viscometer, and a RI detector (Waters 410 Differential Refractometer). All samples were diluted to 1.0 mg/mL by 0.1 M $NaNO_3$ and passed through a 0.45 μm filter. Each run was done at 37^oC, 1.0 mL/min flow rate and with an injection volume of 202.5 μL. The columns were calibrated utilizing eight narrow molecular weight Pullulan standards (5.3, 12.3, 23.6, 53.9, 112, 228, 478 kDa). One GPC run was 40 min, with data acquired and analyzed by Empower 2 (Waters Corp.) GPC software.

2.3 Results

2.3.1 Fourier Transform Infrared Spectroscopy Analysis

Functionalization of Aln with either azide or alkyne end groups were confirmed with FTIR-ATR and ^{1}H-NMR. Figure 6 shows the FTIR-ATR spectrum of Aln (A), Aln-Az (B), and Aln-Alk (C). Azide functionalization was confirmed by the appearance of the azide stretching peak at 2114.1 cm^{-1}. However, alkyne functionality was more difficult to confirm with FTIR because alkyne stretching occurred around 3300 cm^{-1}, a location that coincides with O-H stretching (3100-3500 cm^{-1}). Therefore, alkyne functionalization was confirmed with ^{1}H-NMR.

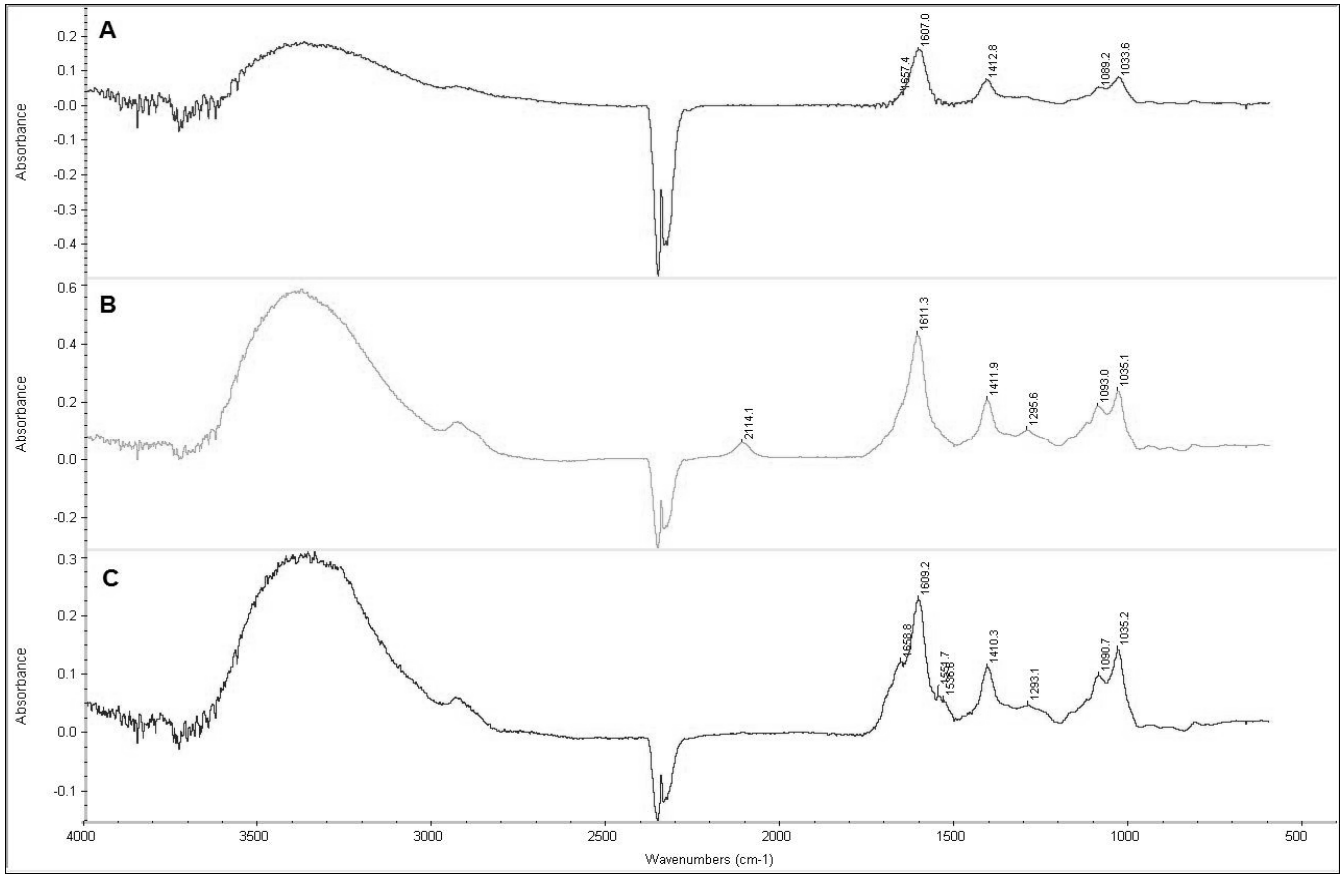

Figure 6. FTIR-ATR spectrum of alginate (A), alginate-azide (B), alginate-alkyne (C).
Aln was functionalized with either Az or Alk functional groups. Functionalization was confirmed utilizing a Nicolet FTIR- spectrometer with a single bounce Ge ATR attachment. A spectrum was collected after 128 scans, at 4cm^{-1} resolution, and ATR correction was performed. Azide functionalization was confirmed by the appearance of the azide stretching peak at 2114.1 cm^{-1}.

2.3.2 Nuclear Magnetic Resonance Analysis

Characteristics peaks of the starting materials, namely PA (Figure 7), AA (Figure 8), Aln (Figure 9 A), and HA (Figure 10 A) were determined by ^{1}H-NMR analysis and compared to literature values[64-66]. For spectra taken at 80^{o}C, the peaks were referenced in relation to the characteristic D_2O peak at 4.19 ppm. For spectra taken at 25^{o}C, the peaks were referenced to D_2O at 4.80 ppm. All spectra were scaled to the highest peak present that was not water. Identifiable peaks for the functional groups of the starting materials are summarized in Table 1.

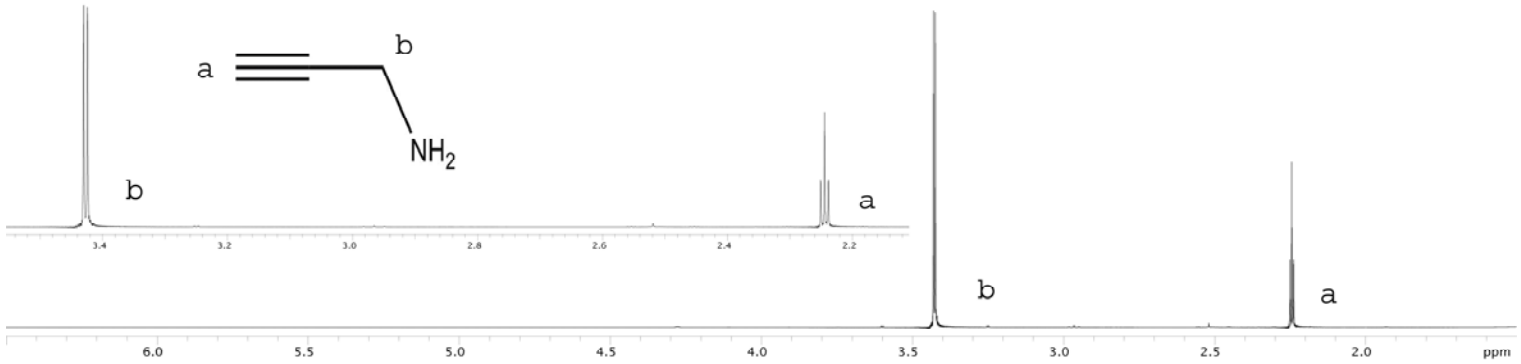

Figure 7. ^{1}H NMR spectra of propargylamine in $CDCl_3$ at 25^{o}C.
The assignment of the spectra is indicated in the figure with labeled peaks corresponding to the appropriate chemical species. Values for the assignments are listed in Table 1.

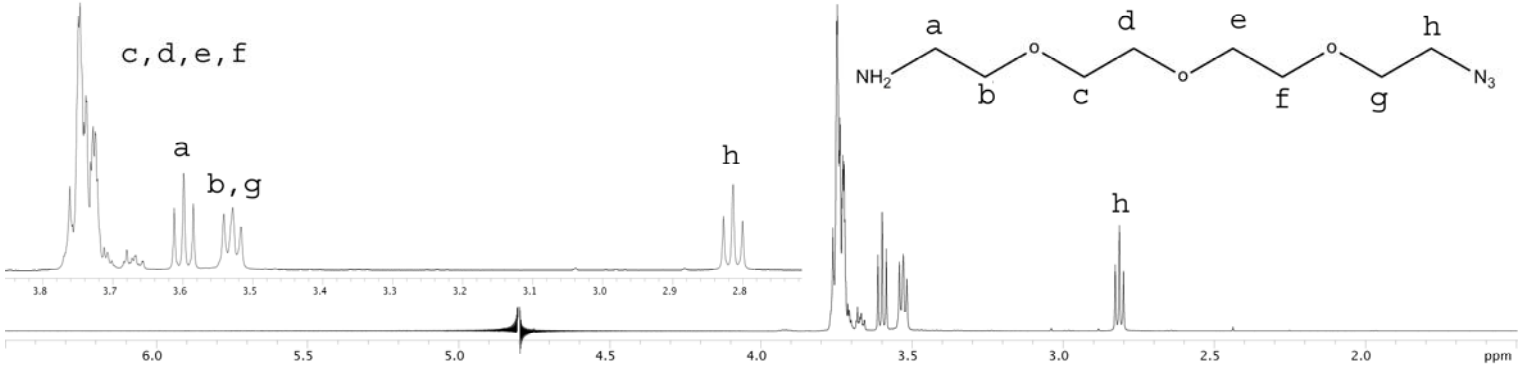

Figure 8. ^{1}H NMR spectra of 11-Azido-3,6,9 trioxaudecan-1-amine in D_2O at 25^{o}C.
The assignment of the spectra is indicated in the figure with labeled peaks corresponding to the appropriate chemical species. Values for the assignments are listed in Table 1.

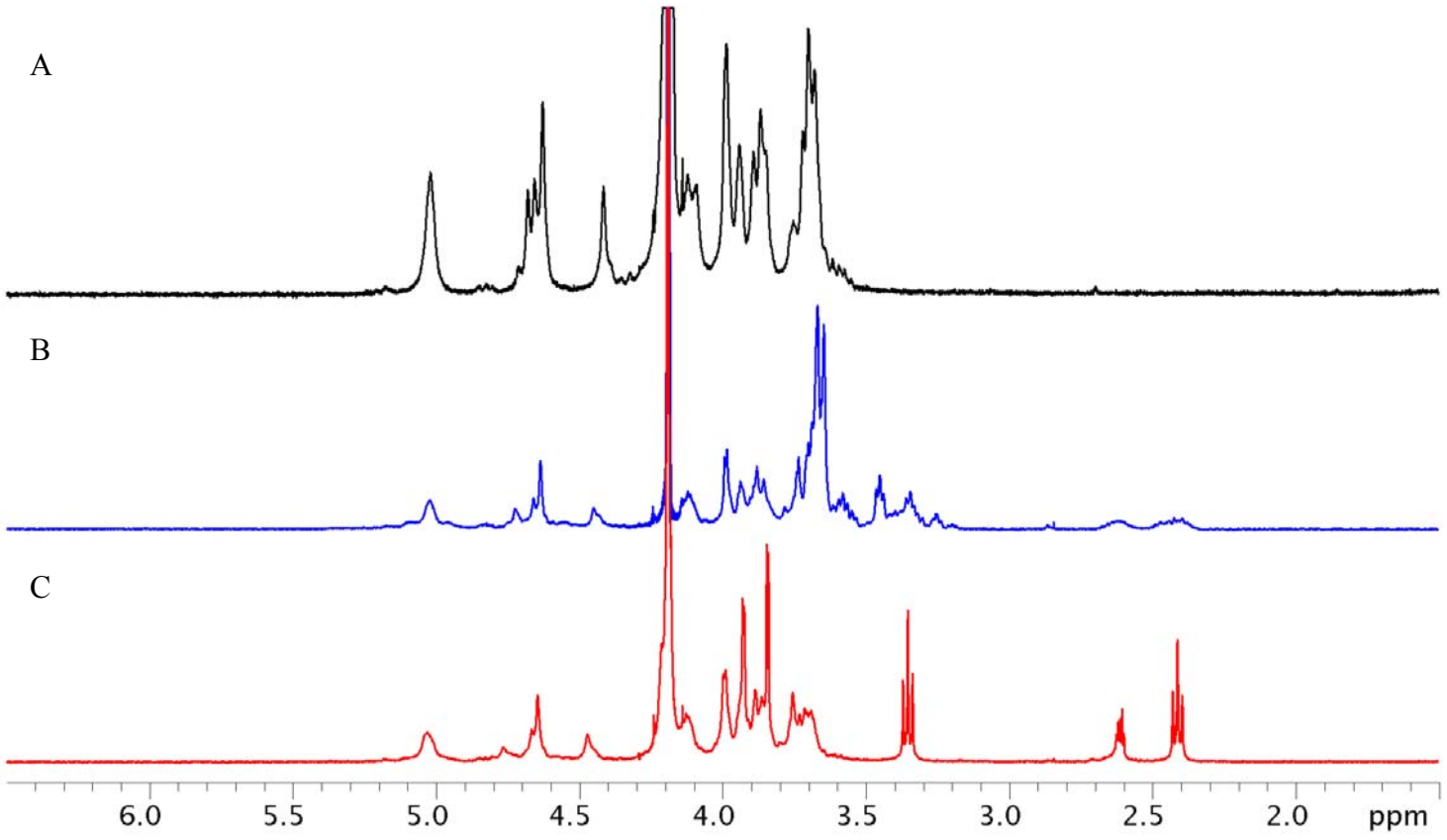

Figure 9. ^{1}H NMR spectra of hydrolyzed alginate (A, black), alginate-azide (B, blue), alginate-alkyne (C, red) in D_2O at 10 mg/mL at 80^{o}C.
Functionalized Aln samples were lyophilized twice in D_2O and ^{1}H NMR spectra was performed at 80^{o}C. Assignments are summarized in Table 1 and Table 2.

Table 1. Summary of characteristic ^{1}H-NMR peaks of starting materials.

Starting Material	Characteristic Peak δ (ppm)
11-Azido-3,6,9 trioxaudecan-1amine	
R-C<u>H</u>$_2$-N$_3$	2.81
R-C<u>H</u>$_2$-OR	3.53
H$_2$N-C<u>H</u>$_2$-R	3.60
(O-(C<u>H</u>$_2$)$_2$-O)$_2$	3.74
Propargylamine	
C≡C-<u>H</u>	2.25
R-C-<u>H</u>$_2$-R	3.43
Alginate*	
Alpha reducing ends	5.20
G (H-1)	5.07
Beta reducing ends	4.87
G<u>G</u>M (H-5)	4.76
M<u>G</u>M (H-5)	4.74
<u>M</u>G (H-1)	4.70
<u>M</u>M (H-1)	4.68
<u>G</u>G (H-5)	4.46
Hyaluronic Acid	
C<u>H</u>$_3$C(O)NH	2.05
GlcUA	
H-1	4.48
H-2	3.34
H-3	3.51
H-4	3.51
H-5	3.73
GlcNAc	
H-1	4.56
H-2	3.84
H-3	3.74
H-4	--
H-5	3.51
H-6^{a}	3.92
H-6^{b}	3.94

*Only the relevant peaks are listed for alginate characterization.

Aln is composed of two subunits, β-D-mannuronate (M) and α-L-guluronate (G) units. Given that Aln is a natural biopolymer, the composition can vary and the chain sequence is random, with GG, MM, MGM, and GMG blocks. Aln (Sigma) was

first hydrolyzed to decrease the MW and viscosity (η) of the biopolymer and to better identify significant peaks associated with Aln (Figure 9 A). Integrations of the relevant Aln peaks, as identified by ASTM standard F2259-03, were performed for characterization of Aln (Sigma). The fraction of G (F_G) in Aln (Sigma) was found to be 0.46±0.01 when calculated according to the ASTM standard F2259-03 procedure[67]. According to the manufacturer, Aln from Pronova has a $F_G \geq 0.60$. Other characteristics of Aln (Sigma) such as the fraction of monads, diads, triads, number average of block length, and degree of polymerization (DP_n) are summarized in Table 2.

Table 2. Summary of results from NMR analysis of alginate.

Characterization of Alginate (Sigma)	
Fraction of Monads	
F_G	0.44±0.01
F_M	0.56±0.01
Fraction of Diads	
$F_{\underline{G}G}$	0.24±0.01
$F_{\underline{M}M}$	0.35±0.01
$F_{\underline{M}G}=F_{\underline{G}M}$	0.21±0.01
Fraction of Triads	
F_{GGG}	0.20±0.01
$F_{M\underline{G}M}$	0.16±0.01
$F_{G\underline{G}M}=F_{M\underline{G}G}$	0.04±0.01
Number Average of Block Length	
N_G	2.16±0.11
$N_{G>1}$	6.89±0.69
N_M	2.71±0.14
Degree of Polymerization	
DP_n	17.65

Aln functionalization can occur via any of the carboxylate groups on either the G or M block. The G residue is just a C-5 epimer of the M residue. Functionalization of Aln with either Alk or Az groups causes distinct changes in the characteristic Aln spectra. For example, the peak at 5.02 ppm is associated with the first proton of the G

block (G-1) (Figure 2). This peak is actually composed of two overlapping peaks associated with the different conformations associated with the H-1 of the G block. After functionalization, this peak became broader and less well defined. Another interesting change in the spectra of functionalized Aln as compared to Aln was the disappearance or shift of the peak associated with H-5 of MGM that normally appears at 4.70 ppm. Functionalization of Aln with AA to form Aln-Az was confirmed by the appearance of peaks at 3.47 ppm (t) and 3.76 ppm (m) associated with the methylene protons of AA (Figure 8). Functionalization of Aln with PA to form Aln-Alk was confirmed by the appearance of peaks at 2.42 ppm (t) and 3.35 ppm (t) associated with the terminal alkyne protons (C≡C-H) and the methylene protons (R-CH_2-C=CH), respectively.

While HA is composed of only two repeating subunits (GlcUA and GlcNA), the spectra is still quite complex with significant peak overlap (Figure 10 A). The complexity of HA ^{1}H-NMR spectra increases with increasing MW[65, 66]. Functionalization of HA caused significant changes in the HA spectra. The peak associated with the acetyl group of GlcNA that appears at 2.05 ppm disappeared after functionalization with AA or Az. The acetyl group is not involved with either functionalization reaction. Functionalization on HA can only occur via the carboxylate group of the GlcUA subunit; forming an amide followed by the desired functional group (Figure 3). Azide functionalization was confirmed by the appearance of peak (m) at 3.68-3.76 ppm associated with the methylene protons of the PEG unit and a peak at 2.82 ppm associated with the methylene protons adjacent to the azide

group (Figure 10 B). Alkyne functionalization was confirmed by the appearance of a peak at 2.92 ppm associated with the alkyne proton (Figure 10 C).

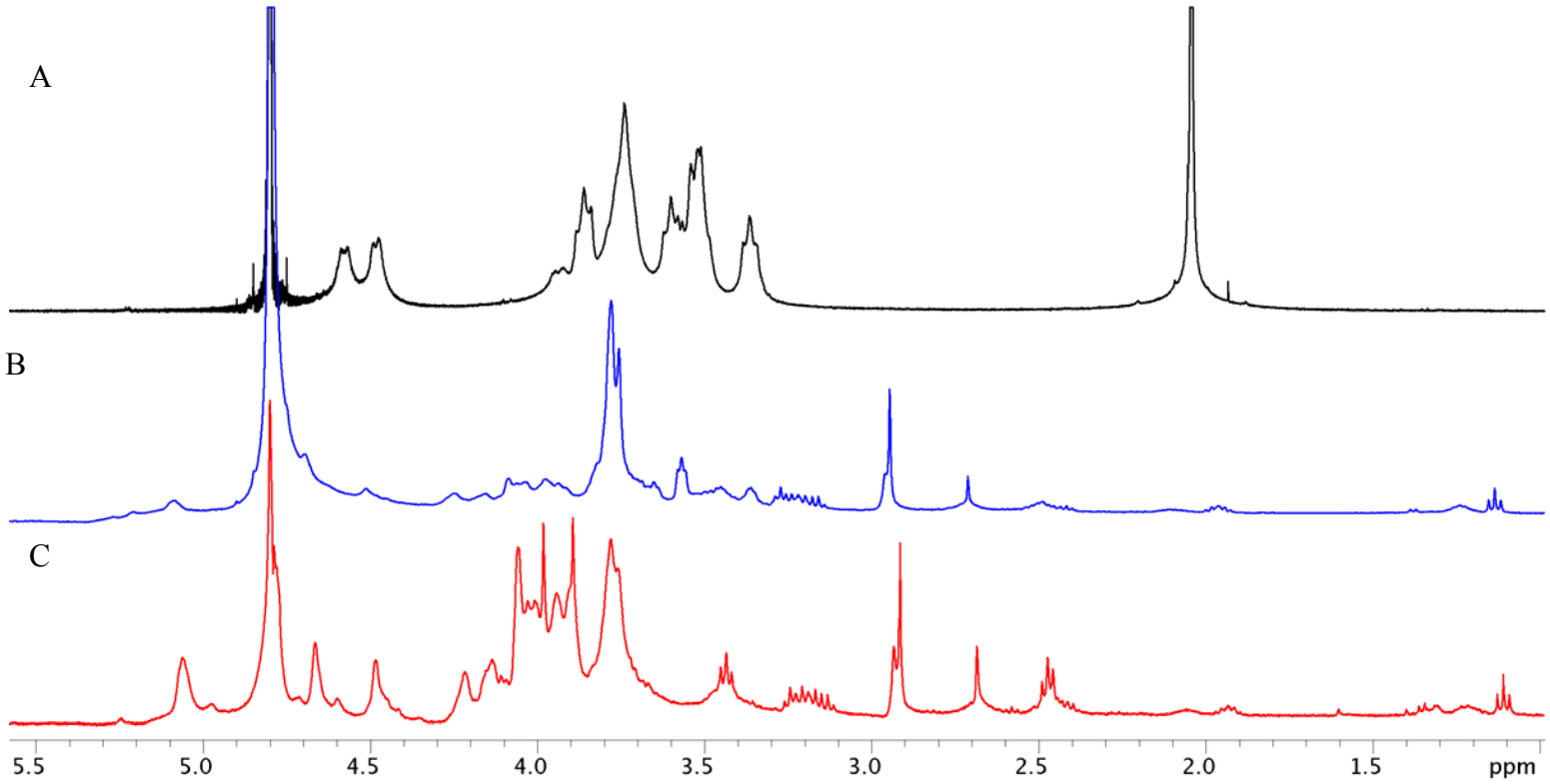

Figure 10. ^{1}H NMR spectra of hyaluronic acid (A, black), hyaluronic acid-azide (B-blue), hyaluronic acid-alkyne (C-red) in D_2O at 10 mg/mL at 25^{o}C. HA and functionalized HA samples were lyophilized twice in D_2O and ^{1}H NMR spectra were performed at 25^{o}C on a Varian 400 MHz NMR. Assignments of the starting materials are summarized in Table 1.

2.3.3 Gel Permeation Chromatography Analysis

GPC was utilized to determined the M_W, M_W/M_n, and degree of branching of Aln and HA before and after functionalization. HAln samples that were used for NMR were also analyzed with GPC. Results are summarized in Table 3.

Aln from Pronova (Alginate SLG20) is employed in this lab for encapsulation of therapeutic cells such as islets. According to the manufacturer, it has a low LPS content (≤100 EU/g), viscosity of ≤ 100 mPas and G content of $F_G \geq 0.60$. Pronova Aln was purchased from Sigma and utilized for functionalization with either Az or Alk end groups. Aln from Sigma was found to have M_W of 179 kDa and M_W/M_n of 2.81 whereas Pronova Aln has a lower M_W and a much narrower size distribution (Mw = 45K and M_W/Mn~1.4).

Representative viscosity law plots of Aln (Figure 11 A), Aln-Alk (Figure 11 B), Aln-Az (Figure 11 C), HA (Figure 11 D), HA-Az (Figure 11 E), and HA-Alk (Figure 11 F) are summarized in Figure 11. Functionalization of Aln with the alkyne yielded a slight increase in the M_n and the M_W/M_n as compared to Aln. Functionalization with the azide caused a significant increase in M_n and M_W/M_n as compared to Aln. Increases in M_W and M_W/M_n support that the functionalization of alginate was successful.

Table 3. Summary of GPC results for functionalized polysaccharides.

	M_n (kDa)	M_W (kDa)	M_W/M_n	M_P (kDa)	g' $x10^{-3}$	α	K	[η] (dL/g)
Aln[1]	33.33±0.00	45.22±0.19	1.36±0.01	38.00±0.33	4.603±0.045	1.438±0.020	5.63±1.14 $x10^{-8}$	0.310±0.05
Aln[2]	63.83±0.36	179.06±3.24	2.81±0.06	101.96±0.45	16.412±0.28	1.206±0.018	4.76±0.86$x10^{-6}$	1.206±0.018
Aln-Alk[2]	69.04±0.29	197.10±0.27	2.86±0.02	114.74±0.43	12.484±0.089	1.124±0.006	8.20±5.94$x10^{-6}$	3.357±0.015
Aln-Az[2]	103.11±0.49	435.13±1.22	4.22±0.01	176.51±6.28	4.551±0.029	1.082±0.013	6.50±9.19 $x10^{-6}$	2.631±0.021
HAln[2]	30.91±0.84	40.43±1.22	1.31±0.00	34.00±1.22	4.661±0.037	1.495±0.018	3.290±0.38 $x10^{-8}$	0.292±0.000
HAln-Alk[2]	28.52±0.15	38.90±0.08	1.37±0.01	30.18±0.19	5.911±0.045	1.234±0.008	6.87±0.70 $x10^{-7}$	0.334±0.004
HAln-Az[2]	25.91±0.13	35.45±0.10	1.37±0.00	27.09±0.14	6.774±0.066	1.191±0.007	1.28±0.11 $x10^{-7}$	0.354±0.001
HA	41.65±0.47	63.95±0.10	1.54±0.03	53.42±0.20	0.96±0.01	0.818±0.034	1.27±0.45$x10^{-4}$	0.988±0.005
HA-Alk	40.40±0.19	68.04±0.16	1.69±0.01	59.70±0.57	1.10±0.04	0.599±0.042	9.35±3.75$x10^{-4}$	0.766±0.000
HA-Az	32.89±0.04	59.99±0.02	1.83±0.01	50.69±0.04	0.98±0.01	0.726±0.003	2.57±0.06 $x10^{-4}$	0.699±0.005

[1]Alginate Source: Pronova; [2]Alginate Source: Sigma. Results are the average of two runs per sample.

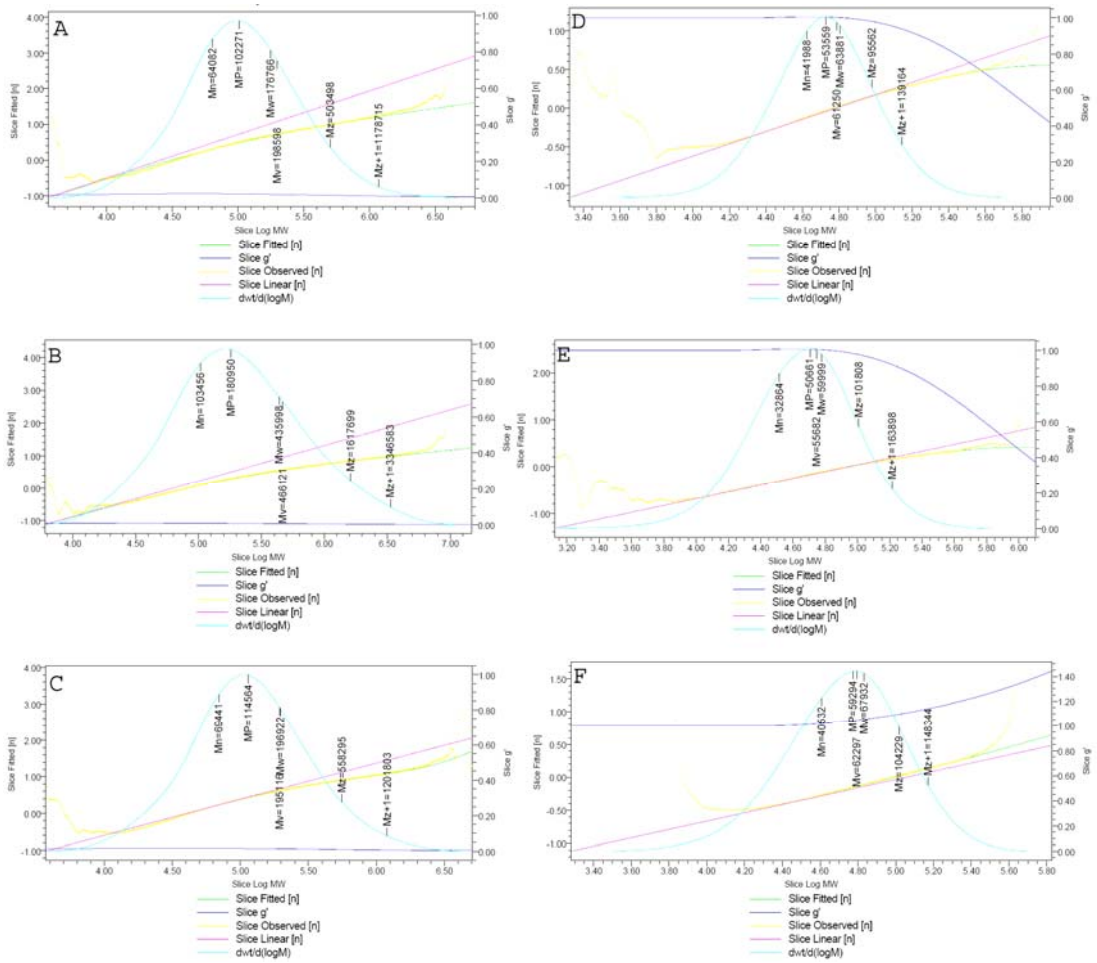

Figure 11. Viscosity law plots of alginate (A), alginate-azide (B), alginate-alkyne (C), hyaluronic acid (D), hyaluronic acid-azide (E), hyaluronic acid-alkyne (F).
Functionalized polysaccharides were dissolved in 0.1 M $NaNO_3$ to a final concentration of 1 mg/mL, filtered, and analyzed via GPC to determine the M_W, M_n, M_W/M_n, M_P, g', and α. Results are summarized in Table 3.

Change in viscosity and index branching were used as additional indicators for alginate functionalization. Alginate is a linear anionic polyelectrolyte with strong electrostatic repulsion which leads to a stiff extended molecular confirmation and high viscosity. Successful functionalization of alginate should result in increased polymer flexibility and reduced viscosity. The Mark-Houwink equation (Equation 1) relates the polymer intrinsic viscosity to the M_W of a linear polymer as:

Equation 1

$$[\eta] = KM_w^{\alpha}$$

where K and α are the constants that depend on conformation and stiffness of the polymer chain and polymer interaction with the solvent. The value for α ranges from zero (for globular proteins) to 2.0 (for rod-like molecules) if dissolved in a good solvent. Typical α values for alginate range from 0.9 to 1.13 depending on the composition. M-rich Alns are more flexible than G-rich Alns thus have lower α values[68]. The α obtained for unfunctionalized Aln of 1.206 was similar to literature values[68, 69]. For unfunctionalized and functionalized Alns, the α's were found to be above 0.8, suggesting a rigid and more extended confirmation.

The functionalization of alginate caused noticeable deviation from linearity in the log-log viscosity vs M_W curves and decreases in polymer viscosity and in α (Figure 11). These data suggest a relatively more flexible confirmation likely due to reduced electrostatic repulsion between polymer chains resulting from functionalization/branching. In agreement with M_W trends, the Az functional group causes the greatest decrease in α as compared to Alk functionalization.

The overall branching index (g') was used as another indicator of functionalization. The g' is defined as the ratio of the radius of gyration of the branched polymer (s_b) and the liner polymer (s_l) or the ratio of the branched intrinsic viscosity (η_b) and the linear intrinsic viscosity (η_l) (Equation 2). As the degree of branching increases, the g' decreases. As mentioned earlier, branching results in increased polymer flexibility and corresponding decreases in both radius of gyration and viscosity[70]. As expected, both g' and η decreased with increasing M_W of

functionalized Aln. The g' decreased four fold for Aln-Az as compared to Aln due to long chain branching. Long chain branching is defined as a polymer branch with 6 or more carbon atoms[71, 72]. The Az functional group is a chain of 12 carbon units, thus functionalization of alginate with this functionality was considered to lead to a long chain branching. Functionalization with the alkyne did not greatly decrease the g' due to short chain branching which is defined as less than 3-6 carbon atoms.

Equation 2

$$g' = \frac{s_b^2}{s_l^2} \approx \left(\frac{\eta_b}{\eta_l} \right)^{\varepsilon}$$

where $2/3 \leq \varepsilon \leq 2$

GPC data for HAln samples are summarized in Table 3. HAln was thought to be a good model to establish quantitative degree of functionalization due to the low MW of the hydrolyzed alginate. However the changes in MW and viscosity trends due to functionalization for HAln did not correlate with trends for functionalized Aln. According to the GPC manufacturer, the intrinsic viscosity is unaffected by long chain branching at low MW. Therefore, there was a MW threshold at which branching affects on η and MW become apparent. Most likely the MW of HAln is below that threshold. Acidic hydrolysis of alginate for 1.5 hr reduced the M_W and η of alginate from 179.06 to 40.43 kDa, and Mw/Mn from 2.81 to 1.31.

Pronova Aln has a higher F_G, lower M_W, and narrower M_W/Mn compared to Aln (Sigma) and due to these factors is expected to undergo more ionic crosslinking, leading to more stable gels than Aln from Sigma. However, due to high cost of Pronova alginate it was not used in functionalization nor stability studies.

HA (Figure 11 D) and functionalized HA (Figure 11 E-F) were also analyzed via GPC to determine M_W, M_W/M_n, and to confirm functionalization. The starting M_W

of HA was 35 kDa as stated by the manufacturer. However, the M_W was found to be 63.95 ±0.10 kDa with a polydispersity of 1.54±0.03. Functionalization of HA with Alk (Figure 11 E) caused a slight increase in M_W and polydispersity for HA-Alk, 68.04±0.16 kDa and 1.69±0.01 respectively, as compared to HA. However, HA functionalized with Az had a decrease in M_W to 59.99±0.02 kDa and an increase in polydispersity of 1.83±0.01 (Figure 11 F). The correlation between chain length and the affects on MW and η were not evident possibly due to the MW of HA and functionalized HA.

2.4 Conclusions

Synthesis of HA and Aln with pendant alkyne and azide functionalities was performed via amidation reaction[30]. Qualitative degree of functionalization was confirmed via FTIR, NMR, and/or GPC techniques. However, given the complex structures and their interactions with solvents for both Aln and HA accurate quantitative degree of functionalization could not be resolved.

^{1}H-NMR confirmed functionalization by comparing the spectra of the starting materials with that of the functionalized polysaccharides. Functionalization of Aln caused distinct changes in the characteristic spectra of Aln such as the appearance of peaks associated with the functional group and band broadening of some characteristic Aln peaks. However, quantitative degree of functionalization or spatial distribution of functional groups along the Aln chain (i.e., preferential functionalization of the G-block or M-block) could not be determined with ^{1}H-NMR.

It was observed that Aln-Az does not form a stable three dimensional hydrogel structure when attempted to crosslink with Ca^{+2} ions suggesting that the G-

blocks are no longer available for effective ionic crosslinking. This observation, together with the GPC results of increased branching and flexibility, implies that Az functionalization may occur at the G-block or that long-chain Az branching may disrupt the ability of Ca^{+2} to ionically interact with the G-blocks of Aln through steric hindrance effects. On the other hand, when Aln-Alk was reacted with Ca^{+2} ions Aln capsules formed suggesting that functionalization with short-chain Alk branches does not inhibit Aln-Alk's ability of to ionically crosslink via the G block.

2.5 Future Work

Determining the extent of functionalization is difficult given Aln's complex chemical structure. More sensitive techniques such as ^{1}H high resolution magic angle spin NMR (^{1}H HR-MAS NMR) should be attempted for quantitative degree of functionalization and crosslinking[30]. This solid state NMR technique would be able to detect the proton associated with the triazole ring that is formed as a result of the 'click' reaction[30]. The intensity of this peak could be utilized for quantifying the degree of crosslinking present which in turn could be used to estimate the extent of functionalization. GPC with Multiangle Laser Light Scattering (MALLS) should be used for more accurate branching analyses and absolute molecular weight determination.

Chapter 3: Comparison of Material Properties Between Ionic and Covalent Alginate Hydrogels

3.1 Introduction

Aln and HA were functionalized via amidation chemistry to contain azide or alkyne functional groups as described in Chapter 2. The functionalization was confirmed with FTIR, NMR, and GPC techniques. The objective of the experiments in this chapter was to evaluate and compare the stability and transport properties of novel, covalently crosslinked 'click' Aln capsules with that of Ca^{+2}-crosslinked Aln capsules. The diffusion properties of these capsules were studied via adsorption /desorption of dye-labeled dextrans of known molecular weight. Also, the affects of the ionic strength of solvent media on gel swelling and diffusion properties were assessed.

3.2 Methods

3.2.1 Materials

Neutral dextrans conjugated with Texas Red® dye, with nominal molecular weight ranging from 3 to 70 kDa, were purchased from Invitrogen. Stock solutions of Texas Red® labeled dextrans were prepared as follows: each dextran was diluted to 2 mg/mL with d.i. H_2O, passed through a 0.45 μm filter, aliquoted out, and frozen at -20^{o}C until use. Complete medium (CM) contained RPMI 1640 medium with 10% fetal calf serum, 2 mM glutamine, 100 U/mL penicillin, and 100 μg/mL streptomycin. Calcium and copper ion selective electrodes (ISE) along with appropriate ionic

strength adjusters (ISA) (4M KCl or 5M $NaNO_3$, respectively) and Ca^{+2} and Cu^{+2} standard solutions were purchased from Cole Palmer and used according to the manufacturer's instructions.

3.2.2 Formation of Ionically or Covalently Crosslinked Capsules

A 2% w/v Aln solution was passed through a Nisco electrostatic microencapsulator (1.1 mm O.D. Needle, 7.5 KV, 20 mL/hr pump speed) into a gelation bath containing 50 mM $CaCl_2$ and 200 mM mannitol. The capsules were allowed to gel for 30 min then removed from the gelation bath, washed with PBS with Ca^{+2}, Mg^{+2}, and used immediately.

Covalently crosslinked Aln capsules were also fabricated using an electrostatic microencapsulator. The 2%w/v functionalized Aln solution comprised of 1 part Aln, 1part Aln-Alk, and 1 part Aln-Az, and the gelation bath was comprised of 50 mM $CuSO_4$ and 200 mM mannitol. The capsules were allowed to gel for 20 min, removed from the gelation bath, and placed in a co-catalyst bath of 20 mM sodium ascorbate (NaAsc) for approximately 20 min. NaAsc reduces Cu(II) to Cu(I) to catalyze the 'click' reaction. The excess NaAsc was removed and replaced with 20 mM EDTA. The capsules were incubated overnight to ensure complete removal of any Cu^{+2}/Cu^{+1}. The capsules were washed to remove excess EDTA and used immediately.

3.2.3 Synthesis of Ionically and 'Click' Crosslinked Capsules for Potentiometric Titration

Ionically, Ca^{+2} or Cu^{+2}, crosslinked Aln capsules were fabricated by passing 2% (w/v) Aln through an electrostatic microencapsulator into a gelation bath of either 57.5364 mM $CaCl_2$ and 201.5447 mM mannitol or 49.6826 mM $CuSO_4$ and 203.1584 mM mannitol with the following settings: 7.5 KV, 20 mL/hr pump speed, 1.1 mm O.D. needle, and 12 mm needle height. The capsules were allowed to gel for approximately 30 min. The excess gelation solution was decanted off and the capsules were placed on an absorbent towel to remove any excess gelation solution and to aliquot into batches. Depending on the total number of capsules present, three batches containing 40 or 60 capsules were placed into microfuge tubes. The exact number of capsules was recorded depending on the type of crosslinking used. To the microfuge tube, d.i.H_2O was added and stored at room temperature until use.

Covalently crosslinked 'click' Aln capsules were fabricated using an electrostatic microencapsulator as stated above with the exception that the 2%w/v functionalized Aln solution comprised of 1 part Aln, 1part Aln-Az, and 1 part Aln-Alk. The capsules gelled for approximately 20 min in a 49.6826 mM $CuSO_4$ and 203.1584 mM mannitol bath and then placed in an approximately 15 mM NaAsc bath for another 20 min to undergo the 'click' reaction. The capsules were removed from the NaAsc bath and placed in EDTA (approximately 50 mM, pH<7) overnight to remove any $Cu^{+2/+1}$. The following day the EDTA was discarded and the capsules were washed with d.i.H_2O to remove any excess EDTA. The capsules were clear in

appearance and sorted into three equal batches as stated above. Each batch contained 80 capsules.

3.2.4 Potentiometric Titration

A calcium or copper ion selective electrode (ISE) was used to detect the presence of ionic (Ca^{+2} or Cu^{+2}) crosslinks. A calibration curve for either calcium or copper was constructed following the manufacturer's (Cole Palmer) instructions.

EDTA titration against ionically or covalently crosslinked capsules was performed following the manufacturer's instructions for the ISE. For Ca^{+2}-crosslinked capsules, 40 capsules were placed into a beaker containing 50 mL d.i.H_2O and 1 mL Ca-ISA (4M KCl). The electrode was placed in the beaker, allowed to stabilized, and the mV reading was recorded as a function of EDTA added. For Cu^{+2}- or 'click' crosslinked capsules, 60 or 80 capsules, respectively, were placed in a beaker containing 50 mL d.i.H_2O, 1 mL Cu-ISA (5M $NaNO_3$), and 0.1 mL ~1N HCl. The electrode was placed in the beaker, allowed to stabilized, and the mV reading was recorded as a function of the volume of EDTA added. For 'click' capsules, after the addition of EDTA, standard Cu^{+2} was employed as a back titrant to determine the excess number of moles of EDTA present.

3.2.5 Water Content and Volumetric Swelling Ratio of Ionically or Covalently Crosslinked Capsules

Calcium or 'click' crosslinked capsules were fabricated as described in section 3.2.2. The diameter of the preswollen capsules was recorded (n =20). Each type of crosslinked capsules were then spilt into three equal groups and incubated overnight

in one of the following: PBS (with Mg^{+2}, Ca^{+2}), PBS (with no Mg^{+2}, Ca^{+2}), or d.i.H_2O to achieve equilibrium swelling. The capsules were removed, blotted with a Kim Wipe® to remove excess moisture, and separated into three equal batches (each batch contained 100 capsules) for each type of crosslink and swelling media. Each batch was weighed in its swollen (W_{sw}) or dry state (W_d). The three batches of capsules were dried overnight in a vacuum oven set at 40°C. The capsules were reswollen in PBS (with Mg^{+2}, Ca^{+2}), PBS (with no Mg^{+2}, Ca^{+2}), or d.i.H_2O and the reswelling was monitored for up to 24 hrs. This was recorded by taking digital photographs (Nikon D40). The capsule diameter was analyzed utilizing Image J®. The swollen (D_{sw}) and dry (D_d) capsule diameters for each of the three batches (n =20) were recorded and the volumetric swelling ratio (VSR) was calculated as:

Equation 3

$$VSR = \frac{D_{sw}^3}{D_d^3}$$

Initial WC was determined using the equation:

Equation 4

$$W.C. = \left(\frac{W_{sw} - W_d}{W_{sw}} \right) \times 100\%$$

3.2.6 Gel Permeation Chromatography of Texas Red® Labeled Dextrans

The M_n, M_W, M_n/M_W, and hydrodynamic radius (R_h) of dextrans conjugated with Texas Red® dye was determined by GPC as described in Section 2.2.6. The columns were calibrated utilizing dextrans standards of known M_W and relatively narrow

M_W/M_n (American Polymer Standards Corp) [1, 4, 20, 41, 80, and 225 kDa]. Data were acquired and analyzed by employing Empower software (Version 2.0, Waters).

The R_h (Equation 5) was calculated utilizing the Einstein viscosity relationship where the hydrated polymer molecules were modeled as hydrodynamic spheres that would increase the viscosity to the same degree that solid, spherical particles of volume V would; where [η] is the intrinsic viscosity (Equation 6), M is the M_w, and N is Avogadro's number[73]. Equation 6 is the Mark-Houwink equation that applies to dextrans below 10^5 MW and describes the relationship between intrinsic viscosity and M_W for dextrans in water[73].

Equation 5

$$R_h = \left(\frac{3[\eta]M}{10\pi N} \right)^{1/3} (cm)$$

Equation 6

$$[\eta] = 0.0978(M_w)^{0.5}$$

3.2.7 Modeling Diffusion of Texas Red® Labeled Dextrans of Known Molecular Weight

Either ionic or covalently crosslinked capsules were placed on an absorbent towel and split into sixteen equal batches into microfuge tubes. Any excess gelation solution was washed and replaced with either d.i.H_2O, PBS (no Ca^{+2}, Mg^{+2}), or CM. Texas Red® dye labeled dextran (3,000, 10,000, 40,000, or 70,000 M_W) in d.i.H_2O was added to a final concentration of 1.0 mg/mL and the capsules were incubated overnight at 20°C to ensure adequate absorption. On the following day, the capsules, 96-well plate, and solvents were equilibrated to 37°C. Excess dextran and moisture was removed from the capsules by blotting the capsules on a Kim Wipe®. Using

tweezers, one capsule was added per well of a 96-well plate for each condition and MW of dextran (n =6). For each condition, 200 μL of either d.i.H_2O, PBS (no Ca^{+2}, Mg^{+2}), or CM was added. The plate was immediately placed in the Tecan Plate Reader and a kinetic program started. The kinetic program consisted of shaking the plate for 1 min to ensure adequate mixing before each reading, measuring the fluorescence in six areas of each well, and taking a measurement every 5 min at an excitation of 595 nm and emission of 615 nm for approximately 20 hrs. Data was analyzed with Excel® by first removing data points associated with the fluorescent capsule utilizing the well-map produced by the Tecan plate reader software and eliminating values that were more than two standard deviations higher than the expected value.

The average diffusion coefficients for each M_W of Texas Red® labeled dextran with respect to media and type of cross-link present was estimated by two methods. The first method utilized the initial rate of dextran desorption and determine the average diffusion coefficient (D) by fitting the linear portion of the desorption curve to Equation 7:

Equation 7

$$\frac{M_t}{M_\infty} = 6\left(\frac{Dt}{\pi a^2}\right)^{\frac{1}{2}}$$

where M_t is the amount of dextran diffused out of the capsule at time t, M_∞ is the amount that has diffused at time equal infinity, t is time, and a is the radius of the hydrogel sphere[74]. Time infinity was taken as the last measured time point.

The second method to estimate the D was to fit the data from each desorption profile to the solution for Fickian diffusion through a sphere with uniform initial,

equal surface concentration conditions, and near sink conditions (Equation 8). Fickian diffusion is defined as simple, passive diffusion from a region of high concentration to a region of low concentration and is determined by the following equation:

Equation 8

$$\frac{M_t}{M_\infty} = 1 - \frac{6}{\pi^2}\sum_{n=1}^{\infty}\frac{1}{n^2}\exp\left(\frac{-Dn^2\pi^2 t}{a^2}\right)$$

Matlab© was employed to fit the data to the Equation 8 by minimizing the error between the data point and estimated point. Each data point for the actual fractional release was the average of six capsules. The function, fmincon, was utilized in Matlab® to find a constrained minimum of the sum of squared errors function (Equation 9) utilizing an initial estimate determined from values obtained from the linear regression analysis. Comparisons between the experimental desorption profiles and the predicated profiles were made to discuss Fickian versus non-Fickian diffusion dextrans through ionically and covalently crosslinked Aln hydrogels.

Equation 9

$$f = \sum\left(\frac{M_t}{M_{\infty\ actual}} - \frac{M_t}{M_{\infty\ estimate}}\right)^2$$

The R_h for each MW of Texas Red® labeled dextran, as estimated by GPC methods, was used to calculate infinite diffusion coefficient (D_o) by employing the Stokes–Einstein equation (Equation 10),

Equation 10

$$D_o = \frac{k_B T}{6\pi\eta R_h}$$

where k_B, η and T are the Boltzmann constant, the solvent viscosity (water at 37^{o}C = 0.7068 mPas), and the absolute temperature, respectively.

3.2.8 Statistical Analysis

Data are expressed as mean ± standard deviation of *n* independent observations. Statistical significance was calculated using the two-tailed unpaired Student's *t*-test or ANOVA. A $p \leq 0.1$ was considered statistically significant.

3.3 Results

3.3.1 Formation of Ionically or Covalently Crosslinked Capsules

Ionic or covalently ('click') crosslinked capsules were fabricated utilizing an electrostatic microencapsulator. Capsule size primarily depended on the needle outer diameter, voltage, and height from the swelling bath. Visually, there was no significant difference in the appearance between ionically and covalently crosslinked capsules. During the fabrication process, the 'click' capsules tended to float on top of the ionic swelling bath whereas the unfunctionalized Aln capsules immediately sank when exposed to the swelling bath. This difference could be due to the differences in viscosity and density of the functionalized and the unfunctionalized Aln solutions as discussed in Chapter 2. 'Click' capsules seemed to have a more 'textured' surface (Figure 12 C and. D).

3.3.2 Potentiometric Titration

When ionically crosslinked capsules are exposed to EDTA, they swell and disintegrate indicating the loss of ionic crosslinks due to EDTA chelation (Figure 12 A and B). Conversely, the covalently crosslinked 'click' capsules do not swell nor

dissolve in the presence of EDTA (Figure 12 C and D); qualitatively confirming the presence and stability of triazole crosslinks.

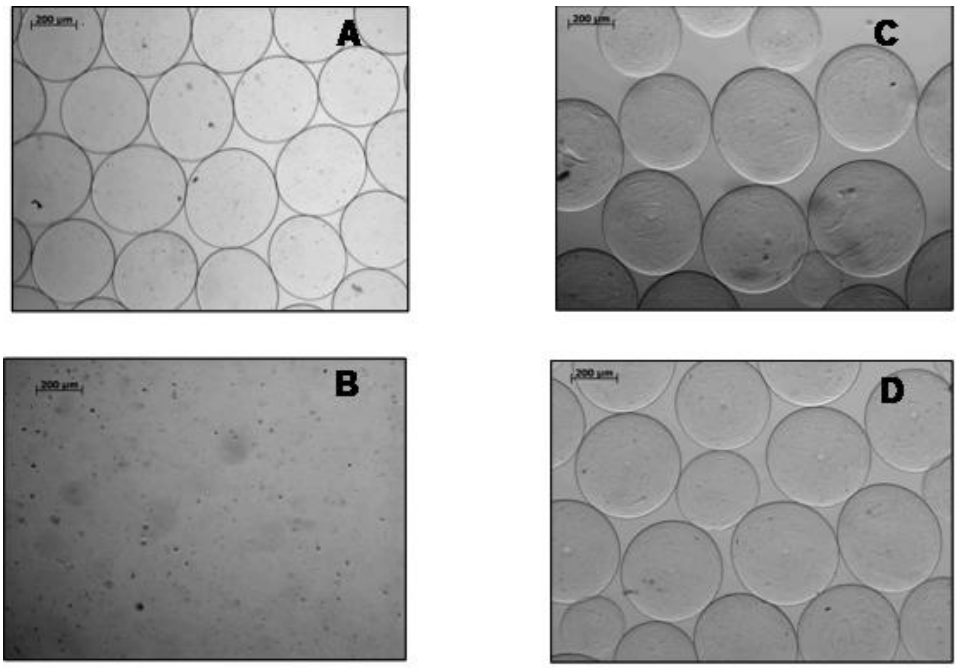

Figure 12. Stability of Ca^{+2} vs. 'click' capsules in the presence of EDTA.
(A) Ca^{+2}-crosslinked capsules (approximately 350 μm in diameter) in d.i. H_2O with a homogeneous, spherical shape. (B) Ca^{+2}-crosslinked capsules in the presence of EDTA. The capsules dissolved as Ca^{+2}, forming the ionic crosslinks, chelated with EDTA. (C) 'Click' capsules in d.i.H_2O (approximately 350 μm in diameter) with a homogenous, spherical shape. (D) 'Click' capsules in the presence of EDTA. The capsules are still present even after 10 min exposure to EDTA with no apparent swelling or disintegration in structure indicating the presence of covalent crosslinking.

The EDTA solutions were standardized using ion specific standard solutions obtained from the manufacturer (Figure 13). As EDTA was added, the ionically crosslinked capsules (Ca^{+2} or Cu^{+2}) were observed to swell along with a corresponding decrease in voltage of the electrode reader. At the beginning of the titration, longer equilibration times were needed for the signal to stabilize; presumably due to the release of ions from the hydrogel into the media. For all titration experiments, the endpoint corresponded to a sharp decrease in voltage.

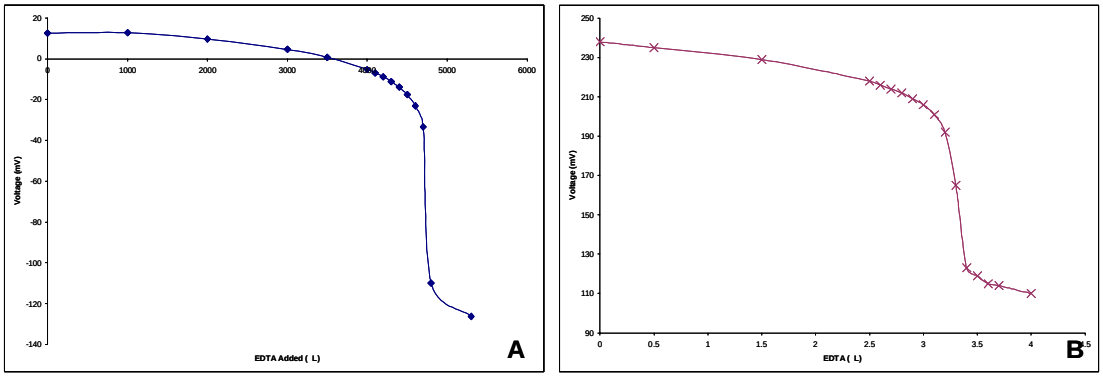

Figure 13. Representative EDTA standardization curves.
(A) EDTA titration against Ca^{+2}. (B) EDTA titration against Cu^{+2}. A sharp decrease in voltage corresponded to the endpoint of the titration.

The endpoint of the titration usually occurred right after the visual disappearance of the ionically crosslinked capsules (Figure 14 A and B). For Ca^{+2}-crosslinked capsules, each trial contained 40 clear appearing capsules within a diameter range of 1.8-2.2 mm. The average endpoint was 1,350 μL of EDTA (12.1 mM) which corresponded to $4.06 \pm 0.03 \times 10^{-7}$ mol Ca^{+2} per capsule. For Cu^{+2}-crosslinked capsules, each trial contained 60 bright blue capsules. The average endpoint was determined to be 4,067 μL of EDTA (10.0 mM) which corresponded to $6.77 \pm 0.17 \times 10^{-7}$ mol of Cu^{+2} per capsule. These findings are summarized in Table 4.

Table 4. Summary of mole of ionic crosslinking per capsule by type of crosslink.

Type of Crosslink	Mole of Ionic Crosslink per Capsule ($\times 10^{-7}$)
Ca^{+2}	4.06 ± 0.03
Cu^{+2}	6.77 ± 0.17
'Click'	N/A

Prior to titration, 'click' capsules were first incubated overnight in EDTA to remove all traces of $Cu^{+2/+1}$, the 'click' catalyst that could also serve as an ionic cross linker. The capsules were clear in appearance, similar to the Ca^{+2}-crosslinked capsules. The initial voltage measurement corresponded to voltage measurements that corresponded to previous endpoints of Cu^{+2}/EDTA titrations indicating that no or

very little Cu^{+2} was present (Figure 14 C). As more EDTA was added, there was no change in the voltage. To exhaustively confirm that there were no trace amounts of $Cu^{+2/+1}$ crosslinking present, a back titration using Cu^{+2} standard was performed. The theoretical endpoint for the Cu^{+2} reacting with excess EDTA corresponded with the actual endpoint (data not shown). The 'click' capsules never swelled or dissolved throughout the titration.

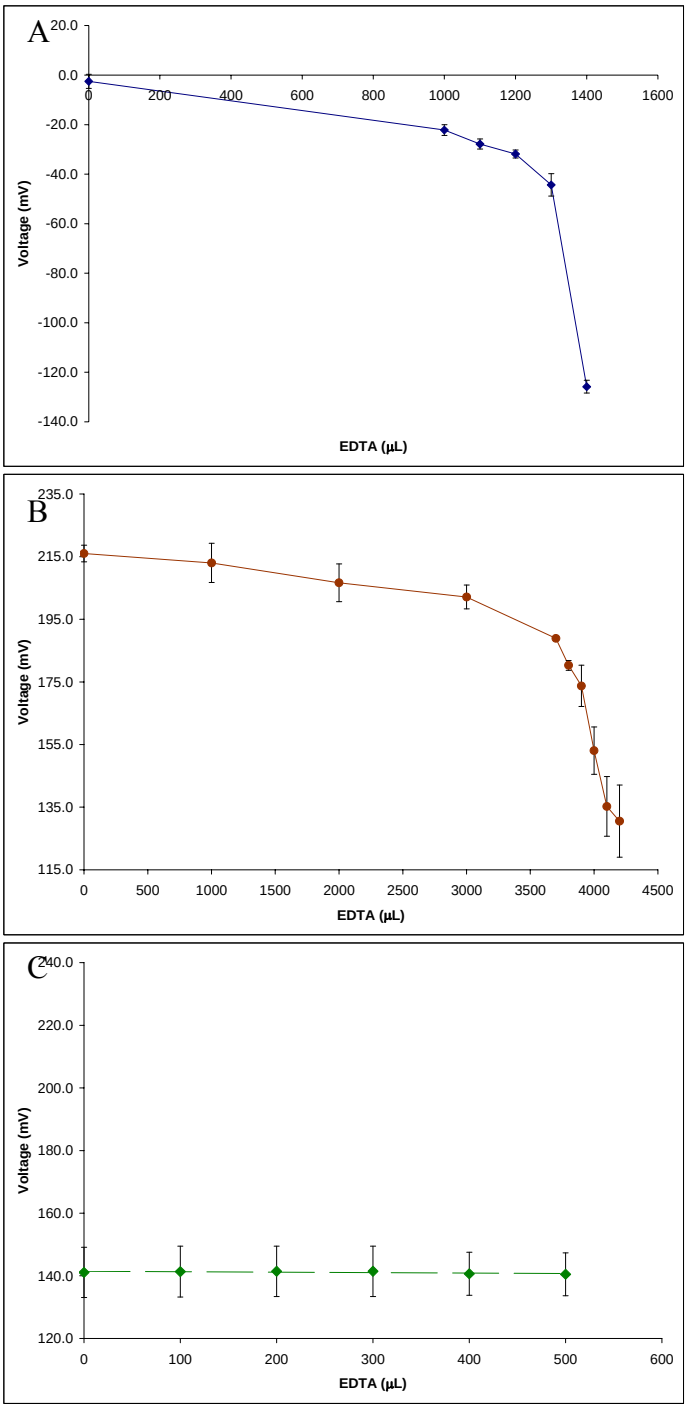

Figure 14. EDTA titration against Ca^{+2} (A), Cu^{+2} (B), or 'click' (C) capsules. Ionically or covalently crosslinked Aln capsules were fabricated with an electrostatic microencapsulator. At least 40 capsules per crosslinking chemistry were placed into a beaker containing 50 mL d.i.H_2O and 1 mL of ISA. An ion specific electrode was placed in the beaker, allowed to stabilized, and the mV reading was recorded as a function of EDTA added. A sharp decrease in voltage corresponds to the endpoint in the titration where EDTA has chelated with the ionic species in a 1:1 ratio. The capsules dissappeared or completely dissolved right before the endpoint.

3.3.3 Volumetric Swelling Ratio and Water Content

The volumetric swelling ratio (VSR) was determined for Ca^{+2}-crosslinked and 'click' crosslinked capsules in d.i.H_2O, PBS (with Ca^{+2}, Mg^{+2}), and PBS (without Ca^{+2}, Mg^{+2}) over a period of 24 hrs. Capsules were fabricated with a microencapsulator. The "preswollen" state was defined as the dimension measured of the capsules right after fabrication but before being incubated in swelling media overnight (n>10). The "swollen" state was defined as the dimension measured of the capsules after being swollen in media (d.i. H_2O, PBS (w/ Ca^{+2}, Mg^{+2}), or PBS (w/o Ca^{+2}, Mg^{+2})) overnight and before the capsules were dried in a vacuum oven (n>10). Finally, the "final" state was defined as the dimension measured of the capsules (n>10) after being reswollen in their respective media after 24 hrs of swelling.

The diameters of the capsules in the various swelling states (preswollen, swollen, dry, and final) are summarized in Table 5. The average diameter of the Ca^{+2}-crosslinked capsules immediately after fabrication was 1.85 ± 0.06 mm (n> 20). Ca^{+2}-crosslinked capsules that were incubated overnight in d.i.H_2O had no significant increase in diameter (1.85 ± 0.06 vs. 1.89±0.09, n=28). For Ca^{+2}-crosslinked capsules that were swollen overnight in PBS (with or without Ca^{+2}, Mg^{+2}), the average diameter increased to 2.10 mm. There was no significant difference in the swollen diameters of Ca^{+2}-crosslinked capsules in PBS (w Ca^{+2}, Mg^{+2}) or PBS (w/o Ca^{+2}, Mg^{+2}).

For 'click' capsules, the preswollen diameter was determined to be 2.21±0.14 mm (n>30) and the diameter significantly increased when the capsules swelled in di.H_2O overnight to 2.42±0.10 mm. However, when capsules were incubated

overnight in PBS (w/ Ca^{+2}, Mg^{+2}) or PBS (w/o Ca^{+2}, Mg^{+2}) the capsules visually and significantly shrank in size (2.06±0.08 mm and 2.01±0.09 mm, respectively). There was no significant difference in diameter between capsules swollen in PBS (w/ Ca^{+2}, Mg^{+2}) and PBS (w/o Ca^{+2}, Mg^{+2}) ($p<0.01$).

Table 5. Summary of preswollen, swollen, dry, and final diameters (mm) of Ca^{+2}- or 'click' crosslinked capsules (n>20 for each measurement).

	Ca^{+2}-Crosslinked			'Click' Crosslinked		
	d.i.H_2O (mm)	PBS (w/ Ca^{+2}, Mg^{+2}) (mm)	PBS (w/o Ca^{+2}, Mg^{+2}) (mm)	d.i.H_2O (mm)	PBS (w/ Ca^{+2}, Mg^{+2}) (mm)	PBS (w/o Ca^{+2}, Mg^{+2}) (mm)
Preswollen		1.85±0.06			2.21±0.14	
Swollen	1.89±0.09	2.10±0.08	2.07±0.12	2.42±0.10	2.06±0.08	2.01±0.09
Dry	0.86±0.08	1.05±0.13	1.12±0.12	0.85±0.7	0.83±0.09	0.88±0.07
Final	0.87±0.08	2.29±0.17	2.39±0.10	1.70±0.11	1.37±0.10	1.30±0.09

The capsules were dehydrated by placing them in a vacuum oven overnight at 40°C and 7 mm Hg. Water swollen Ca^{+2}-crosslinked capsules had an average dry diameter of 0.87±0.08 mm which was significantly less than capsules swollen in PBS (w/ Ca^{+2}, Mg^{+2}) or PBS (w/o Ca^{+2}, Mg^{+2}). There was no significant difference in the dry diameters of capsules that were first swollen in PBS (w/ Ca^{+2}, Mg^{+2}) or PBS (w/o Ca^{+2}, Mg^{+2}) (1.05±0.13 and 1.12±0.12 mm, respectively). The dry diameters of 'click' capsules first swollen in d.i.H_2O, PBS (w/ Ca^{+2}, Mg^{+2}), or PBS (w/o Ca^{+2}, Mg^{+2}) were not significantly different from each other (0.85±0.7, 0.83±0.09, and 0.88± 0.07 mm, respectively).

Dry Ca^{+2}- or 'click' crosslinked capsules were then incubated in their respective swelling media and reswelling was measured as a function of time (Figure 15 and Figure 16). Ca^{+2}-crosslinked capsules that were reswollen in d.i.H_2O did not significantly reswell. However, Ca^{+2}-crosslinked capsules reswollen in PBS (w/ Ca^{+2}, Mg^{+2}) or PBS (w/o Ca^{+2}, Mg^{+2}) did reswell. In general, these capsules reswelled to

their original swollen VSR in less than 30 min and continued to swell reaching an pseudo-equilibrium swelling state in approximately an hour (Figure 15). As the capsules swelled past their original size, cracks and deformations were observed indicating the capsules had begun to burst, resulting in destruction of the hydrogel structure. 'Click' capsules dramatically reswelled in d.i.H_2O or PBS (Figure 16) however never reached their original, swollen VSR. These results are summarized in Table 6.

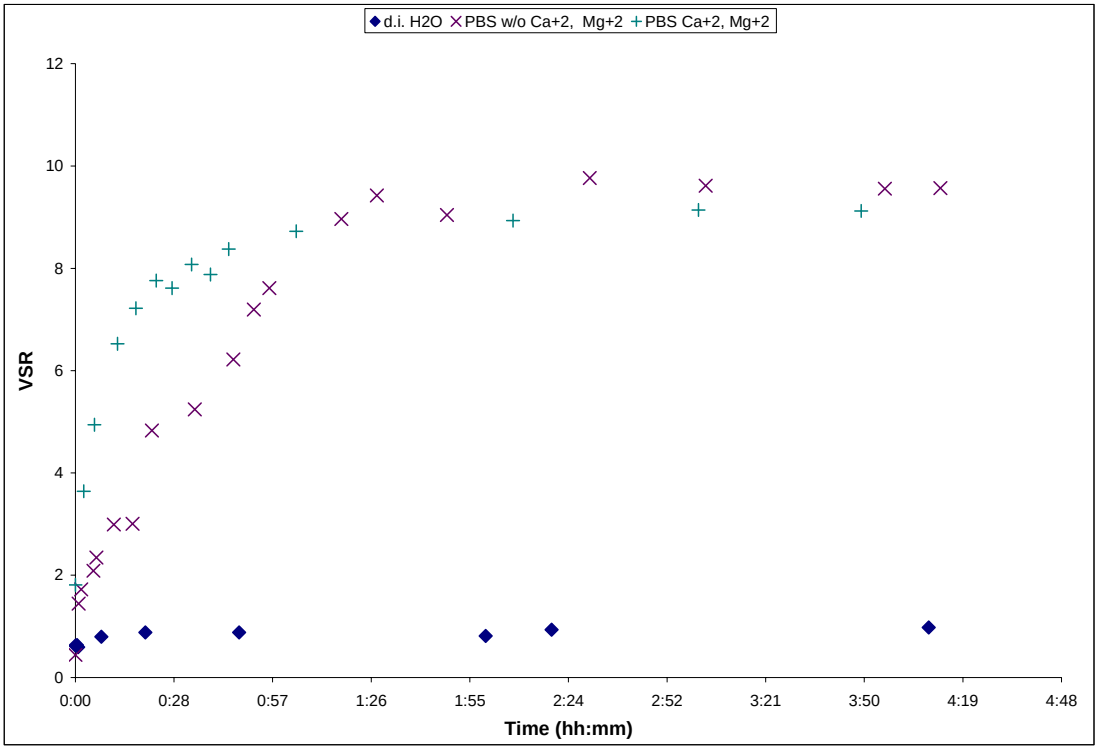

Figure 15. Ca^{+2}-crosslinked capsules reswollen in d.i.H_2O, PBS w/ Ca^{+2}, Mg^{+2}, and PBS w/o Ca^{+2}, Mg^{+2}.
Ca^{+2} -crosslinked capsules were swollen over night in either d.i.H_2O, PBS w/ Ca^{+2}, Mg^{+2}, or PBS w/o Ca^{+2}, Mg^{+2} and their initial swollen diameter was measured. The capsules were dried overnight in a vacuum oven at 40°C and their dried diameter was measured. The capsules were incubated in their respective media and the reswelling was monitored as a function of time. Each measurement is the average of at least 20 capsules.

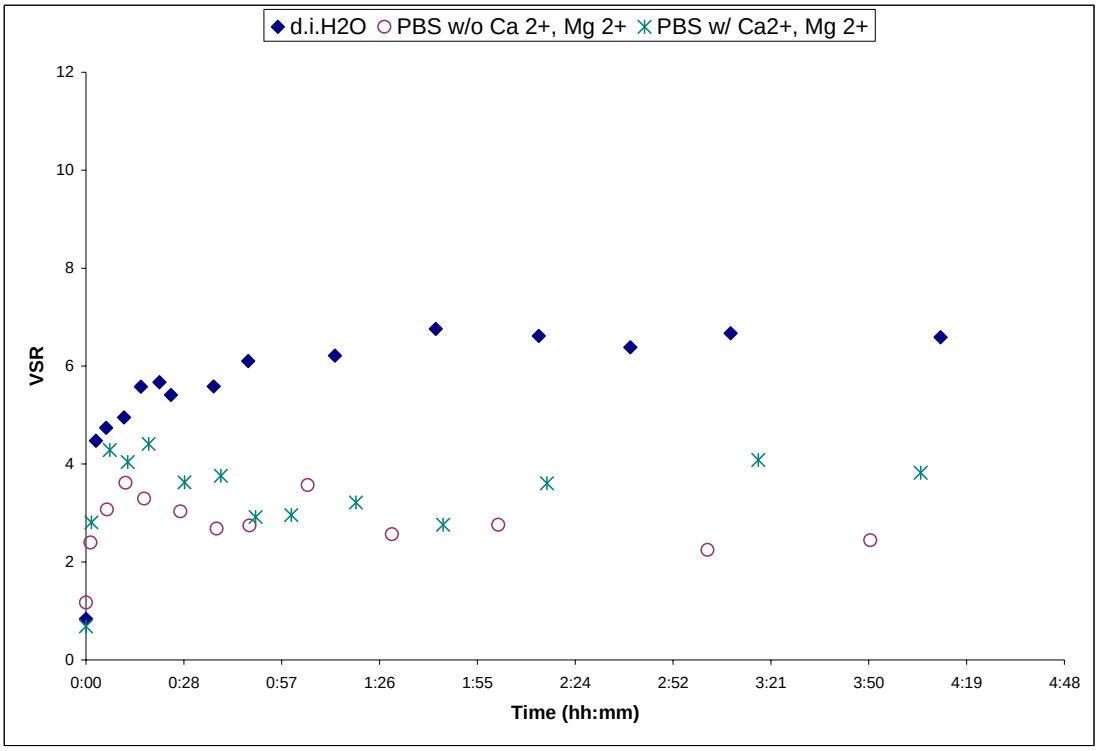

Figure 16. 'Click'-crosslinked capsules reswollen in d.i.H_2O, PBS w/ Ca^{+2}, Mg^{+2}, and PBS w/o Ca^{+2}, Mg^{+2}.
'Click' -crosslinked capsules were swollen over night in either d.i.H_2O, PBS w/ Ca^{+2}, Mg^{+2}, PBS w/o Ca^{+2}, Mg^{+2}. The capsules were dried overnight in a vacuum oven at 40°C. The capsules were incubated in their respective media and the reswelling was monitored as a function of time. Each measurement is the average of at least 20 capsules.

Table 6. Summary of VSR of Ca+2- or 'click' crosslinked capsules in media of varying ionic strength.

	Ca^{+2}-Crosslinked			'Click' Crosslinked		
	d.i.H_2O (mm)	PBS (w/ Ca^{+2}, Mg^{+2}) (mm)	PBS (w/o Ca^{+2}, Mg^{+2}) (mm)	d.i.H_2O (mm)	PBS (w/ Ca^{+2}, Mg^{+2}) (mm)	PBS (w/o Ca^{+2}, Mg^{+2}) (mm)
Preswollen	9.77±2.87	5.46±2.16	4.53±1.46	17.85±5.57	18.84±6.84	16.02±4.93
Swollen	10.44±3.23	8.02±3.21	6.48±2.30	23.52±6.58	15.21±5.05	12.09±3.32
Final	0.98±0.41	10.43±4.65	9.85±3.27	8.24±2.60	4.51±1.70	3.27±1.02

The WC was only measured for Ca^{+2}- or 'click' capsules swollen in d.i.H_2O and PBS (w/o Ca^{+2}, Mg^{+2}) and was determined to be 95.91 ± 0.03 % for Ca^{+2}-crosslinked capsules swollen in PBS (w/o Ca^{+2}, Mg^{+2}) and 96.23 ± 0.04% in d.i.H_2O (Table 7). For 'click' capsules swollen in PBS (w/o Ca^{+2}, Mg^{+2}), the WC was determined to be 95.74 ± 0.13% and increased to 98.36 ± 0.02% for 'click' capsules

swollen d.i.H_2O. As mentioned earlier, 'click' capsules swelled significantly more in water as compared to 'click' capsules in PBS or Ca^{+2} crosslinked capsules in d.i.H_2O. However, when swollen in PBS further ionic crosslinking occurs in the 'click' capsules and they underwent less swelling as indicated by the decrease in the WC.

Table 7. Summary of WC for ionically or covalently crosslinked capsules in media of varying ionic strength (*n* =3, with each trial containing at least 80 capsules).

	d.i.H_2O (%)	PBS (%)
Ca^{+2}	96.23 ± 0.04	95.91 ± 0.03
'Click'	98.36 ± 0.02	95.74 ± 0.13

3.3.4 Gel Permeation Chromatography Determination of the Hydrodynamic Radius and Infinite Diffusion Coefficient of Texas Red® Labeled Dextrans

The M_n, M_W, M_W/M_n, and M_P of Texas Red ® labeled dextrans were determined by GPC (Figure 17). Samples were prepared at 1.0 mg/mL in 0.1 $NaNO_3$ buffer, passed through 0.45 μm filter, and assessed on a Waters Alliance GCPV 2000 system with a 1.0 mL/min flow rate at 40°C. Dextrans standards were used to develop a calibration curve. Results are summarized in Table 8 and Table 9.

Table 8. Summary of GPC analysis of Texas Red® labeled dextrans.

Labeled Dextran Name	M_n (kDa)	M_W (kDa)	M_W/M_n	M_P (kDa)	K	α	g'	Degree of Labeling[1] (dye/dextran)
3 kDa	---	---	---	---	---	---	---	0.5-1
10 kDa	9.74±0.18	22.65±0.34	2.32±0.01	14.60±0.22	4.29±0.13 x10^{-4}	0.419±0.001	0.32±0.01	1-2
40 kDa	11.40±0.06	54.42±0.68	4.78±0.04	55.84±1.24	4.56±0.16 x10^{-4}	0.469±0.002	0.60±0.01	2-6
70 kDa	125.01±10.56	168.04±5.16	1.35±0.07	150.62±8.68	4.63±4.66 x10^{-8}	1.20±0.10	0.34±0.01	3-8

[1]Degree of labeling provided by manufacturer. Results are the average of two runs per sample.

Table 9. Summary of Texas Red® labeled dextran properties.

Labeled Dextran Name	[η]* (mL/g)	R_h (nm)	D_o x10^{-8} (cm^2/s)
3 kDa	---	---	---
10 kDa	14.72±0.11	3.75±0.03	85.63±0.64
40 kDa	22.82±0.14	5.82±0.04	55.24±0.34
70 kDa	40.09±0.62	10.22±0.16	31.44±0.48

*Calculated from $[\eta]=0.0978(Mw)^{0.5}$. Results are the average of two runs per sample.

.

Representative chromatograms of different MW's of labeled dextrans are shown in Figure 17. Refractive index data is shown in red and viscometry data shown in green. The MW and M_W/M_n data for 10 and 40 kDa dextran agreed with manufacturers specifications. GPC chromatograms indicate a broad M_W/M_n for each dextran, with 70 kDa having the broadest. The manufacturer stated that their 70 kDa dextran consisted of dextran of 60 to 90 kDa MW. Dextrans are branched polysaccharides, labeling with dye increases their distribution further. A low MW shoulder peak present only on the RI chromatograms is due to a system solvent peak (Figure 17 A and C). A distinctive lower MW shoulder that is observed on both RI and viscometry chromatograms is most likely due to contaminants such as free Texas Red® dye or buffer salts present in the samples (Figure 17 B).

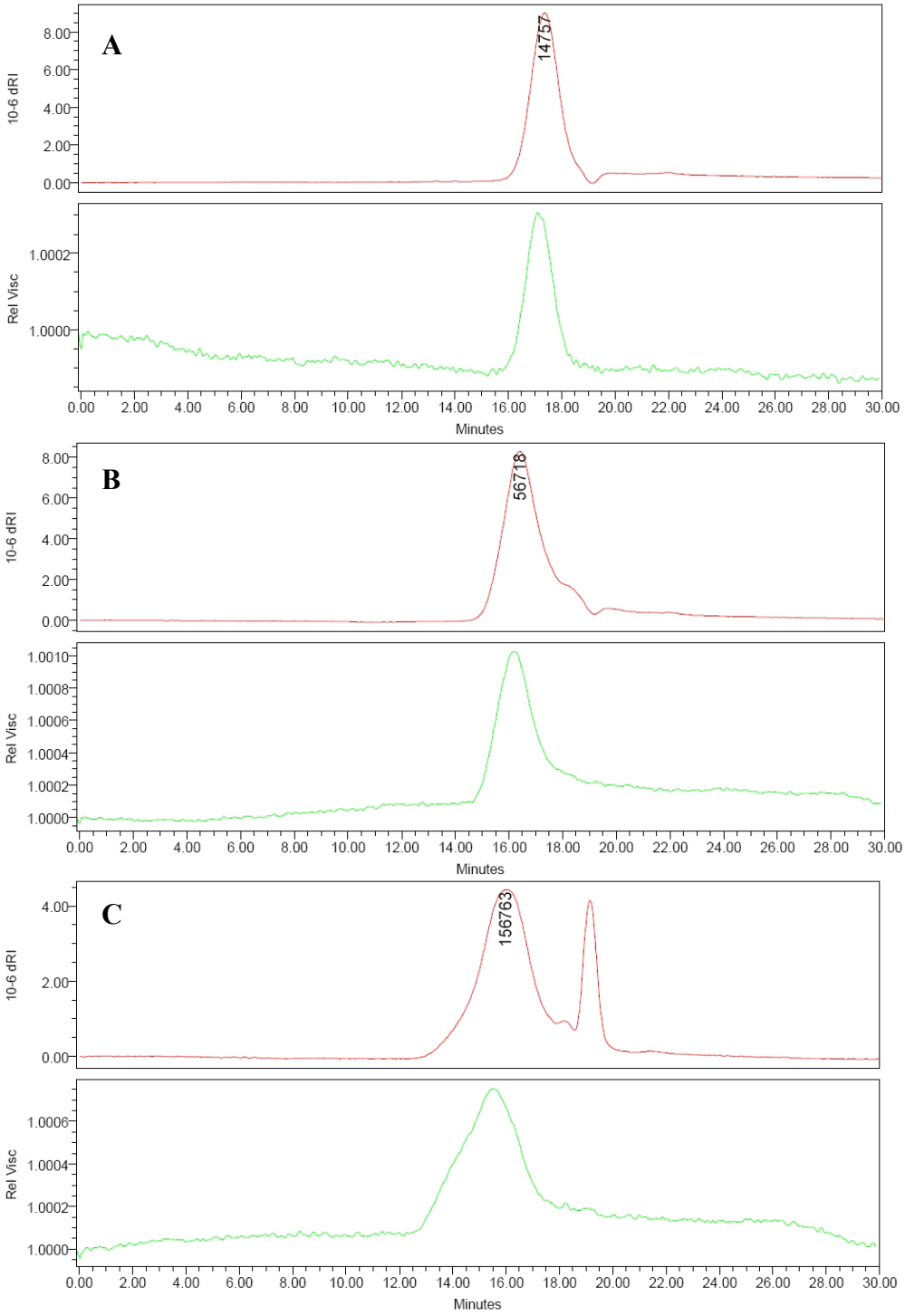

Figure 17. GPC chromatograms of Texas Red® labeled dextrans in 0.1 M $NaNO_3$ at 1.0 mg/mL, 1.0 mL/min.
(A) 10 kDa Texas Red® labeled dextran (B) 40 kDa Texas Red® labeled dextran (C) 70 kDa Texas Red® labeled dextran. Red line: Refractive Index data, Green line: Viscometry data.

The [η] and the M_W data were employed to calculate the hydrodynamic radius (R_h) for each MW of available dextran (Equation 5). The results obtained for the R_h

were in agreement with R_h stated in the literature for dextrans of similar MW[73, 75, 76]. The R_h and the solvent viscosity η were employed to calculate the Do (Equation 10) for each MW dextran and are summarized in **Error! Reference source not found.**.

The [η] of expanded, flexible polymer chains is related to the MW by the Mark-Houwink equation where K and α are constants for a given polymer. For the 10 kDa and 40 kDa dextrans, α was found to be ~ 0.470 and K~$4.44x10^{-4}$. Both α and K depend on the nature of the polymer, the solvent, and the temperature[72]. For flexible polymers in a good solvent α is less than 0.8. In the case of dextran which should be a flexible polymer, the α determined experimentally was in agreement with literature values[73, 77] indicating that 0.1 M $NaNO_3$ was an appropriate buffer.

3.3.5 Modeling of Texas Red® Labeled Dextran Diffusion

The desorption of dextrans of known MW (3-70 kDa) from Ca^{+2}-crosslinked and 'click' crosslinked capsules was studied as a function of time in different medias. Ca^{+2}- and 'click'-crosslinked capsules were fabricated with an electrostatic encapsulator, incubated overnight in 1.0 mg/mL dye labeled dextrans of varying MW, seeded into a 96-well plate, and the desorption of the dye labeled dextran was measured by fluorescence as a function of time.

As expected, the amount of dye labeled dextran absorbed in Ca^{+2}- or 'click' crosslinked capsules depended on the MW of dextrans (Figure 18 and Figure 19). Visually, Ca^{+2}- and 'click'-crosslinked capsules absorbed negligible amounts of 70 kDa dextran and small amounts of 40 kDa dextran suggesting a molecular weight cutoff (MWCO) of around 40-70 kDa.

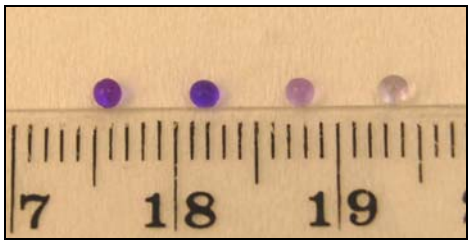

Figure 18. Ca^{+2}-crosslinked capsules after overnight incubation in 1.0 mg/mL Texas Red® labeled dextran (3 kDa, 10 kDa, 40 kDa, 70 kDa from left to right).
Based on visual appearance, Ca^{+2}-crosslinked capsules absorbed very little 40 or 70 kDa Texas Red® labeled dextran indicating a MWCO between 40-70 kDa.

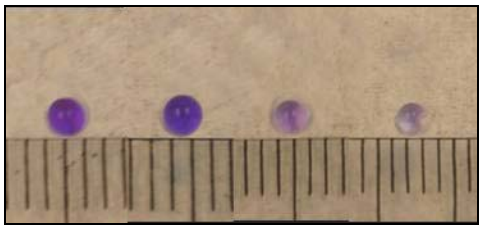

Figure 19. 'Click'-crosslinked capsules after overnight incubation in 1.0 mg/mL Texas Red® labeled dextran (3 kDa, 10 kDa, 40 kDa, 70 kDa from left to right).
Based on visual appearance, 'click'-crosslinked capsules absorbed very little 40 or 70 kDa Texas Red® labeled dextran indicating a MWCO between 40-70 kDa.

As mentioned previsously, Ca^{+2}-crosslinked capsules dissolved overnight in PBS and culture media (CM) but not in d.i.H_2O. However, ionically crosslinked capsules did completely dissolved in PBS after 24 hrs. In CM, capsules were observed to have dissolved or capsule fragments were present at the bottom of the wells. 'Click' crosslinked capsules did not dissolve in any of the solvation media.

The absolute amounts of Texas Red® labeled dextran (3-70 kDa) that desorbed from Ca^{+2}-or 'click' crosslinked Aln capsules (Figure 20-Figure 22). Ca^{+2}-crosslinked capsules absorbed less Texas Red® labeled dextrans than 'click' crosslinked capsules indicating smaller diffusion channels, perhaps due to a greater degree of crosslinking in these capsules. However, 'click' capsules were still present at the end of the experiment indicating superior stability. For Ca^{+2}- and 'click' crosslinked capsules, as the molecular weight of the dextran increased the amount absorbed/desorbed decreased (Figure 20-Figure 22). 'Click' capsules in ionic media

(PBS (Figure 21 B) or CM (Figure 22B)) absorbed/desorbed less dextran (3-70 kDa) than compared to ‘click’ capsules in water (Figure 20 B), likely due to additional ionic crosslinking and reduction in diffusion channel sizes.

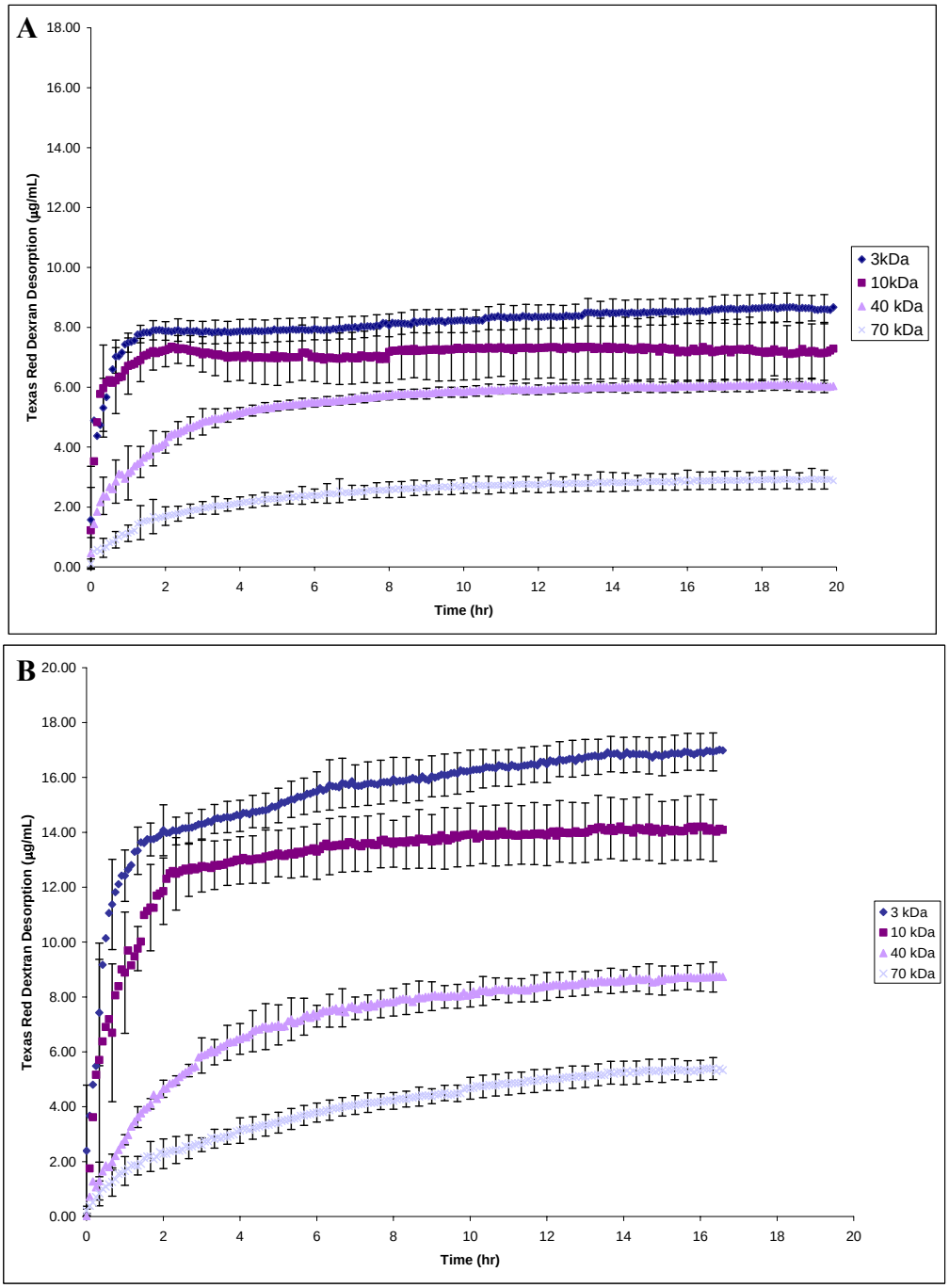

Figure 20. Texas Red® labeled dextran (3-70 kDa) desorption from Ca^{+2}-crosslinked capsules (A) vs. 'click' capsules (B) (each dextran MW *n* =6) in d.i.H_2O.
As the MW of the dextran increased the amount absorbed/desorbed from the capsule decreased. Ca^{+2}-crosslinked capsules overall absorbed/desorbed less dextran than 'click' capsules indicating more crosslinking.

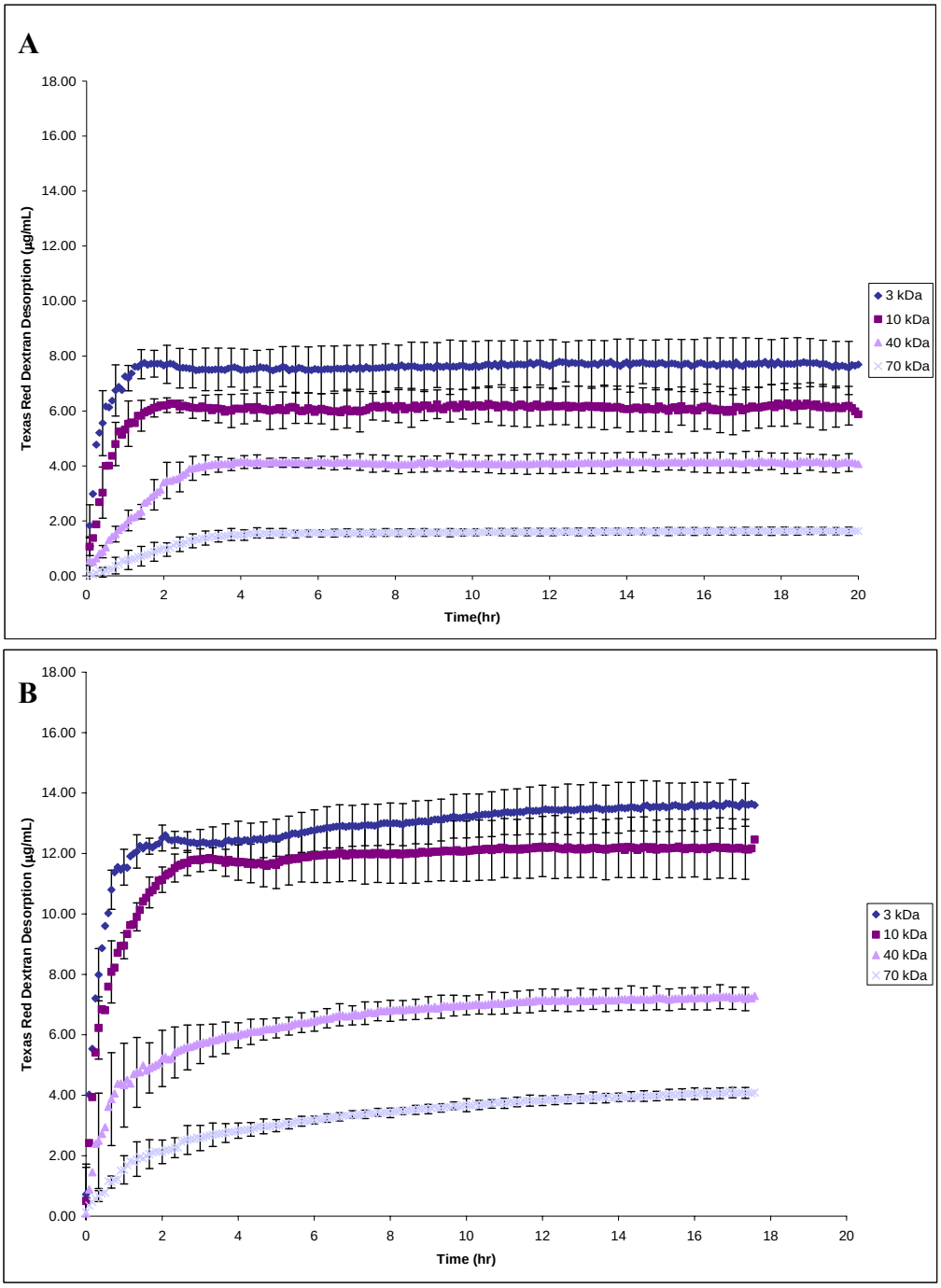

Figure 21. Texas Red® labeled dextran (3-70 kDa) desorption from Ca^{+2}-crosslinked capsules (A) vs. 'click' capsules (B) (each dextran MW *n* =6) in PBS.

As the MW of the dextran increased the amount absorbed/desorbed from the capsule decreased. Ca^{+2}-crosslinked capsules overall absorbed/desorbed less dextran than 'click' capsules indicating more crosslinking.

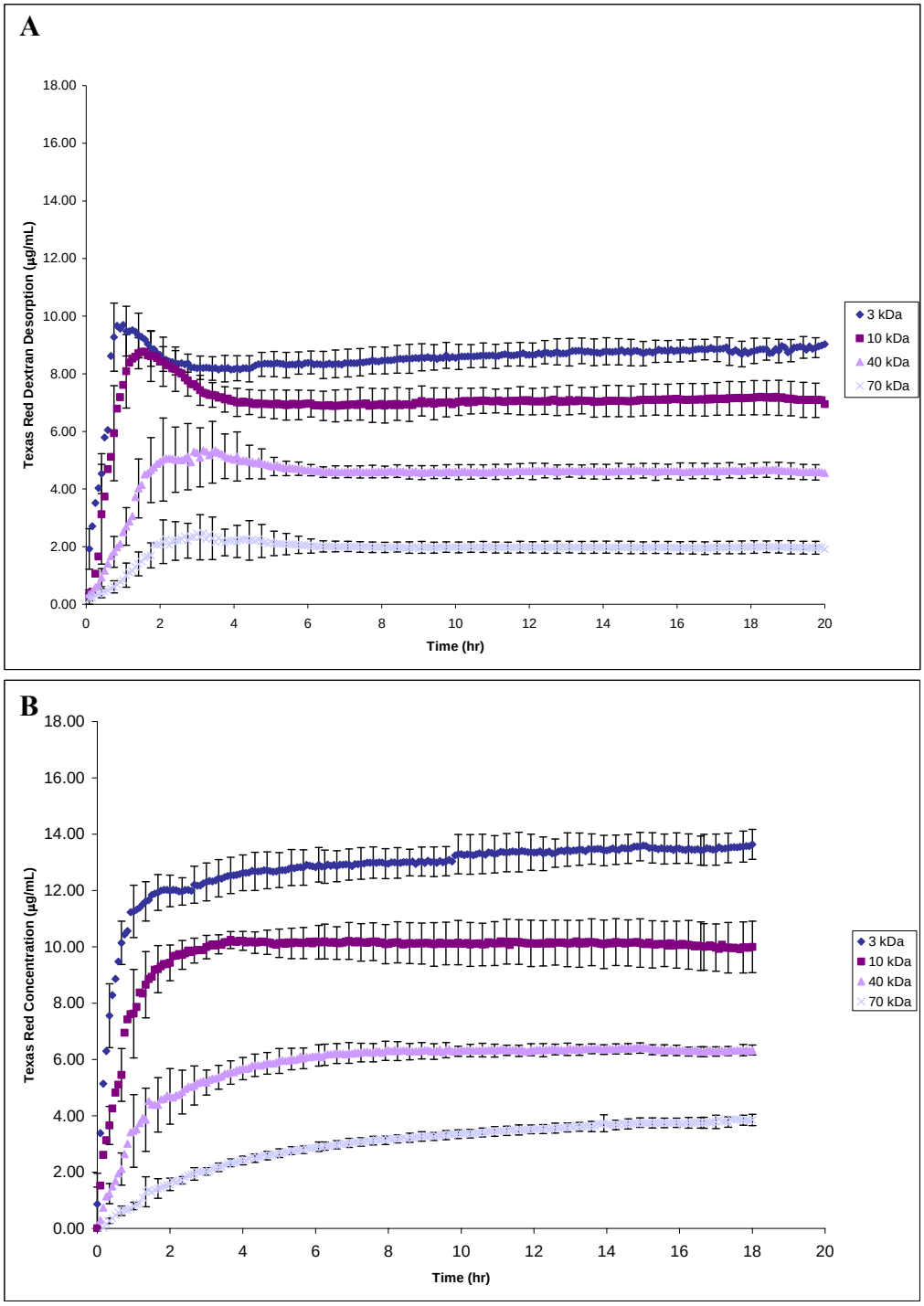

Figure 22. Texas Red® labeled dextran (3-70 kDa) desorption from Ca^{+2}-crosslinked capsules (A) vs. 'click' capsules (B) (each dextran MW *n* =6) in CM.

As the MW of the dextran increased the amount absorbed/desorbed from the capsule decreased. Ca^{+2}-crosslinked capsules overall absorbed/desorbed less dextran than 'click' capsules indicating more crosslinking. However, desorption from Ca^{+2}-crosslinked capsules exhibited a burst release indicative of a degrading capsule.

The first method to determine the D employed Equation 7 which required that the fractional release of the diffusing molecule be linear for at least 50% of the release curve[74]. This was done by employing linear regression analysis for the linear portion of the desorption curve for each dextran in each media. Results are summarized in **Error! Reference source not found.**. For Ca^{+2}-crosslinked capsules, as the ionic strength of the media increased the value of the D for each MW dextran approached the D_o (Table 10). This supports the observation that Ca^{+2}-crosslinked capsules were disintegrating, removing the alginate framework that would impede dextran diffusion. As the ionic strength of the media increased, the D for dextrans in Ca^{+2}-crosslinked capsules increased.

For 'click' capsules, the D was approximately one order of magnitude less then the D_o. There was no strong correlation between the ionic strength of the media and the affect on the D for dextrans in 'click' capsules. The D obtained from the linear regression analysis was used as a starting value in modeling the diffusion in Matlab®.

Table 10. Summary of average diffusion coefficients determined from linear regression analysis utilizing Equation 7.

	Ca^{2+}			'Click'		
	d.i.H_2O D ($x10^8$ cm^2/s)	PBS D ($x10^8$ cm^2/s)	CM D ($x10^8$ cm^2/s)	d.i.H_2O D ($x10^8$ cm^2/s)	PBS D ($x10^8$ cm^2/s)	CM D ($x10^8$ cm^2/s)
3 kDa	34.1	20.4	32.1	25.4	21.8	18.9
10 kDa	10.1	17.9	78.6	12.7	8.31	17.3
40 kDa	3.11	9.35	23.8	5.95	6.12	6.77
70 kDa	3.15	9.01	17.7	2.14	3.24	2.79

The second method used to determine the D of dextrans was to fit the solution for Fickian diffusion (Equation 8) through a hard sphere to desorption profiles by

minimizing the error between the actual data and the estimated data. This was done by employing Matlab® and its optimization toolbox. The estimated diffusion coefficients are summarized in Table 11. For the Ca^{+2}-crosslinked capsules in CM, Matlab® could not converge on a solution when utilizing the equation for Fickian diffusion. Again, with the exception of Ca^{+2}-crosslinked capsules in CM, as the MW of dextran increased the D decreased regardless of the media. Also, as the ionic strength of the solvation media increased the diffusion coefficient of each MW of dextran increased when in Ca^{+2}-crosslinked capsules. The affect of ionic strength on the diffusion coefficient was not seen in 'click' capsules. Also, when comparing diffusion coefficients of Ca^{+2}- or 'click' crosslinked capsules in the same media, 'click' capsules generally had lower or about the same diffusion coefficients for each MW compared to the Ca^{+2}-crosslinked capsules. Even though freshly made Ca^{+2} crosslinked capsules absorbed less dextrans than 'click' capsules, likely due to a tighter crosslinking, their disintegration over time led to higher diffusion coefficients than those for 'click' gels.

Table 11. Summary of average diffusion coefficients determined using Matlab®.

	Ca^{2+}			'Click'		
	d.i.H_2O D (x10^8 cm^2/s)	PBS D (x10^8 cm^2/s)	CM D (x10^8 cm^2/s)	d.i.H_2O D (x10^8 cm^2/s)	PBS D (x10^8 cm^2/s)	CM D (x10^8 cm^2/s)
3 kDa	20.7	21.4	---	13.4	19.6	18.5
10 kDa	12.0	18.5	---	11.2	6.75	17.3
40 kDa	2.58	5.41	---	2.54	4.07	2.89
70 kDa	2.79	4.58	---	1.87	2.35	2.29

The experimental and modeled fractional release of dextran (3-70 kDa) in ionic vs. covalent crosslinked capsules in medias of varying ionic strength is compared in Figure 23(A-E). Figure 23A is a plot of the actual fractional release and

the model for dextran release in d.i. H_2O. The model seems to fit the experimental data for diffusion in d.i.H_2O for both Ca^{+2} and 'click' capsules extremely well. However, as the ionic strength of the media increases (Figure 23 C and E) the model fails to achieve a good fit with the data. When covalent 'click' crosslinking was employed (Figure 23 B, D, and F) the model for Fickian diffusion was a good prediction of the actual data.

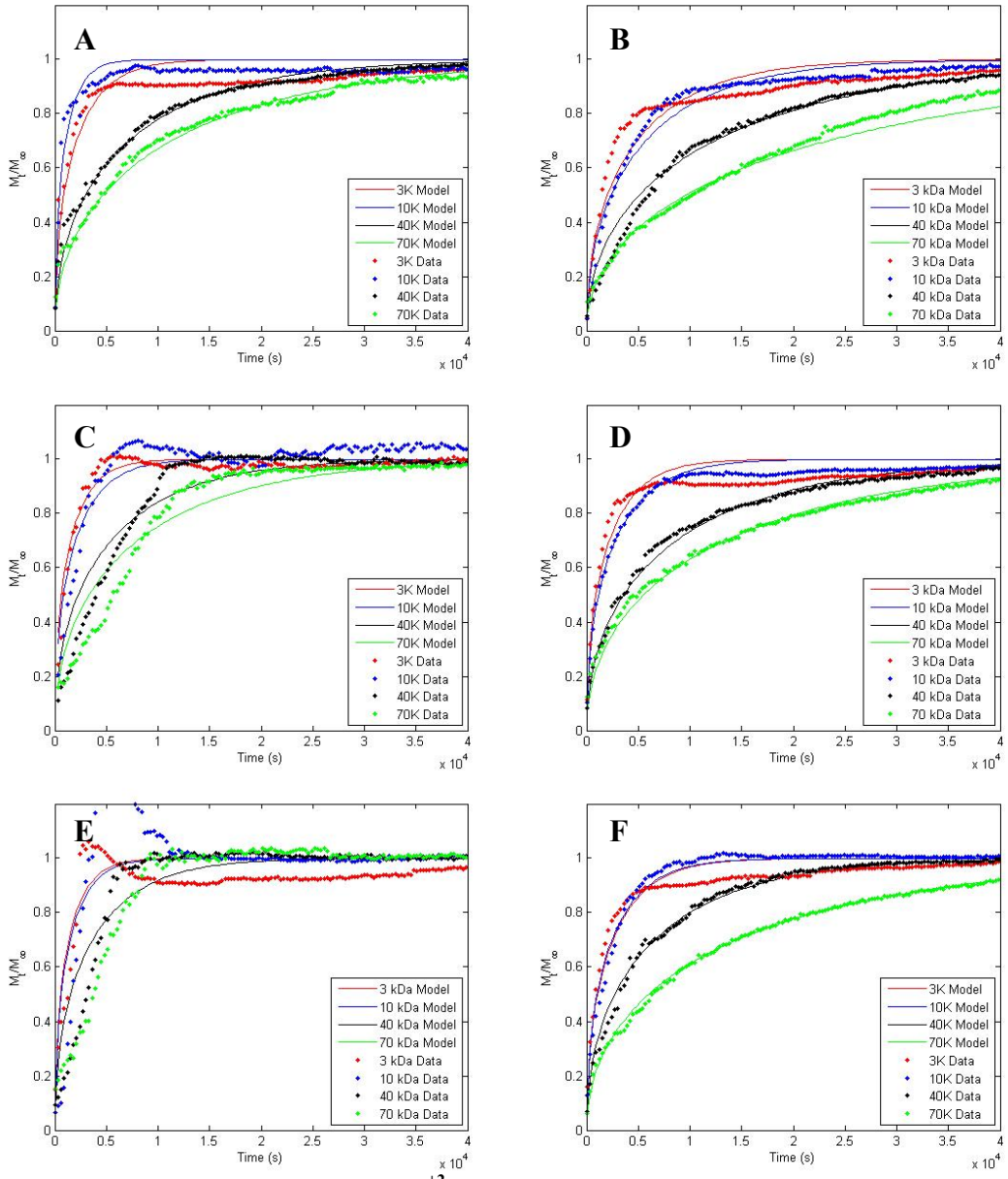

Figure 23. MatLab® simulations (A) Ca^{+2}-crosslinked in d.i. H_2O (B) 'Click' in d.i.H_2O (C) Ca^{+2}-crosslinked in PBS, (D) 'Click' in PBS (E) Ca^{+2}-crosslinked in CM (F) 'Click' in CM.
The error between the actual value and the estimate value was minimized by utilizing the solution for Fickian diffusion and the optimization toolbox in Matlab®.

3.4 Conclusions

The superior stability of 'click' capsules versus ionically crosslinked capsules was observed and demonstrated via titration, swelling, and diffusion measurements.

Cosslinking chemistry and swelling media influence swelling and WC properties of hydrogels. 'Click' capsules swelled more in water as compared to 'click' capsules in PBS or Ca^{+2} crosslinked capsules. Ca^{+2}-crosslinked capsules incubated in d.i.H_2O did not swell significantly during the time period (24 hrs) of the experiment as compared to being incubated in PBS. In d.i. H_2O, there are no ions present to undergo ion exchange with the Ca^{+2}. Therefore, Ca^{+2}-crosslinked capsules in d.i.H_2O should have the maximum amount of crosslinking compared to other ionic media.

Dye-labeled dextrans of different MW's were employed to study the diffusion proprieties of covalently versus ionically crosslinked capsules and also to determine the MWCO of these hydrogels. Fickian diffusion was employed as a model to compare diffusion properties between ionically and covalently crosslinked hydrogel capsules. As the ionic strength of the media increased, the modeling of diffusion from ionically crosslinked capsules was not possible. Therefore, a model that incorporates hydrogel degradation should be employed when modeling diffusion from ionically crosslinked Aln hydrogels[78, 79]. The D of dextran desorbing from Ca^{+2}-crosslinked capsules in CM was almost identical to the Do. As the ionic strength of media increased the Ca^{+2}-crosslinked capsules quickly dissolved removing any impediment against dextran diffusion from the Aln framework. For 'click' capsules the D was

approximately one order of magnitude less than the Do. This was also the case for Ca^{+2}-crosslinked capsules in d.i.H_2O where no ion exchange between the media and the capsule can occur. This was the result of the Aln matrix impeding the diffusion of the dextrans out of the capsules.

The Do's were one order of magnitude higher than the experimentally determined D when calculating the diffusion out of Aln with the exception of Ca^{+2} crosslinked capsules in CM. The Aln mesh frame work, either ionically or covalently crosslinked, served as a barrier that impeded dextran diffusion. This was due to two important factors both related to polymer concentration: exclusion effects and the obstruction effects[8, 78, 79]. For exclusion effects, the volume available to the diffusive molecule is greatly reduced by the polymer to a fraction of the total volume. The polymer also creates obstructive effects by creating impermeable segments that increase the overall path length for the diffusive molecule. These same impediments would also limit the diffusion of nutrients, hormone signals/products, and waste for encapsulated islets of Langerhans.

Dextrans of different MW's were employed to study the diffusion properties of covalently versus ionically crosslinked capsules and also to determine the MWCO of these hydrogels. For ionically crosslinked Aln, the degree of ionic crosslinking and the chemical composition of Aln also determine the MWCO. Aln with a G content higher than 70% and an average G-block length greater than 15 are referred to as "high G" Alns and are the most stable, have the highest porosity, and highest mechanical strength[80]. Diffusion of the encapsulated molecule relies on a number of factors including: charge of the diffusive molecule, MW, shape of the molecule,

polymer flexibility and pH of the solvent[13, 80-83]. The pH of the solvent and the net charge of the molecule can influence the diffusion rates by affecting how the diffusive molecule interacts with the Aln matrix. Chretien et al.[81] described release behavior of FTIC-dextrans from Ca^{+2}-Aln capsules as consisting of two phases: (1) a slow release phase from the progressive erosion of Ca^{+2}-Aln and (2) a fast release profile related to the eroded Ca^{+2}-Aln capsule. This same behavior was seen for dextran diffusion from Ca^{+2}-Aln in media of increasing ionic strength where the capsules were broken or completely dissolved after 24 hrs. 'Click' capsules did not exhibit this kind of behavior because they were still completely intact due to covalent crosslinking.

Neutral dextrans were employed to study diffusion characteristics and determine MWCO to minimize the affect of the net charge of the molecule interacting with the Aln matrix. The diffusion of the molecule depended on the MW molecule and the stability of the hydrogel. Determining the MWCO is an important characteristic for biomaterials meant for immunoisolation. The biomaterial must consist of pores large enough to allow for the diffusion of hormone signals, glucose, and insulin (~5 kDa) for example but small enough to exclude molecules related to an immune response such as components of the complement system, cytokines (γ-IFN: MW~ 17 kDa), and immunoglobulins (IgG antibody: MW~150 kDa)[80, 82]. These immune mediators have been shown to be extremely cytotoxic to β-cells and inhibit insulin release[4, 84]. While both crosslinking chemistries result in pores with a random size distribution, a general MWCO can be determined. Both Ca^{+2}- and 'click'-crosslinked capsules excluded dextrans above the MW of 40 kDa based on the limited

amounts they absorbed/desorbed. 'Click' capsules absorbed higher amounts of dextrans than Ca^{+2} crosslinked capsules indicating larger pores due to less overall crosslinking then Ca^{+2}-crosslinked capsules. However, 'click' capsules still had a MWCO similar to Ca^{+2}-crosslinked capsules which is sufficient for immunoisolation applications.

3.5 Future Work

Dextrans conjugated with Texas Red® were chosen to model protein diffusion over actual protein diffusion for a number of reasons: 1) dextrans conjugated with Texas Red® were neutral, minimizing any charge interaction between the diffusive molecule and the hydrogel 2) dextrans are generally flexible, linear molecules minimizing the interference due to shape affects 3) utilizing dextrans conjugated with Texas Red® provided an economic, fluorescent based assay. We were able to take exponentially more data points using dextrans than if a proteins were employed since everything was contained in the well. Future experiments should use specific proteins and an appropriate protein detection assay to gain a more accurate picture of the diffusivity properties of these novel hydrogels. The shape, rigidity, and charge of protein molecules will influence the diffusion characteristics from these alginate capsules.

The solution for 'Fickian' diffusion was employed as a means of comparing diffusion through stable, 'click' capsules and with that of the instable Ca^{+2}-crosslinked capsules. To model diffusion more accurately through ionically crosslinked capsules, a model that employs hydrogel degradation should be utilized.

Chapter 4: Inflammatory Potential of Functionalized Polysaccharides

4.1 Introduction

Based on our pervious studies, we have demonstrated the applicability of RAW264.7 in screening biomaterials that may activate inflammatory pathways[35, 42, 85, 86]. As a murine macrophage cell line, RAW264.7 produces robust amounts of NO in the presence of an inflammatory signal. The NO breaks down to nitrites and nitrates in solution which can be quantified by fluorometric methods[87]. The experiments in this chapter will determine the inflammatory potential of HA based on MW, unfunctionalized polysaccharides (Aln or HA), and functionalized polysaccharides with either alkyne or azide groups. To elucidate subtle macrophage-mediated NO inflammatory reactions, a variety of simulated inflammatory conditions were employed utilizing LPS and/or murine recombinant γ-interferon (mrIFN-γ). Supernatants from RAW264.7 exposed to these biomaterials were analyzed for nitrite concentration at various time points.

4.2 Methods

4.2.1 Materials

LPS from Escherichia coli serotype O26:B6, murine recombinant interferon gamma (mrIFN-γ), and 2,3-diaminonaphthalene (DAN) were purchased from Sigma. A series

of hyaluronic acid (HA) samples of known molecular weights (4.77, 6.55, 17, 35, 64, 132, 485, 1,100 and 1,700 kDa), and defined low endotoxin content (less than 0.03 EU/mg) were purchased from LifeCore Biomedical. HA oligosaccharides (disaccharide [0.401 kDa], hexamer [1.221 kDa], octamer [1.607 kDa], decamer [1.993 kDa], and dodecamer [2.394 kDa]) derived by digestion of Streptococcal fermentation products with mammalian hyaluronidase and certified low in endotoxin (less than 0.01 EU/mg) were purchased from Iduron. Stock solutions of the different reagents and samples were prepared as follows: HA, functionalized Alns, and functionalized HA samples were diluted in sterile RPMI 1640 at 10.0 (LifeCore samples or functionalized polysaccharides) or 0.5 mg/mL (Iduron samples), filtered through 0.45 μm filters, aliquoted, and stored frozen at -20 ºC. LPS was diluted in dimethyl sulfoxide (DMSO) to a concentration of 250 μg/mL, aliquoted, and stored frozen at -70 ºC. Mouse recombinant interferon-gamma (mrIFN-γ) was initially diluted to 1 mg/mL in phosphate buffered saline pH 8.0 then to 1 μg/mL in CM, aliquoted, and stored frozen at -20 ºC. Stock solutions of DAN, at 20 mg/mL, were prepared by diluting 100 mg DAN in 5 mL of DMSO and freezing aliquots at -20 ºC.

4.2.2 Cell Culture

RAW 264.7 (ATCC TIB71; American Type Culture Collection, Manassas, VA), a murine monocyte/macrophage cell line, were stored in liquid nitrogen. Aliquots were rapidly-thawed and cultured in 5% CO_2/95% air, 70% humidity, at 37ºC until they adhered to the culture flask and the monolayer reached 50% confluency (usually one to two days). The monolayer was harvested with calcium/magnesium-free phosphate buffered saline (PBS w/o Ca^{+2}/Mg^{+2}), then seeded at $1x10^4$ cells/well into 96 well

plates. The cells were allowed to adhere to the bottom of the wells by further culture for 24 hrs at 37ºC in 5% CO_2/95% air. Following adherence, LPS standard and test reagents were added to the wells and incubation was continued for up to 72 hrs. Then 0.1 mL of supernatant was taken from each well and stored at -70 ºC until thawed and assayed for nitrite concentration.

4.2.3 Nitrate Assay

Nitrites were measured in CM supernatants based on the method described by Misko et al[87]. In RAW 264.7 and other cell types, nitrite accumulation in the supernatant is directly correlated with NO production. A 200 µM working nitrite standard was used to prepare nitrite standard curve dilutions of 25, 12.5, 6.25, 3.13, 1.56, 0.78, 0.39, and 0.195 µM concentrations in CM. A working DAN solution of 50 µg/mL was prepared by diluting a 20 mg/mL stock solution with 0.62 N HCl. All assays were conducted in 96-well plates, with each condition performed in quadruplet. In each well, 20 µL of standard, sample, or medium-only was added to 80 µL of deionized water then 10 µL of working DAN solution was added to each well. The plate was allowed to sit in the dark at room temperature for ten minutes. Utilizing the same timing and sequence as for the additions of DAN, 20 µL of 2.8 N NaOH was added to each well, and the plate was gently shaken. The plate was then incubated in the dark for one minute and read in a fluorescence plate reader (Perkin Elmer HTS 7000 Plus BioAssay Reader) with an excitation of 360 nm and an emission of 430 nm.

4.2.4 Assay for Endotoxin Contamination in Hyaluronic Acid and Alginate

LPS, HA (4.77, 6.550, 17, 35, 64, 132, 485, 1,100, and 1,700 kDa), and Aln were assayed according to kit instructions with the Lonza Kinetic-QCL Chromogenic Limulus Amoebocyte Lysate (LAL) Endotoxin Assay (Walkersville, Maryland) with a sensitivity range of 0.005 EU/ml - 50.0 EU/ml.

4.2.5 Statistical Analysis

Data are expressed as mean ± standard deviation of *n* independent observations. Statistical significance was calculated using the two-tailed unpaired Student's *t* test or ANOVA. A $p \leq 0.05$ was considered statistically significant.

4.3 Results

RAW 264.7 cells were cultured in 96-well plates and exposed for up to 72 h to 2 mg/ml of HA of various MW, Aln, HA-Az, HA-Alk, Aln-Az, or Aln-Alk plus or minus 6 EU/ml LPS plus or minus 50 ng/mL mrIFN-γ. In addition to the control condition of the vehicle in the absence of HA, another control of an additional 0.06 EU/ml LPS was included in order to exclude any affects due to LPS impurity present in the HA samples. The highest LPS concentration found from the LAL endotoxin assay of HA and Aln samples was assayed to be less than 0.06 EU/mL per sample per well (data not shown). Cell-free supernatants were obtained and assayed via DAN fluorescence for nitrite concentration. Each experiment was replicated at least twice.

4.3.1 Inflammatory Potential of Hyaluronic Acid as a Function of Molecular Weight

As seen in Figure 24, 0.06 EU/ml of LPS did not significantly change the control responses in the absence of HA (labeled as vehicle-only) for either LPS (6 EU/mL) alone or 6 EU/ml LPS plus mrIFN-γ (50 ng/ml). For the highest inflammatory condition of wells containing 6 EU/ml LPS plus 50 ng/ml mrIFN-γ (Figure 24), the nitrite concentration was significantly increased versus both the vehicle and 0.06 EU/ml LPS controls in the presence of 4,770 and 6,550 kDa HA, but not significantly changed by 17 and 35 kDa HA, and significantly decreased by HA samples of molecular weights 64, 132, 254, 485, 1,100, and 1,700 kDa. For the lesser inflammatory state of RAW 264.7 stimulated only by 6 EU/ml LPS in the absence of mrIFN-γ (Figure 24), different effects were observed by the presence of HA. In this case, large and significant increases in nitrite accumulation versus the vehicle and 0.06 EU/ml LPS controls by HA were observed for molecular weights 132, 254, 485, and 1,100 kDa. As seen in Figure 25, for nitrite accumulation when only mrIFN-γ was present (no extra LPS), only 6.55 and 17 kDa HA samples showed clear increases. For unstimulated RAW 264.7, only the 4.77 kDa sample produced a small but significant increase versus vehicle and 0.06 EU/ml controls.

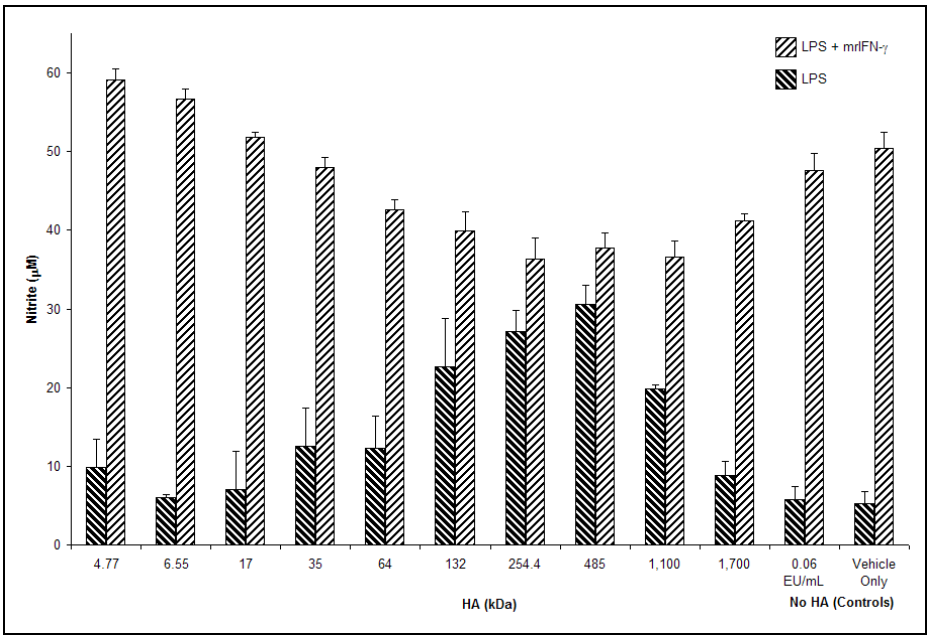

Figure 24. Effect of HA of different molecular weights on nitric oxide (NO) response of RAW 264.7 cells to endotoxin ±mrIFN-γ in the presence of 6 EU/mL LPS.
RAW 264.7 was seeded at 10^4 cells/well in a 96-well plate, allowed to adhere overnight, then incubated for 48 h at 37°C in the presence of 6.0 endotoxin units (EU)/mL of lipopolysaccharide (LPS) ±50 ng/mL mrIFN-γ, plus 2mg/mL HA samples of different molecular weights, as compared to an additional 0.06 EU/mL control or vehicle only. Supernatants were removed at 48 h for nitrite assay. Data shown are mean ± 1 standard deviation of 4 replicate wells per condition.

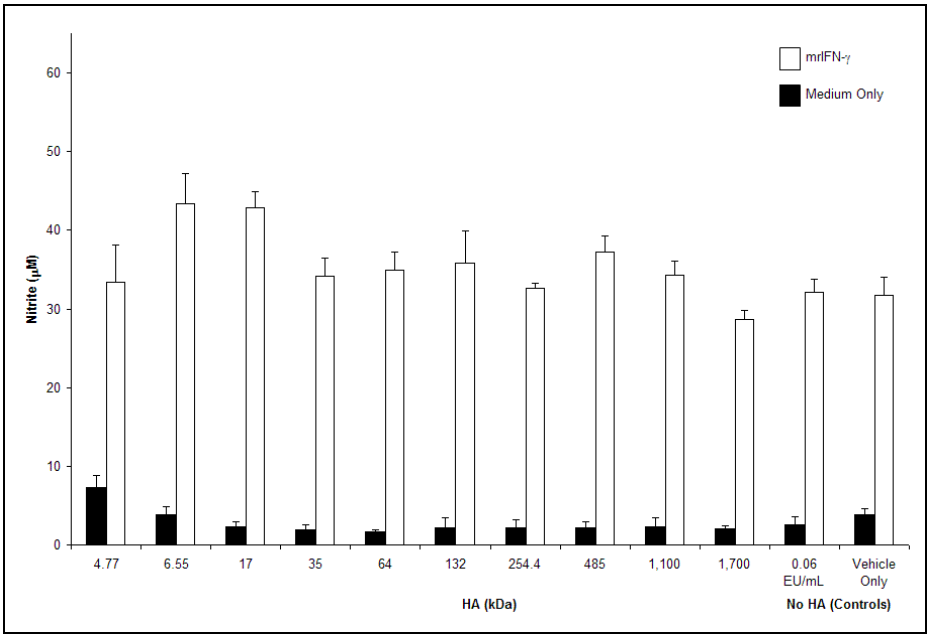

Figure 25. Effect of HA of different molecular weights on nitric oxide (NO) response of RAW 264.7 cells to endotoxin ±mrIFN-γ.
RAW 264.7 was seeded at 10^4 cells/well in a 96-well plate, allowed to adhere overnight, then incubated for 48 h at 37°C in the presence of or absence of 50 ng/mL mrIFN-γ, plus 2 mg/mL HA samples of different molecular weights as compared to an additional 0.06 EU/mL control or vehicle only. Supernatants were removed at 48 h for nitrite assay. Data shown are mean ± 1 standard deviation of 4 replicate wells per condition.

These data suggest that when LPS is reduced to below 0.03 EU/mg, no or little direct affect on RAW 264.7 NO production by HA occurs. However, as the cells are stimulated by inflammatory mediators like LPS contamination or sensitizing cytokines, MW of HA seems to exert an increasingly prominent stimulatory effect as the level of nitrite increases. Looking at a separate series of HA fragments of even lower MW and at 25 μg/mL (80X reduction over the previous experiments; Figure 26), no overall effect was observed on RAW 264.7 nitrite accumulation either in a basal state, stimulated by LPS (6 EU/mL) alone, stimulated by mrIFN-γ alone, or by LPS plus mrIFN-γ. HA disaccharide (0.401 kDa) or hexamer (1.221 kDa), octamer (1.607 kDa), decamer (1.993 kDa), or dodecamer (2.394 kDa) produced no significant changes to nitrite accumulation from RAW 264.7 in either an unstimulated or inflammatory state. Thus, the smallest fragments of HA did not stimulate RAW 264.7 cells in terms of NO production whether the cells were in either a basal or activated state.

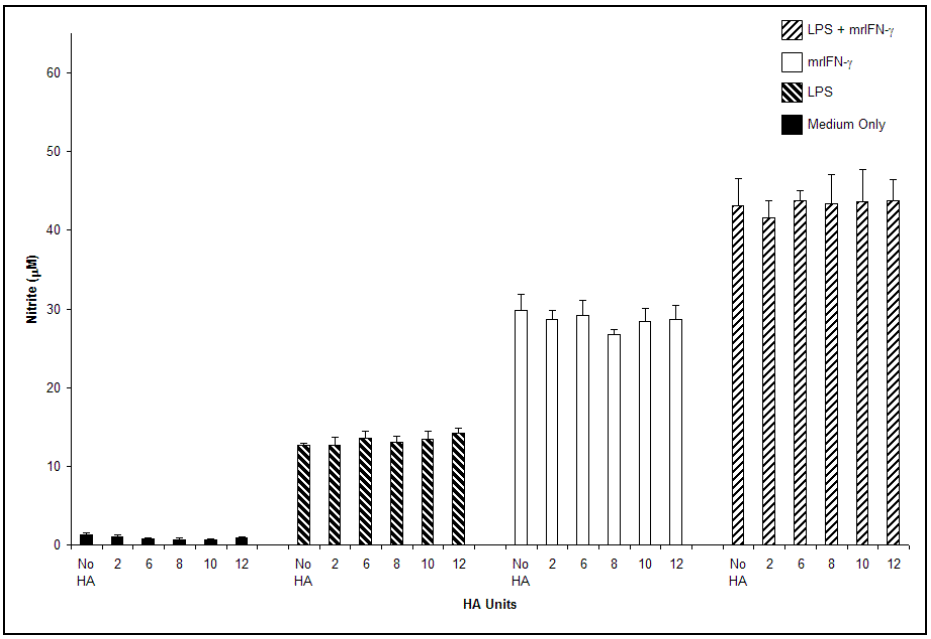

Figure 26. Effect of HA oligosaccharides on nitric oxide (NO) response of RAW 264.7 cells in the presence or absence of 6 EU/ml LPS ±mrIFN-γ.
RAW 264.7 was seeded at 10^4 cells/well in a 96-well plate, allowed to adhere overnight, and then incubated for 48 h at 37°C in the presence or absence of 6.0 EU/mL of LPS ±50 ng/mL mrIFN-γ ±25 μg/mL HA samples of different molecular weights. Supernatants were removed at 48 h for nitrite assay. Data shown are mean ± 1 standard deviation of 4 replicate wells per condition

4.3.2 Inflammatory Potential of Functionalized Hyaluronic Acid

HA (35 kDa starting MW) was functionalized in the manner described in section 2.2.2. Nitrite accumulation increased over time and in response to sensitizing reagents such as LPS and/or mrIFN-γ. All results were compared to unfunctionalized HA (35 kDa MW). Over the time course of the experiment (up to 72 hrs), there was no statistical difference in nitrite accumulation from HA functionalized with azide or alkyne groups as compared to unfunctionalized HA in the absence of inflammatory mediators or sensitizing cytokines such as LPS or mrIFN-γ, respectively (Figure 27 A). In the presence of the sensitizing cytokine mrIFN-γ, after 48 hrs there was a significant increase in nitrite accumulation due to exposure to HA-Az or HA-Alk compared to HA (Figure 27 B). In the presence of an additional 6 EU/mL LPS, there

was no significant difference in nitrite accumulation between HA-Alk and HA, but a significant inhibition in nitrite accumulation due to HA-Az compared to HA after 24 hrs was observed (Figure 27 C). However, in the presence of both LPS (6 EU/mL LPS) and mrIFN-γ (simulating a high inflammatory state), there was a significant increase in nitrite accumulation after 48 hrs from HA-Az and HA-Alk as compared to HA (Figure 27 D).

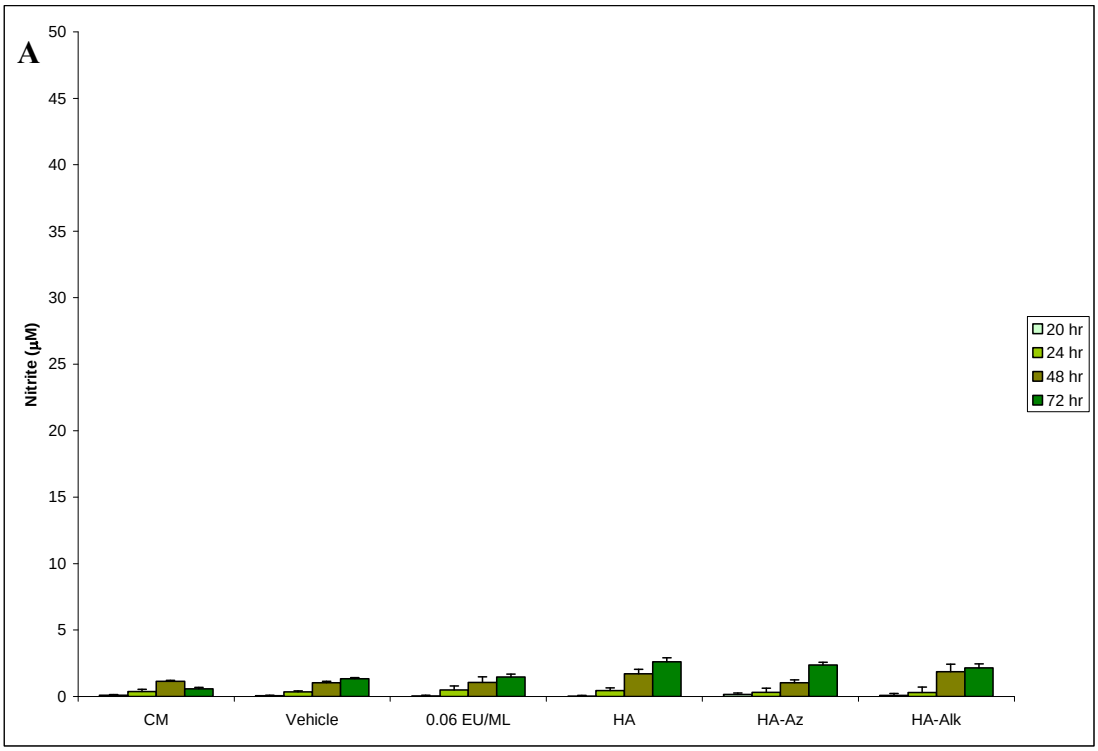

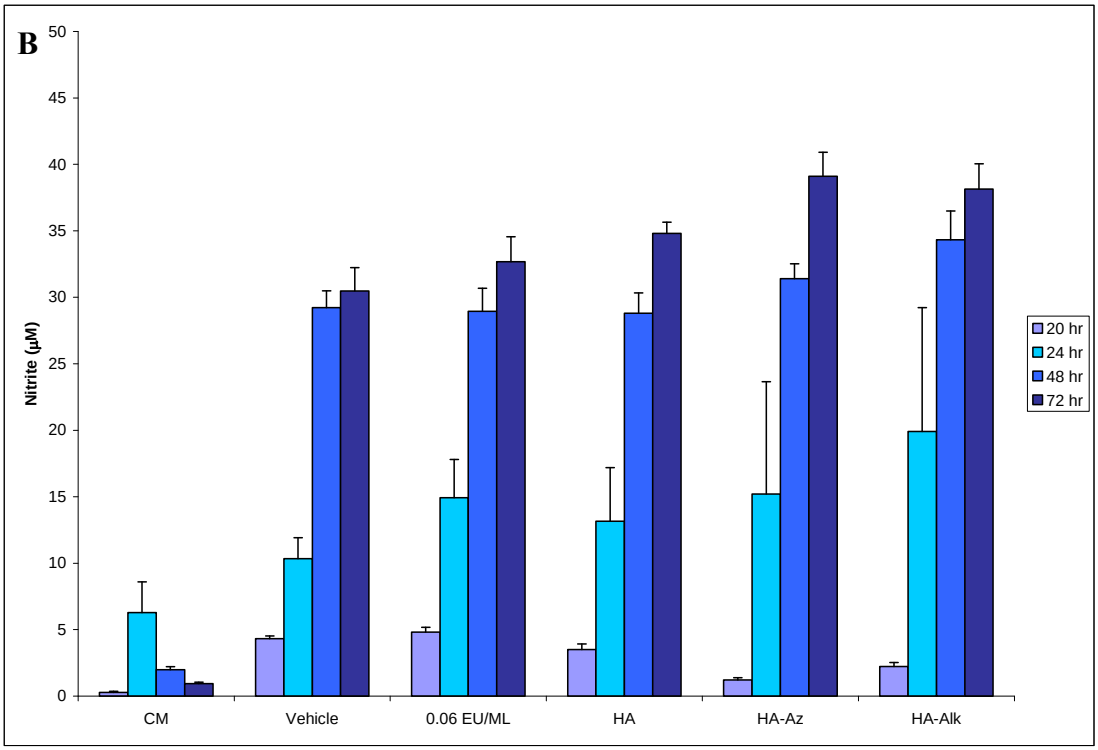
B
Nitrite (µM)
50
45
40
35
30
25
20
15
10
5
0
CM
Vehicle
0.06 EU/ML
HA
HA-Az
HA-Alk
20 hr
24 hr
48 hr
72 hr

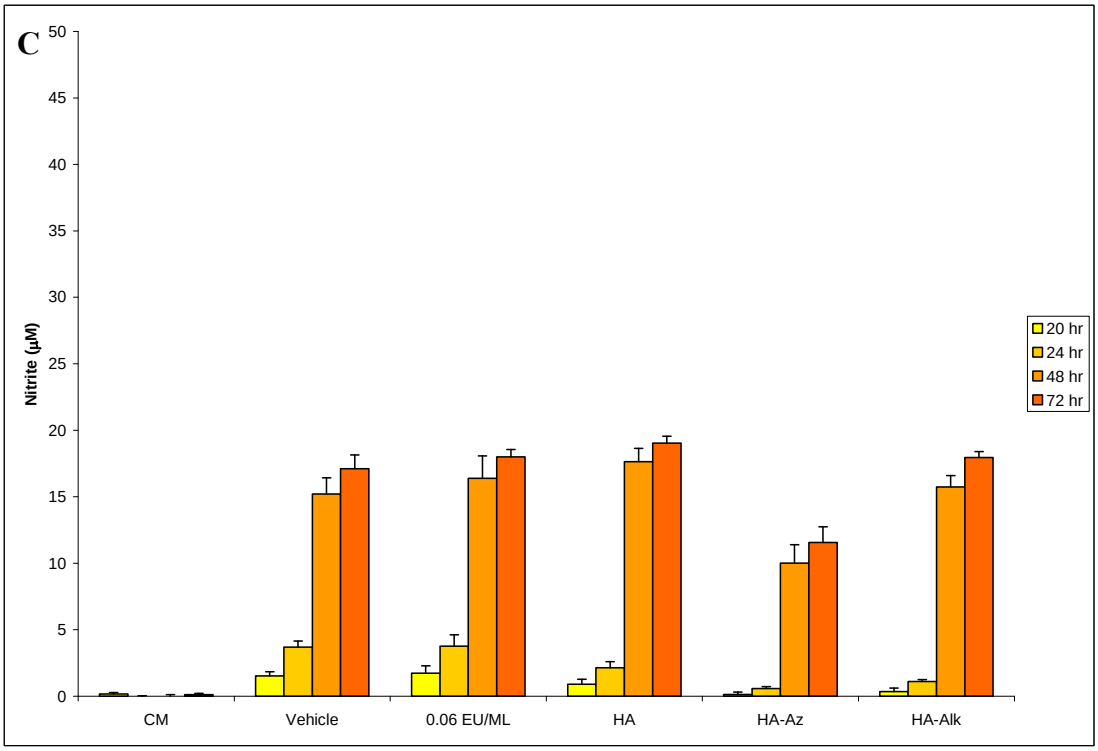
C
Nitrite (µM)
50
45
40
35
30
25
20
15
10
5
0
CM
Vehicle
0.06 EU/ML
HA
HA-Az
HA-Alk
20 hr
24 hr
48 hr
72 hr

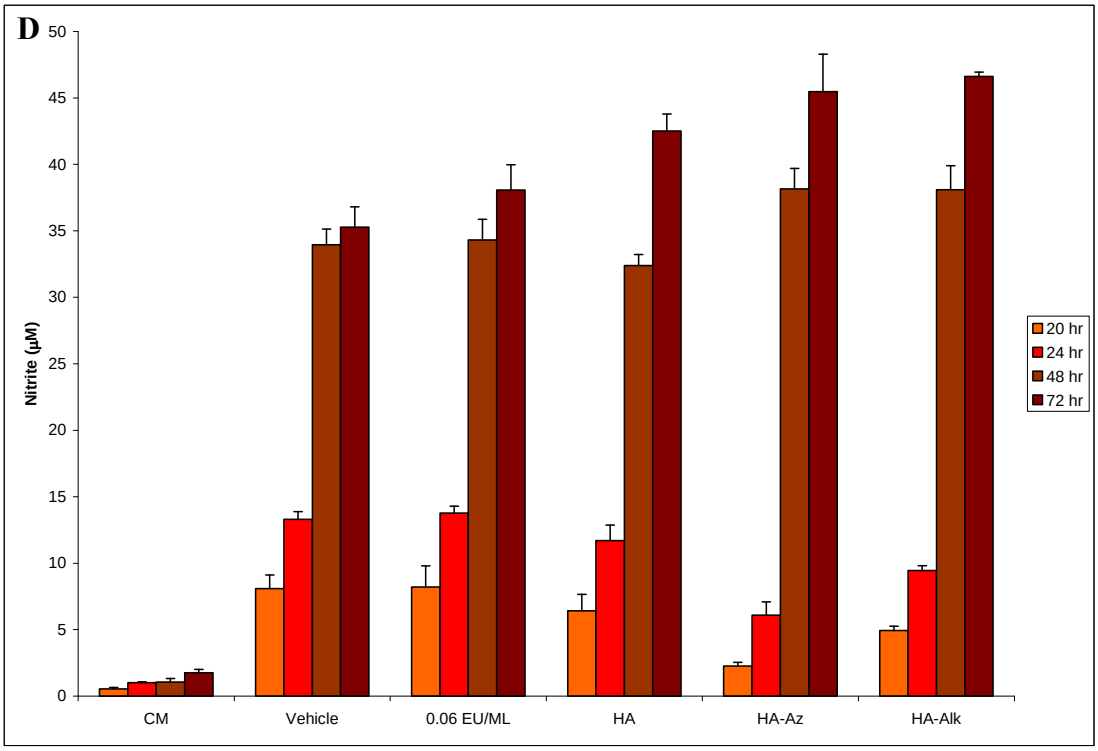

Figure 27. Effect of functionalized HA on nitric oxide (NO) response of RAW 264.7 ±endotoxin ±mrIFN-γ.
RAW 264.7 was seeded at 10^4 cells/well in a 96-well plate, allowed to adhere overnight, then incubated for up to 72 h at 37°C in the presence of 2 mg/mL HA samples of either unfunctionalized HA or functionalized HA with Azide or Alkyne functional groups as compared to an additional 0.06 EU/mL control or vehicle only. A) In the absence of endotoxin (6 EU/mL) and 50 ng/mL mrIFN-γ. B) In the presence of 50 ng/mL mrIFN-γ. C) In the presence of an additional 6 EU/mL LPS. D) In the presence of an additional 6 EU/mL and 50 ng/mL mrIFN-γ. Supernatants were removed at different time points for nitrite assay. Data shown are mean ± 1 standard deviation of 4 replicate wells per condition.

4.3.3 Inflammatory Potential of Functionalized Alginate

Aln was functionalized with either azide or alkyne functional end groups as described in section 2.2.2. The inflammatory effect of functionalized Alns was compared to unfunctionalized Aln by measuring the NO production of RAW264.7 cells in the presence of these polysaccharides (2 mg/mL) and in the presence or absence of two inflammatory mediators, LPS and mrIFN-γ.

In the basal state, with no additional LPS or mrIFN-γ present, neither Aln-Az or Aln-Alk stimulated RAW264.7 cells to produce significantly more NO than unfunctionalized Aln over the entire time course of the experiment (up to 72 hr)

(Figure 28 A). In the presence of the sensitizing cytokine mrIFN-γ, Aln-Az and Aln-Alk stimulated RAW264.7 cells to produce significantly more NO compared to Aln after 48 hrs (Figure 28 B). In the presence of an additional 6 EU/mL LPS, there was no significant difference in NO production of RAW264.7 cells in the presence of either functionalized Aln (Aln-Az or Aln-Alk) compared to unfunctionalized Aln (Figure 28 C) even after 72 hrs exposure. However, in the presence of both mrIFN-γ and 6 EU/mL LPS there was a significant increase in NO production from RAW264.7 cells when in the presence of Aln-Az or Aln-Alk compared to Aln after 48 hrs (Figure 28 D).

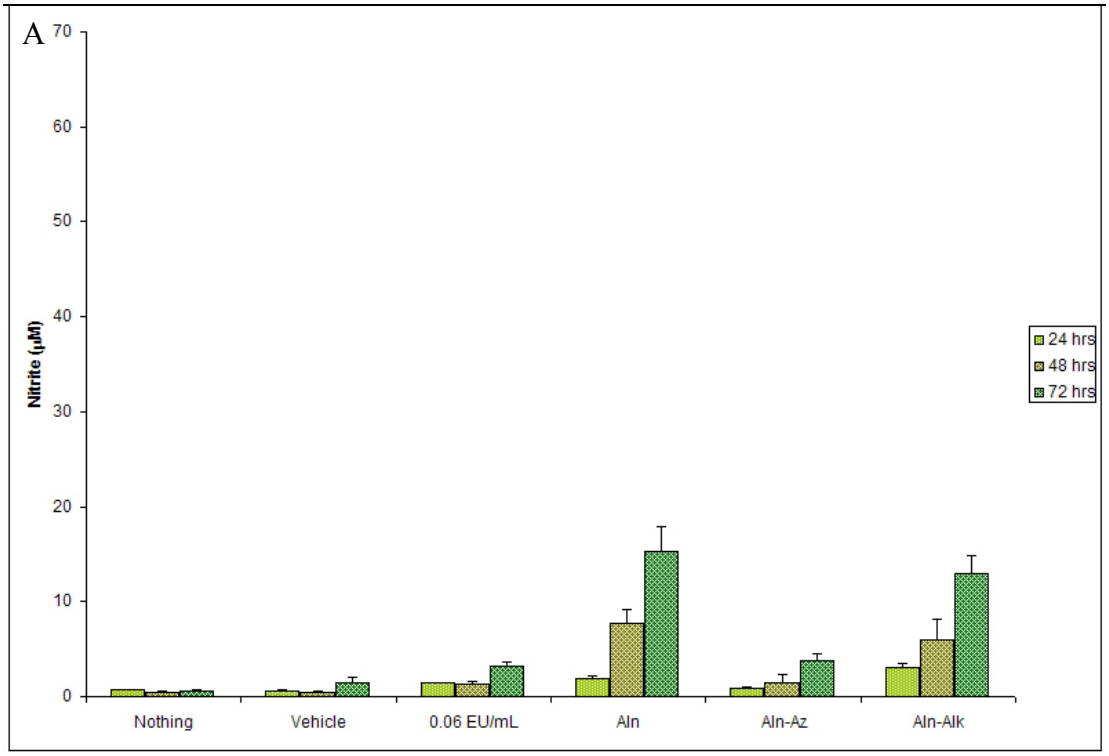

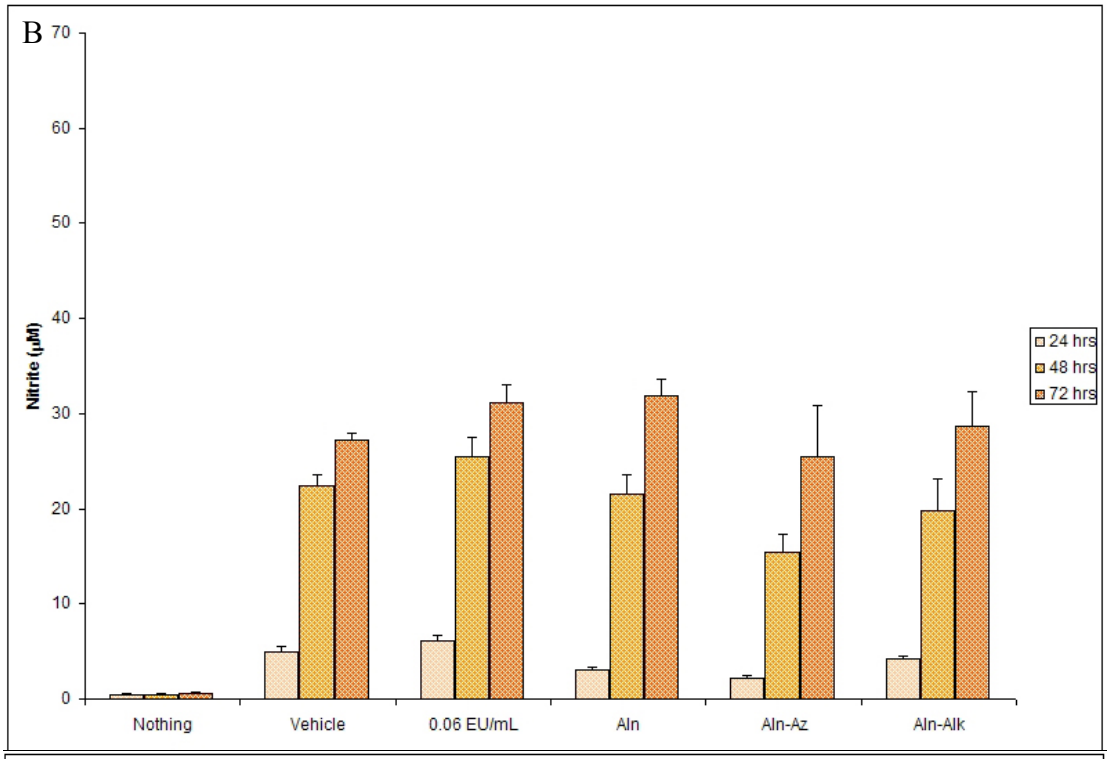
B
Nitrite (μM)
70
60
50
40
30
20
10
0
24 hrs
48 hrs
72 hrs
Nothing
Vehicle
0.06 EU/mL
Aln
Aln-Az
Aln-Alk

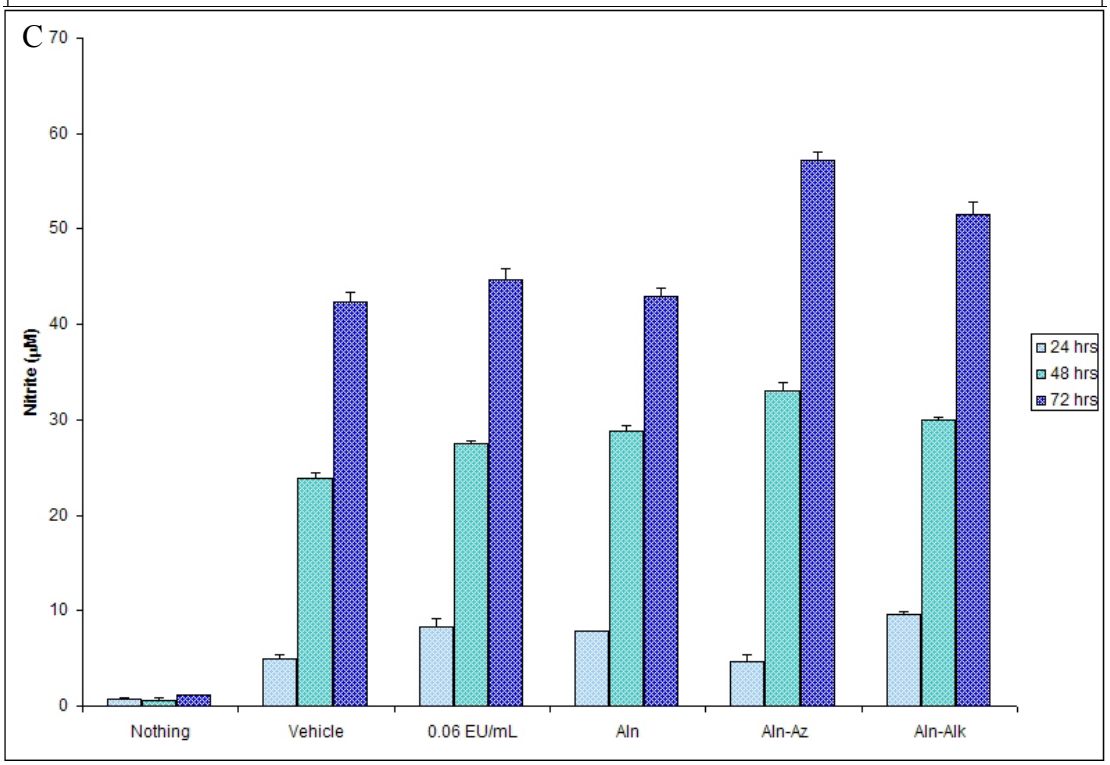
C
Nitrite (μM)
70
60
50
40
30
20
10
0
24 hrs
48 hrs
72 hrs
Nothing
Vehicle
0.06 EU/mL
Aln
Aln-Az
Aln-Alk

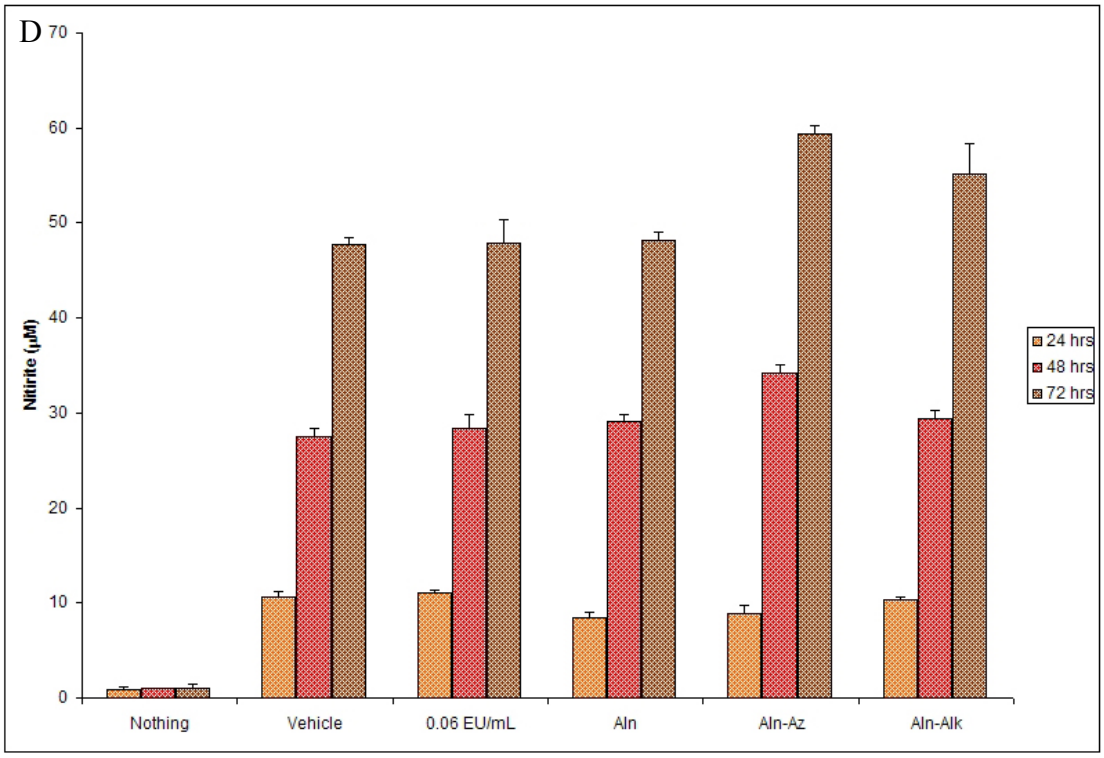

Figure 28. Effect of functionalized alginate on nitric oxide (NO) response of RAW 264.7 ±endotoxin ± mrIFN-γ.
RAW 264.7 was seeded at 10^4 cells/well in a 96-well plate, allowed to adhere overnight, and then incubated for up to 72 h at 37°C in the presence of 2 mg/mL Aln samples of either unfunctionalized Aln or functionalized Aln with azide or alkyne functional groups as compared to an additional 0.06 EU/mL control or vehicle only. A) In the absence of endotoxin (6 EU/mL) and 50 ng/mL mrIFN-γ. B) In the presence of 50 ng/mL mrIFN-γ. C) In the presence of an additional 6 EU/mL LPS. D) In the presence of an additional 6 EU/mL and 50 ng/mL mrIFN-γ. Supernatants were removed at different time points for nitrite assay. Data shown are mean ± 1 standard deviation of 4 replicate wells per condition.

4.4 Conclusions

In order to address the question of whether LMW-HA or functionalized polysaccharides with azide or alkyne groups may be inflammatory, murine macrophage cultures were exposed to a range of molecular weights of HA of defined low endotoxin content (less than 0.03 EU/mg HA), from the unitary disaccharide up to 1,700 kDa, and functionalized polysaccharides at concentrations of either 25 μg/mL or 2 mg/ml. The cell line RAW 264.7 produced a robust nitric oxide

inflammatory response, as assessed by an increase in nitrite concentration, when exposed to LPS, mrIFN-γ, or LPS plus mrIFN-γ.

This robust NO response from RAW264.7 cells in the presence of LPS plus mrIFN-γ was moderately inhibited by HMW-HA and slightly enhance by LMW-HA. For a lesser inflammatory state produced by LPS in the absence of mrIFN-γ, HMW-HA increased the NO response while LMW inhibited it. For stimulation by mrIFN-γ only, a significant enhancement was observed at the lower molecular weights. For the basal state of RAW 264.7 (no LPS or mrIFN-γ), molecular weight of HA had little or no direct inflammatory effect. In addition, the smallest HA fragments (below 5 kDa), that in previous literature has been suggested as having a drug-effect [38,39], tested at a concentration 80X more dilute than the other HA samples, produced no significant change in the NO response in RAW 264.7 cells either directly or by indirectly modulating the response to LPS ±mrIFN-γ.

In general, functionalized HA (either with Alk or Az functional groups) did not stimulate an inflammatory response from murine macrophages in the basal state (no LPS or mrIFN-γ present). Only in the presence of an acute inflammatory state, including mrIFN-γ and in the absence or presence of LPS did functionalized HA produce a significant increase in NO production compared to HA at later time points. This modest increase in NO production could be due to the functional groups themselves or impurities left over from functionalization reaction.

HA of 35 kDa was chosen for functionalization for two reasons. Primarily, from our pervious results (Figures 18 and 19) HA of 35 kDa MW did not instigate an inflammatory response from murine macrophages in any of the inflammatory states

tested. Second, when 35 kDa HA was functionalized with either an azide or alkyne functional group there was no appreciable increase in the solution viscosity after the reaction was performed.

Functionalized Alns demonstrated similar results compared to functionalized HA. There was no significant increase in NO production from functionalized Alns from RAW264.7 cells in their basal state (no mrIFN-γ or 6 EU/mL LPS present). Also, functionalized Alns only stimulated RAW264.7 cells to produce significant amounts of NO when either in the presence of the sensitizing cytokine mrIFN-γ or in the presence of LPS and mrIFN-γ.

The increase in NO production could be due to the presence of the functional groups or due to contaminates left behind from the functionalization reaction. The functionalization of these polysaccharides was not done under aseptic conditions. After the functionalization and recovery of the final product of these polysaccharides they were treated under sterile conditions. Aliquots were prepared with sterile RPMI and passed through 0.45 μm filters. Polysaccharides functionalized with Azide functional groups would not pass through a 0.22 μm filter at the concentration prepared (10 mg/mL). One example of a ubiquitous contaminant is LPS which is very difficult to remove and could have been introduced during the functionalization reaction. Another possibility is that functionalization of these polysaccharides initiates an inflammatory response by the murine macrophages. In that case, further experiments need to be performed to determine if the degree of functionalization corresponds to the degree of inflammatory potential. And if so, what degree of functionalization is sufficient to not initiate an inflammatory response.

4.5 Future Work

Other MW's of HA should be functionalized with azide or alkyne groups and screened for initiating an inflammatory response utilizing murine macrophages. The degree of functionalization should be kept relatively the same. If it seems that the functionalization of HA with either azide or alkyne groups produce proinflammatory HA then different degrees of functionalization should be studied. The minimum amount of functionalization should be utilized to avoid inflammatory potential of modified biomaterials while maintaining a sufficient amount of end groups that are able to undergo 'click' chemistry and contain the desired material properties. Screening the starting materials with RAW264.7 cells might be difficult as propargylamine is known to be very toxic and the ologiometric polyethylene glycol (PEG) azide linker is expensive and in limited supply to test at similar concentrations utilized in the above experiments.

As stated before, the degree of functionalization of Aln with either azide or alkyne functional groups could be altered and the affects on the NO response in RAW264.7cells could be studied to determine if there is a correlation between the amount of functionalization and NO production. The purity of these functionalized polysaccharides should be assessed with HPLC and to determine if the increased inflammatory response is due to contamination. The LPS content could be assessed with the LAL endotoxin assay to determine if LPS contamination is a potential issue.

The murine cell line RAW264.7 has been extensively studied for a number of applications. Our previous work has focused on utilizing RAW264.7 cells in an assay to screen biomaterials for their inflammatory potential prior to implantation in the

body[35, 42, 85, 86]. However, a human cell line would be preferable as a model for NO-mediated inflammatory responses as an *in vitro* screening method for novel biomaterials intended for implantation. As shown in our pervious work, primary splenocytes derived from rat or human sources produce highly variable results when exposed to biomaterials such as different MW's of HA[85]. The inflammatory potential of functionalized, novel biomaterials should be confirmed with other *in vitro* or *in vivo* models.

Chapter 5: Cytotoxicity of Functionalized Polysaccharides and 'Click' Reagents

5.1 Introduction

In chapter 4, the inflammatory potential of functionalized polysaccharides was investigated by employing RAW264.7 cells and measuring NO production (nitrates/nitrites) under a variety of simulated inflammatory conditions (± LPS, ±γ-IFN). In general, the functionalized Alns or HA's stimulate only modest inflammatory responses from RAW264.7 cells. These modest increases in NO production could be due to contamination in the biomaterial or to the degree of functionalization. The remaining half of the dissertation will focus on employing functionalized Aln to encapsulate therapeutic cells. These capsules utilize 'click' chemistry to form covalent crosslinks, increasing the overall capsule stability.

The aim of the experiments in this chapter was to determine the cytotoxicity of all the components and establish optimal conditions that would be used in the implementation of 'click' chemistry for therapeutic cell encapsulation. Another goal was to substantiate the results from Chapter 4 with quantifying the amount of alive or dead cells present. In other words, the cytotoxicity of the functionalized Alns needed to be assessed to determine if a decrease in NO production was the result of increased cell lethality in response to the functionalized Aln.

The cytotoxicity of the 'click' reagents also needed to be assessed. The 'click' reaction relies on utilizing $CuSO_4$, NaAsc, and EDTA of which $CuSO_4$ and EDTA are known to be harmful to cells. Divalent copper has been known as an antibiotic since

antiquity and EDTA chelates with any divalent cation including those that are necessary for cell function. The concentration and time of exposure by cells to these chemicals needs to be optimized to minimize their cytotoxic effect. This could be achieved by employing the Live/Dead ® Viability assay and quantifying cell death over a relevant period of time (up to 1 hr) in the presence of these chemicals in various concentrations and combinations.

5.2 Methods

5.2.1 Materials

LPS from Escherichia coli serotype O26:B6, murine recombinant interferon gamma (mrIFN-γ), and 2,3-diaminonaphthalene (DAN) were purchased from Sigma. Stock solutions of the different reagents and samples were prepared as follows: Aln, Aln-Az, and Aln-Alk samples were diluted in sterile RPMI 1640 at 10.0 mg/mL, filtered through 0.45 μm filters, aliquoted, then stored at 4 ºC. LPS was diluted in dimethyl sulfoxide (DMSO) to a concentration of 250 μg/mL, aliquoted, and stored at -70 ºC. Mouse recombinant interferon-gamma was initially diluted to 1 mg/mL in phosphate buffered saline pH 8.0, then to 1 μg/mL in complete medium (RPMI 1640 medium containing 10% fetal calf serum, 2 mM glutamine, 100 U/mL penicillin, and 100 μg/mL streptomycin)(CM), aliquoted, and stored at -20 ºC. Stock solutions of DAN, at 20 mg/mL, were prepared by diluting 100 mg DAN in 5 mL of DMSO, and aliquots stored at -20 ºC. Stock solutions of $CuSO_4$, EDTA, and NaAsc were made with d.i. H_2O (0.2 M) and stored at 4^{o}C.

5.2.2 Cell Culture

RAW264.7 was cultured and seeded into 96 well microtiter plates in the same manner as described in section 4.2.2. For functionalized Alns, after the supernatants were removed at each time point for nitrite analysis (section 4.2.3). The plate was immediately assayed for cytotoxicity utilizing the live/dead assay. For determining the cytotoxicity of 'click' reagents, the 96-well microtiter plates were cultured and seeded as described in section 4.2.2. Following the adherence period of 24 hrs, RAW264.67 cells were exposed to varying concentrations of EDTA, $CuSO_4$, and/or NaAsc (0-10 mM). Cell death was monitored as function of time for up to 1 hr.

5.2.3 Live/Dead Cytotoxicity Assay

The manufacturer's instructions were followed. Briefly, after each time point (0, 24, 48, or 72 hrs) or before the addition 'click' reagents the supernatant was removed and the plate was washed three times with PBS (w/ Ca^{+2}, Mg^{+2}) to remove any residual CM (which could interfere with the live/dead assay). Control wells were killed using Triton X-100 at a final concentration of 0.5% for 10 min. Ethidium homodimer-1 (EthD-1) and/or Calcein-AM (CalAM) solutions were added to each sample well at a final concentration of 2 μM and 0.5 μM, respectively. The plate was allowed to incubate for 30 min. For functionalized Aln's, the plates were measured with a Tecan fluorescence plate reader at an excitation of 530 ± 12.5 nm and emission of 645 ± 20 nm (EthD-1) or an excitation of 485 ± 10 nm and emission of 530 ± 12.5 nm (CalAM). For the 'click' reactants, the reagents were added then fluorescence was measured every 5 min for up to 1 hr with the Tecan plate reader.

5.2.4 Statistical Analysis

Data are expressed as mean ± standard deviation of *n* independent observations. Statistical significance was calculated using the two-tailed unpaired Student's *t* test or ANOVA. A $p \leq 0.05$ was considered statistically significant.

5.3 Results

RAW264.7 cells were utilized to determine the cytotoxic effects of all the regents employed in the 'click' reaction. RAW264.7 cells were seeded at $1x10^4$ cells/well in 96-well plates, allowed to adhere overnight, and exposed to functionalized Alns or to varying concentrations of 'click' reactants. Cell death was monitored over time as a measure of cytotoxicity by employing EthD-1 which binds to the DNA of damaged or dead cells and/or Cal-AM which is an inclusion dye.

5.3.1 Cytotoxicity of Functionalized Alginates

In Chapter 4, the inflammatory potential of functionalized Alns was investigated by employing RAW264.7 cells and measuring NO production (nitrates/nitrites) under a variety of simulated inflammatory conditions (± LPS, ±γ-IFN). In general, the functionalized Alns did not stimulate overt inflammatory responses from RAW264.7 cells. To confirm that these results were not the result of increased cell lethality from the cytotoxic effects of functionalized Aln, the live/dead viability was assessed.

The cell viability was assessed at 24, 48, and 72 hrs. The general trends for 48 and 72 hrs were the same as for 24 hrs therefore only data from 24 hrs will be shown to expedite the discussion. The amount of LPS contamination in Aln was quantified utilizing the LAL kinetic assay and found to be approximately 0.06 EUg/mL. Since

LPS is a known stimulator of NO production from RAW264.7 cells this amount was employed as a control. Any inflammatory response equal this control was considered to be stimulation due to LPS contamination. When RAW264.7 cells are in the presence of inflammatory stimuli their proliferation either slows or stops as they differentiate. In general at 24 hrs, there was no significant difference ($p \geq 0.05$) between the fraction of RAW264.7 cells that were alive stimulated with Aln as compared to Aln functionalized with an azide or alkyne functional groups under any inflammatory condition (± LPS, ±γ-IFN) (Figure 29). Similar results were obtained for quantification of dead RAW264.7 cells when comparing functionalized Alns to unfunctionalized Aln. At 24 hrs, in general Aln-Alk and Aln-Az were not significantly different than Aln indicating no affect on cell viability by functionalized Alns (Figure 30). Together, these results suggest the neither Aln-Az nor Aln-Alk were cytotoxic toward RAW264.7 cells. Also, with the results from section 4.3.3 these data suggest that while functionalized Aln might elicit a modest increase in NO production from RAW264.7 cells they are not affecting cell viability.

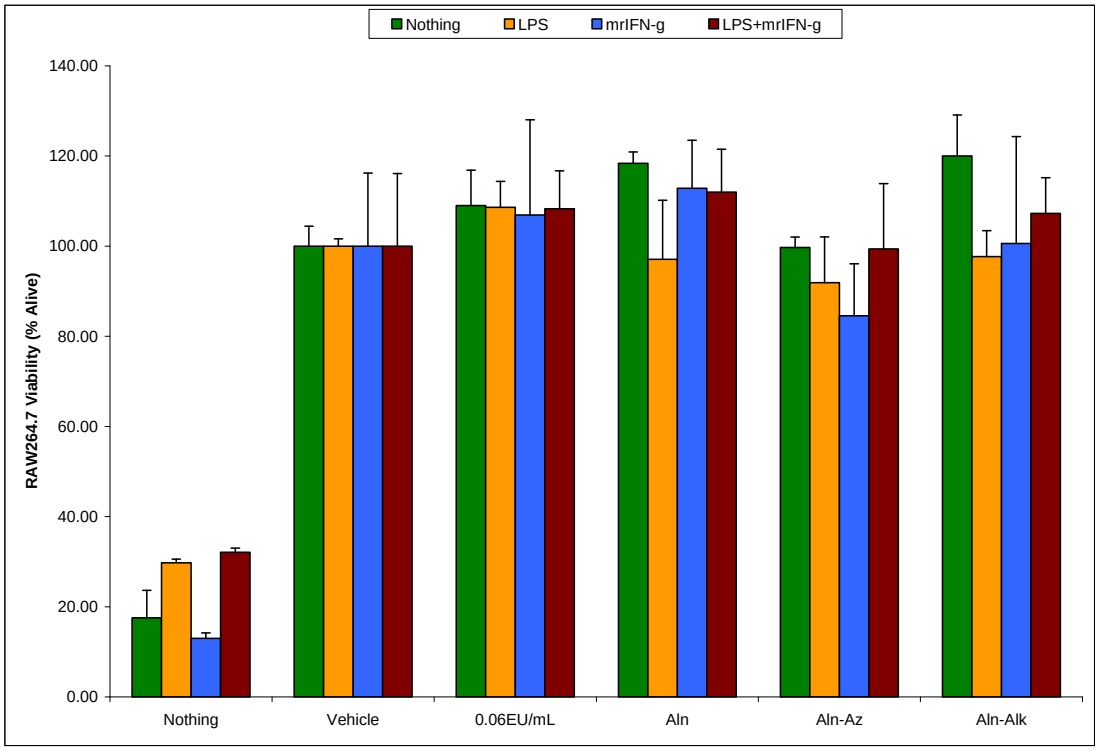

Figure 29. Effect of functionalized alginates on RAW264.7 cell viability ('Alive'). RAW264.7 was seed at 10^4 cells/well into a 96-well plate, then incubated for 24 h at 37°C in the presence of or absence of 50 ng/mL mrIFN-γ, plus 2 mg/mL Aln or functionalized Aln samples as compared to an additional 0.06 EU/mL control or vehicle only. After measuring the accumulated nitrite concentration in the supernatant the cell viability was quantified utilizing a Live/Dead® Assay kit. Data shown are mean ± 1 standard deviation of 4 replicate wells per condition.

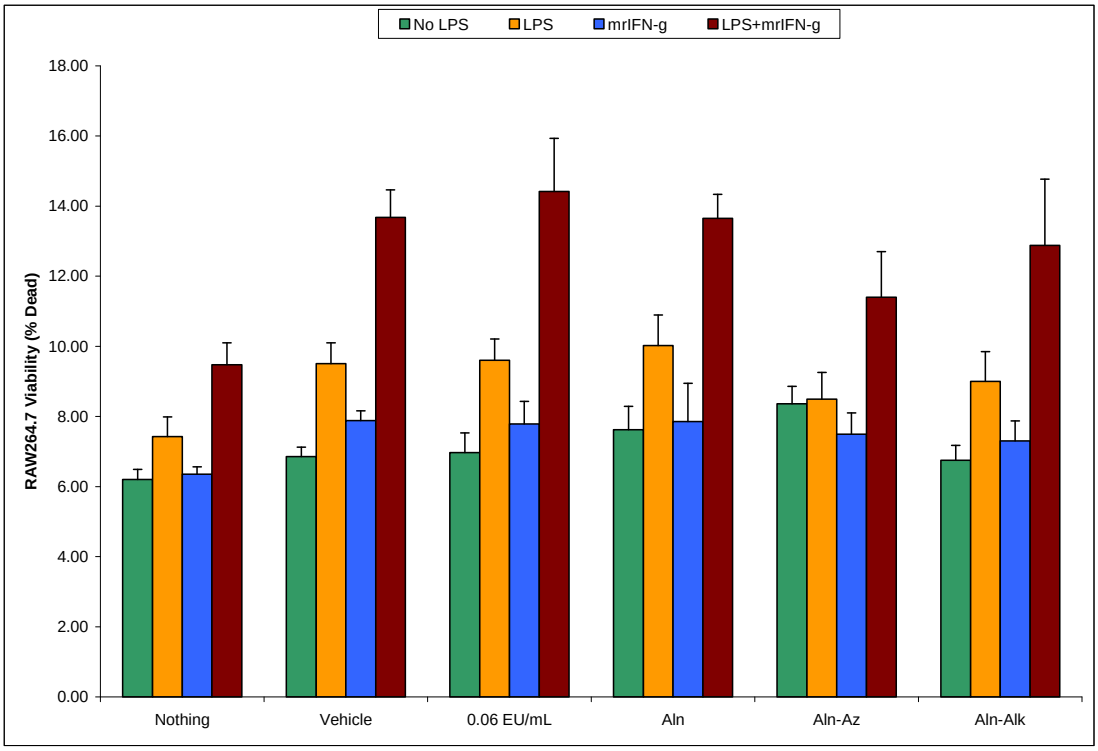

Figure 30. Effect of functionalized alginates on RAW264.7 cell viability ('Dead'). RAW264.7 was seed at 10^4 cells/well into a 96-well plate, then incubated for 24 h at 37°C in the presence of or absence of 50 ng/mL mrIFN-γ, plus 2 mg/mL Aln or functionalized Aln samples as compared to an additional 0.06 EU/mL control or vehicle only. After measuring the accumulated nitrite concentration in the supernatant the cell viability was quantified utilizing a Live/Dead® Assay kit. Data shown are mean ± 1 standard deviation of 4 replicate wells per condition.

5.3.2 Cytotoxicity of 'Click' Reagents Alone or In Combination

Generally, EDTA and $CuSO_4$ are known to be toxic towards cells. EDTA chelates with Ca^{+2} or other divalent cations important for cellular function and CuSO4 has been shown to act as an antibiotic. However, toxicity is a function of concentration and time of exposure. Therefore, to be able to effectively utilize the 'click' reaction chemistry scheme for encapsulating cells a live/dead assay was employed to monitor cell viability as a function of time, concentration, and reagent. RAW264.7 cells were exposed to varying concentrations and combinations of EDTA, $CuSO_4$, and NaAsc and cell death was monitored for up to 1 hr. Ionic crosslinking of Aln usually

proceeds for 30 min. Ideally, the whole encapsulation scheme should be kept under an hour to maintain optimal cell viability.

Triton X was used as a positive control to produce cell death as a function of time (Figure 31). Triton X is a surfactant that disrupts the cellular membrane of cells, killing them rapidly (under 10 min). RAW264.7 cells were first incubated in the presence of EthD-1 which enters cells with damaged membranes, binds to nucleic acids, where EthD-1 subsequently undergoes a 40-fold increase in fluorescence. Triton X was added (final concentration 0.5%), the plate was shaken to ensure adequate mixing, and the fluorescence was monitored over time for up to an hour. An hour was chosen as the time frame because normally, when following the manufacturer's instructions, the cells are exposed for 10 min to Triton X then incubated with EthD-1 for 30-45 min before the fluorescence is measured. The fluorescence increases rapidly and starts to plateau after 50 min. For a cytotoxic compound, the live/dead assay can be utilized to monitor cell death.

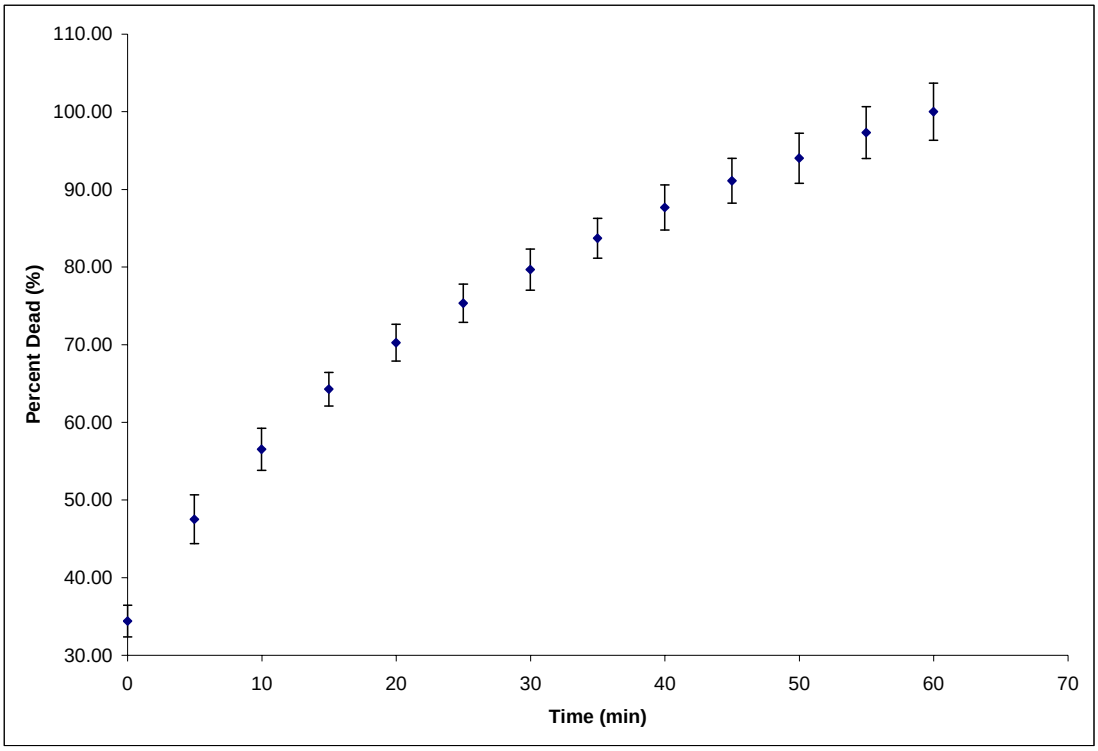

Figure 31. Effect of 0.5% Triton on RAW264.7 cell viability as a function of time. RAW264.7 was seed at 10^4 cells/well into a 96-well plate, allowed to adhere overnight, washed three times with PBS (w/ Ca^{+2}, Mg^{+2}) , incubated for 30 min in the presence of 4 μM EthD-1 working solution, and exposed to 0.5% v/v TritonX-100. Fluorescence was measured every 5 min up to 70 min. Data shown are mean ± 1 standard deviation of 4 replicate wells per condition.

Ascorbic acid reduces Cu^{+2} to Cu^{+1} and Cu^0 and was utilized in the 'click' reaction to quickly and effectively reduce Cu^{+2} to Cu^{+1}. Cu^{+1} was utilized as a catalyst of the reaction between an azide and alkyne to form the 1,2,3, triazole ring. Ascorbic acid is also an antioxidant and given the high concentrations that are utilized in most 'click' reaction schemes it is unknown whether NaAsc would be cytotoxic. Ranging in final concentration from 0 to $1x10^4$ μM, NaAsc was added to RAW264.7 cells that had been preincubated in EthD-1 and the fluorescence was measured over time (Figure 32). In general, the concentration of NaAsc had no overt affect on cell viability as the results of each concentration tested were not higher than the vehicle control (10 μL of d.i.H_2O).

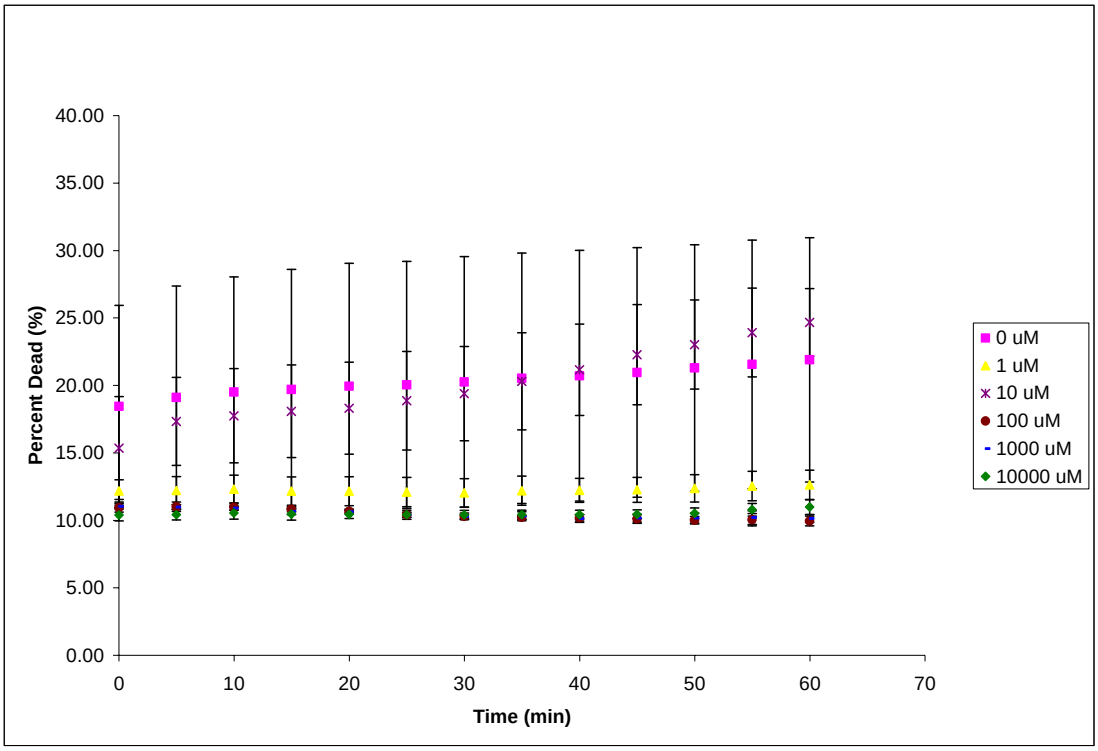

Figure 32. Effect of NaAsc on RAW264.7 cell viability as a function of time.
RAW264.7 was seed at 10^4 cells/well into a 96-well plate, allowed to adhere overnight, washed three times with PBS (w/ Ca^{+2}, Mg^{+2}) , incubated for 30 min in the presence of 4 μM EthD-1 working solution, and exposed to NaAsc (0-10 mM). Fluorescence was measured every 5 min up to 60 min. Data shown are mean ±1 standard deviation of 4 replicate wells per condition.

EDTA is utilized at the end of the 'click' reaction to remove $Cu^{+2/+1/0}$ from the surrounding solution and the hydrogel capsules through chelation. EDTA had an original pH =4.4. However, as EDTA chelates with Cu the pH continues to drop as more protons are released into the solution; creating potentially a toxic environment for cells. EDTA could also theoretically chelate with any Ca^{+2} or Mg^{+2} present necessary for cell attachment and cell function. This is unlikely since EDTA chelates with Ca^{+2} at a pH>8. As before, EDTA ranging in final concentration from 0 to $1x10^4$ μM was used to treat RAW264.7 cells preincubated in EthD-1 and the fluorescence was measured over time (Figure 33). For each concentration tested, there was no significant increase in cell death compared to the vehicle control (10 μL of d.i. H_2O).

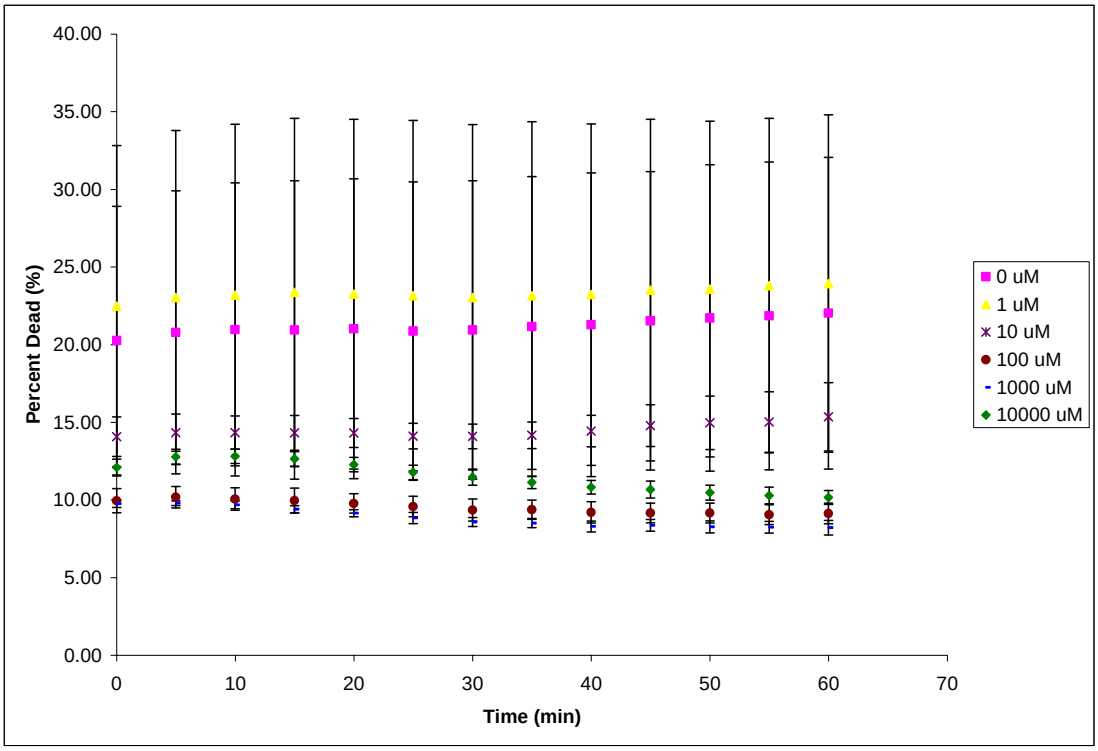

Figure 33. Effect of EDTA on RAW264.7 cell viability as a function of time.
RAW264.7 was seed at 10^4 cells/well into a 96-well plate, allowed to adhere overnight, washed three times with PBS (w/ Ca^{+2}, Mg^{+2}) , incubated for 30 min in the presence of 4 μM EthD-1 working solution, and exposed to EDTA (0-10 mM). Fluorescence was measured every 5 min up to 60 min. Data shown are mean ±1 standard deviation of 4 replicate wells per condition.

$CuSO_4$ is employed as the source of Cu^{+2} for the 'click' reaction and it is known to be cytotoxic to cells. However, at what concentrations and time of exposure is not readily known. Therefore, RAW264.7 preincubated with EthD-1 was exposed to differing concentrations of $CuSO_4$ (0-$1x10^4$ μM) for up to 65 min (Figure 34). Usually in the literature 5 mM $CuSO_4$ and 10 mM NaAsc are employed for the 'click' reaction. Surprisingly, as the concentration of Cu^{+2} increased the fluorescence dramatically decreased and also decreased over time. At the end of the experiment, the observation was made that at the highest concentrations of Cu^{+2} the copper had precipitated out of solution and coated the bottom of the well. Only at the later time points (after 45 min) and at higher Cu^{+2} concentrations (above $1x10^3$ μM) did the fluorescence increase indicating possible cell death.

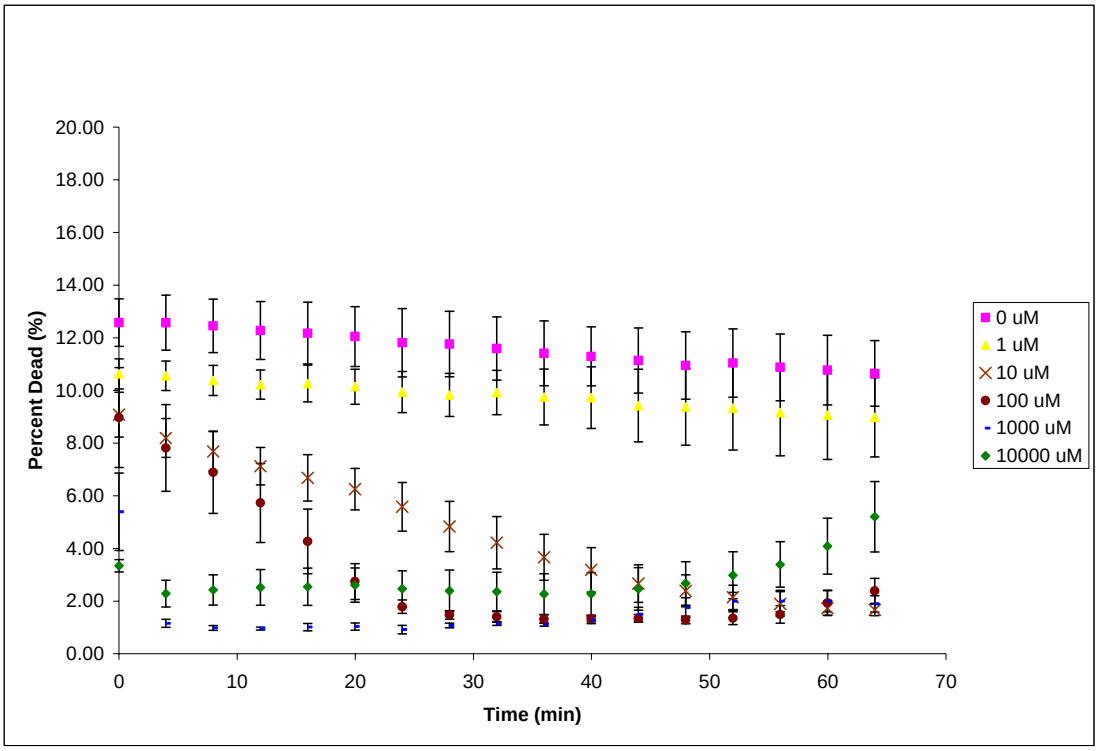

Figure 34. Effect of $CuSO_4$ on RAW264.7 cell viability as a function of time.
RAW264.7 was seed at 10^4 cells/well into a 96-well plate, allowed to adhere overnight, washed three times with PBS (w/ Ca^{+2}, Mg^{+2}) , incubated for 30 min in the presence of 4 µM EthD-1 working solution, and exposed to $CuSO_4$ (0-10 mM). Fluorescence was measured every 5 min up to 70 min. Data shown are mean ±1 standard deviation of 4 replicate wells per condition.

Given the decrease in fluorescence correlated with the Cu^{+2} concentration, the experiment was repeated but with all the cells being exposed to Trition X (0.5%) for 10 min before the addition of Cu^{+2} (Figure 35). This would determine if the Cu^{+2} was interfering with EthD-1. Figure 35 clearly illustrates the affect of Cu^{+2} on fluorescence and apparent cell death as the percent dead sharply decreased with increasing concentrations of Cu^{+2} and over time. Again, at the highest concentration of Cu^{+2} tested, after 45 min the percent dead started to increase again. The results indicated an interference of Cu^{+2} with EthD-1.

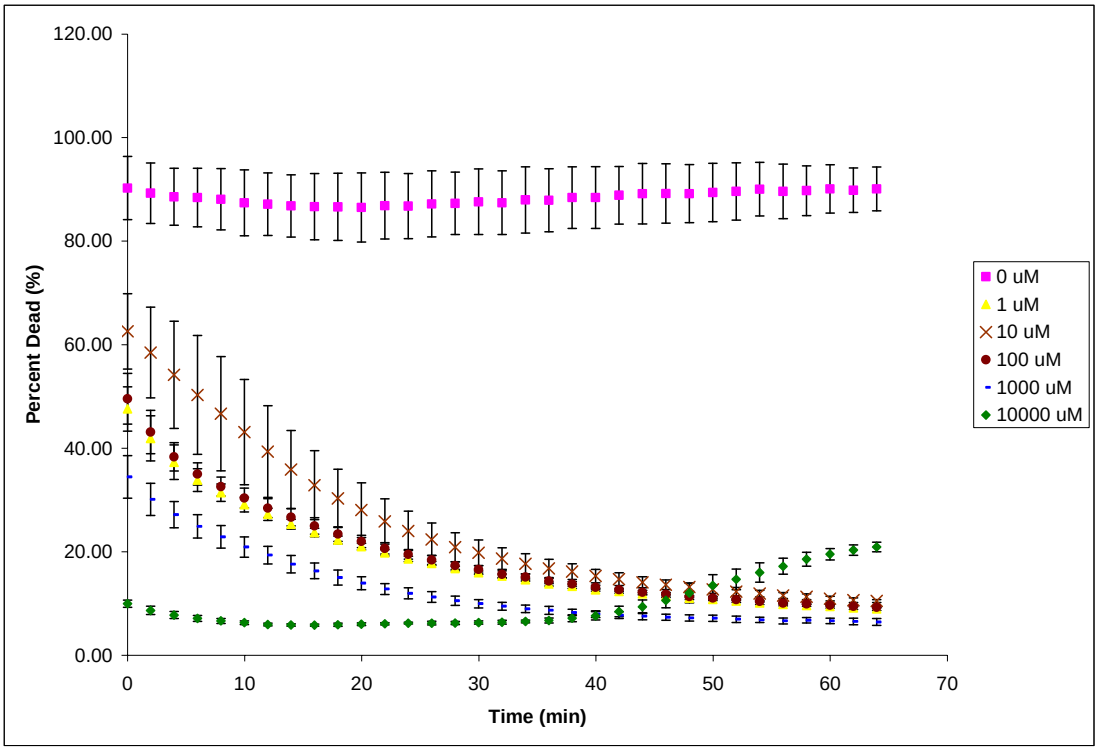

Figure 35. Effect of $CuSO_4$ on dead RAW264.7 as a function of time.
RAW264.7 was seed at 10^4 cells/well into a 96-well plate, allowed to adhere overnight, washed three times with PBS (w/ Ca^{+2}, Mg^{+2}) , incubated for 10 min with 0.5 % Triton, incubated for 30 min in the presence of 4 µM EthD-1 working solution, and exposed to $CuSO_4$ (0-10 mM). Fluorescence was measured every 5 min up to 70 min. Data shown are mean ±1 standard deviation of 4 replicate wells per condition.

While EDTA and NaAsc alone seemed to be non-cytotoxic at the concentrations and over the timeframe tested, the experiments were repeated but with different combinations of EDTA, NaAsc, and $CuSO_4$ to rule out any toxic combinatorial effect. Equal concentrations of EDTA, NaAsc, and/or $CuSO_4$ were used to treat RAW264.7 cells and the fluorescence was measured over time. The first combination was EDTA and $CuSO_4$ exposure (Figure 36). The results suggest that EDTA chelated Cu^{+2} driving the pH down causing cytotoxicity. Above 100 µM $CuSO_4$ and EDTA, the percent dead started to increase after 30 min indicating possible cell death.

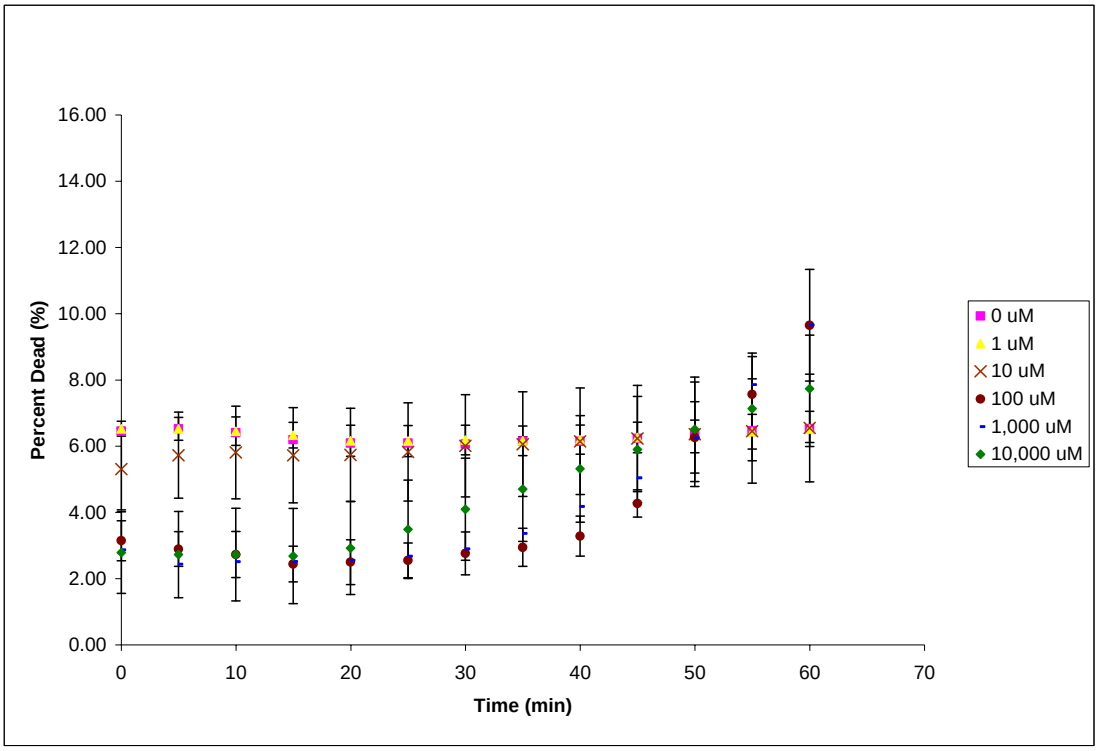

Figure 36. Effect of EDTA and $CuSO_4$ in combination on RAW264.7 cell viability as a function of time.
RAW264.7 was seed at 10^4 cells/well into a 96-well plate, allowed to adhere overnight, washed three times with PBS (w/ Ca^{+2}, Mg^{+2}) , incubated for 30 min in the presence of 4 μM EthD-1 working solution, and exposed to $CuSO_4$ and EDTA (0-10 mM). Fluorescence was measured every 5 min up to 60 min. Data shown are mean ±1 standard deviation of 4 replicate wells per condition.

NaAsc in combination with $CuSO_4$ was tested under a variety of concentrations for up to an hour (Figure 37). Again, NaAsc will reduce Cu^{+2} to Cu^0 over time. The results suggest that as the concentration of $CuSO_4$ and NaAsc increased there was a decrease in percent of cell death most likely due to copper interference. However, the effect was not quite as dramatic as in Figure 34.

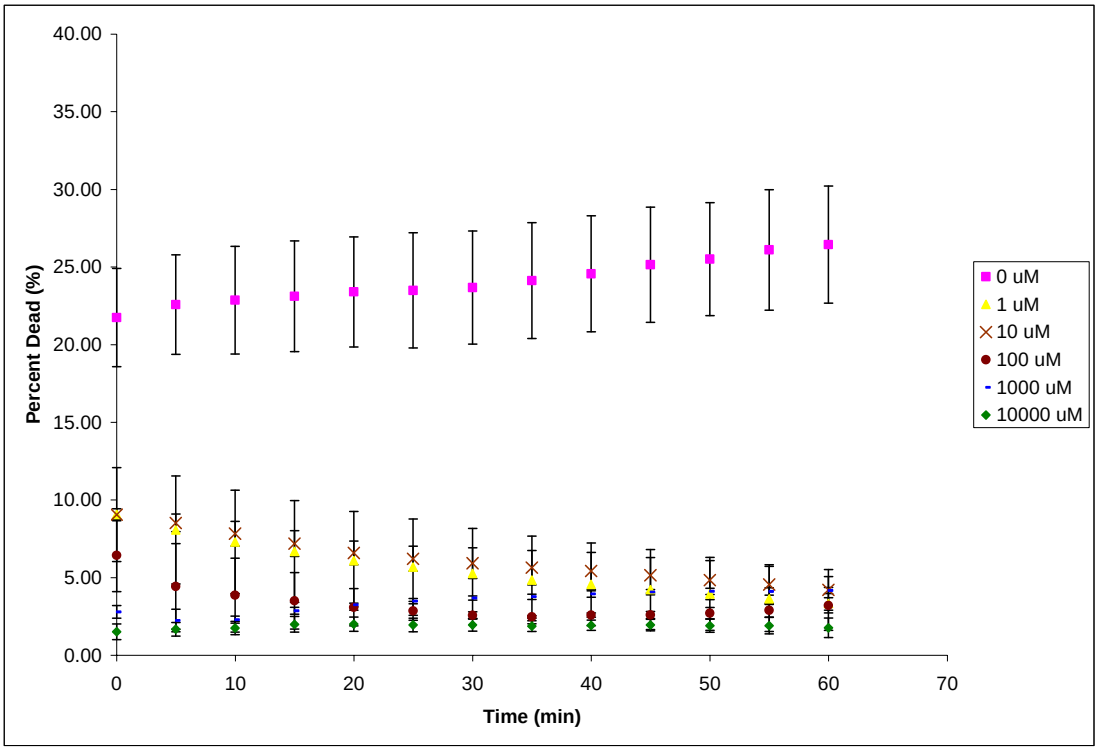

Figure 37. Effect of EDTA and NaAsc in combination on RAW264.7 cell viability as a function of time.
RAW264.7 was seed at 10^4 cells/well into a 96-well plate, allowed to adhere overnight, washed three times with PBS (w/ Ca^{+2}, Mg^{+2}) , incubated for 30 min in the presence of 4 μM EthD-1 working solution, and exposed to $CuSO_4$ and NaAsc (0-10 mM). Fluorescence was measured every 5 min up to 60 min. Data shown are mean ±1 standard deviation of 4 replicate wells per condition.

For completeness, different combinations of EDTA and NaAsc were tested (Figure 38). As expected, there was no effect on cell death for the concentrations tested, over the time of the experiment. There was no increase in cell death compared to the vehicle control (10 μL of d.i. H_2O) for any combination of EDTA and NaAsc tested.

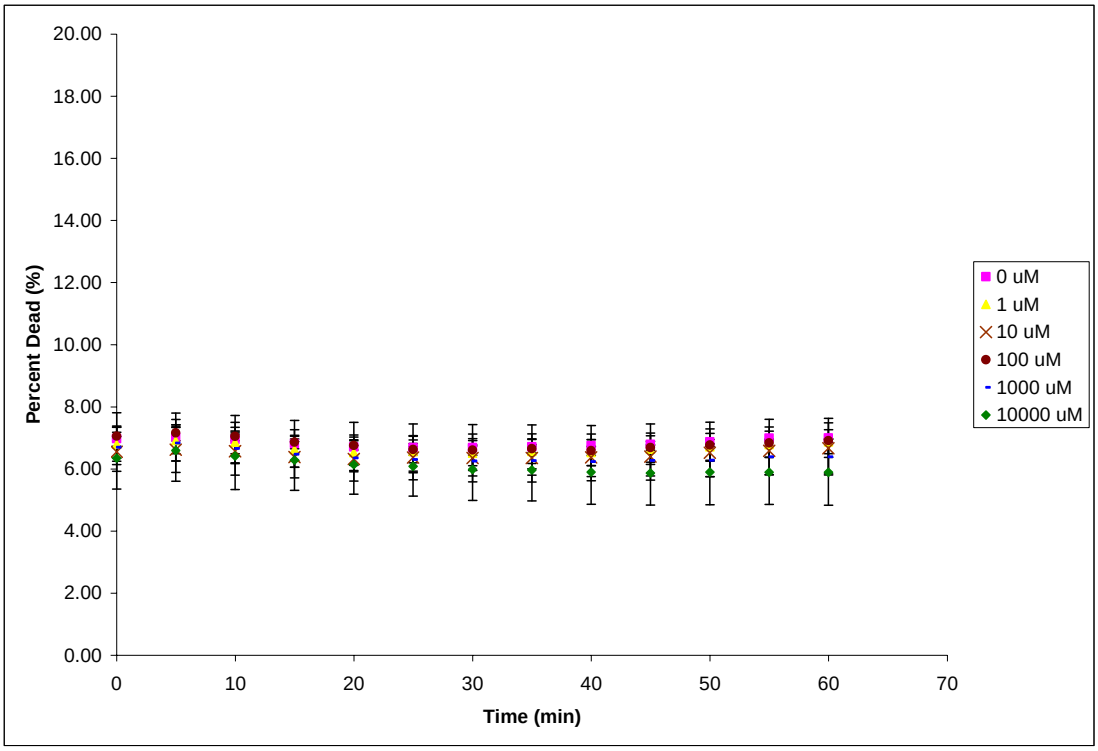

Figure 38. Effect of EDTA and NaAsc in combination on RAW264.7 cell viability as a function of time.
RAW264.7 was seed at 10^4 cells/well into a 96-well plate, allowed to adhere overnight, washed three times with PBS (w/ Ca^{+2}, Mg^{+2}) , incubated for 30 min in the presence of 4 μM EthD-1 working solution, and exposed to NaAsc and EDTA (0-10 mM). Fluorescence was measured every 5 min up to 60 min. Data shown are mean ±1 standard deviation of 4 replicate wells per condition.

Finally, all three (EDTA, NaAsc, $CuSO_4$) were tested in combination at different concentrations for up to an hour (Figure 39). This was done to determine if there was a cytotoxic effect due to all three being in combination and to establish the optimal conditions for encapsulating therapeutic cells. While 10 μM of EDTA, $CuSO_4$, and NaAsc was the only combination that was above the vehicle control (30 μL of d.i.H_2O), it was within the standard deviation of the measurement. Therefore, it was not considered to be a significant increase or biologically relevant.

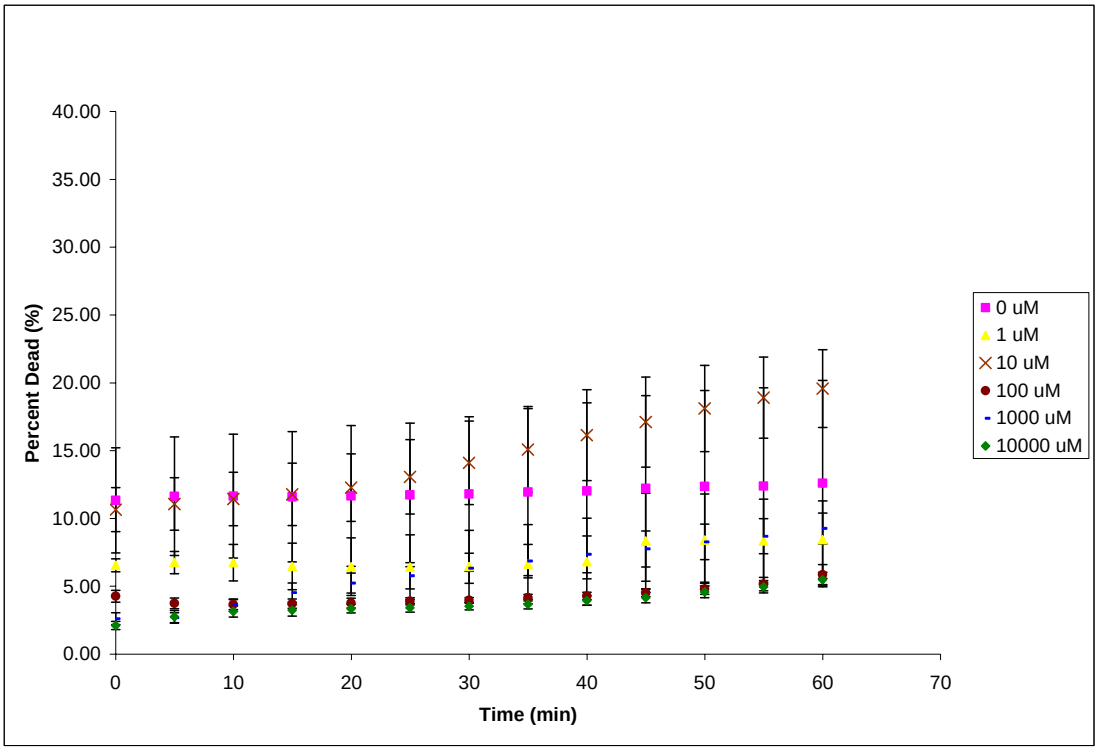

Figure 39. Effect of EDTA, NaAsc, and $CuSO_4$ in combination on RAW264.7 cell viability as a function of time.
RAW264.7 was seed at 10^4 cells/well into a 96-well plate, allowed to adhere overnight, washed three times with PBS (w/ Ca^{+2}, Mg^{+2}) , incubated for 30 min in the presence of 4 μM EthD-1 working solution, and exposed to EDTA, NaAsc, $CuSO_4$ (0-10 mM) in combination. Fluorescence was measured every 5 min up to 60 min. Data shown are mean ±1 standard deviation of 4 replicate wells per condition.

5.4 Conclusions

5.4.1 Cytotoxicity of Functionalized Alginates

The goal of determining the cytotoxicity of functionalized Alns was to determine if cell viability was affected by functionalized Alns. Taken together with results from Chapter 4, functionalized Alns did not affect cell viability of RAW264.7 cells and that the increase in NO production from RAW264.7 cells did not affect cell viability. Since functionalized Alns did not affect cell viability under a variety of simulated inflammatory situations, functionalized Alns can be employed for therapeutic cell encapsulation.

5.4.2 Cytotoxicity of 'Click' Reagents

Toxicity is based on the identity of the chemical species, concentration, and the amount of exposure to the 'click' reagents in question. EDTA and Cu^{+2} are known to be cytotoxic to cells. Therefore, to utilize 'click' chemistry in a cellular encapsulation technique the concentrations and exposures times of these potentially cytotoxic agents need to be established. RAW264.7 cells are a robust, immortal macrophage cell line and were employed to investigate the cytotoxicity of 'click' reagents due to prior experience, fast replication, and ease of use. EthD-1 binds to the nucleic acids found in cells with damaged membranes and undergoes a 40-fold increase in fluorescence. Triton X is a surfactant that is commonly used as a positive control with the live/dead assay in mammalian cells. Observationally, Triton X immediately disrupts cellular membranes causing them to lyses. Therefore, Triton X was suitable as a positive control in the live/dead cytotoxic assay for mammalian cells to determine the cytotoxicity of the reagents utilized in the 'click' reaction. In practice, capsules would first be ionically crosslinked for a maximum of 30 min, then covalently crosslinked via the 'click' reaction for a maximum of 15 min. Then the covalently crosslinked capsules would be exposed to EDTA for a maximum of 20 min to remove any copper residue. At most, encapsulated cells would be potentially exposed to cytotoxic reagents for a maximum of 30 min. In optimizing the experimental conditions utilizing RAW264.7 cells, if the cells are dead and exposed to EthD-1 the fluorescence stabilizes after 30 min (data not shown). Therefore, the exposure time of RAW264.7 cells to these cytotoxic agents was chosen to be 1 hr to account for any cell death and dye/nucleic acid reaction time.

Overall, with the exception of copper, the 'click' reagents did not seem to be cytotoxic at the concentrations and timeframe tested. Only when EDTA and Cu^{+2} were present together at concentrations above 100 μM was there an increase in cell death after 30 min. It is unclear whether this is due to Cu^{+2} cytotoxic effect or that as EDTA chelates Cu^{+2} the overall solution pH is decreasing, making the environment toxic. This uncertainty is due to Cu^{+2} somehow interfering with EthD-1, preventing it from functioning properly.

5.5 Future Work

As stated in Chapter 4, future experiments could be performed with primary cell types such as splenocytes from either rats or humans to confirm the results obtained with RAW264.7 cells. The cell viability could also be assessed with the Live/Dead ® assay for these experiments to confirm the results obtained from the nitrite assay.

Copper adversely affected the results from the Live/Dead® assay by interfering with the fluorescence of EthD-1. There could be a number of reasons for this such as copper affecting the way EthD-1 interacts with damaged cells. Therefore assessing the cytotoxic effect of copper on RAW264.7 cells could not be determined utilizing the Live/Dead ® assay. Other inclusion/exclusion dyes might be employed to assess viability that are not affected by copper.

Another variation of this experiment might be to look at longer exposure times to the reagents involved in the 'click' reaction. In these experiments, the reagents and the dyes were co-incubated together and the cell viability was assessed as a function of time. One variation would be to incubate RAW264.7 cells in the presence of the reagents of interest overnight, wash the cells to remove excess chemicals, and then

perform the live/dead assay. This might provide an absolute determination of the cytotoxicity of the reagents. In addition, some of the reagents such as EDTA might interact with the CM. EDTA might chelate ions present in the CM and therefore affect the viability of treated cells.

Another cell type could be utilized that might be more sensitive to the cytotoxic affects of the 'click' reagents. RAW264.7 cells were employed because of the short time it takes for them to adhere to the culture well ensuring sufficient number of cells for determining the cytotoxic effects of functionalized polysaccharides. RIN-5F could be a more applicable cell type since these are immortal β-cells and the ultimate application would be for encapsulation of islets of Langerhans. As stated in Chapter 4, a human derived cell line would be more applicable when determining the inflammatory response of novel biomaterials. This could also be the case with the cytotoxic effect of the 'click' reagents.

Chapter 6: Encapsulation of Therapeutic Cells

6.1 Introduction

The overall goal of the experiments in this chapter were to optimize conditions for employing 'click' chemistry as a crosslinker of Aln to improve hydrogel stability while maintaining encapsulated cell function. The viability, proliferation, and insulin release of RIN-5F cells encapsulated in Ca^{+2}- and/or 'click' crosslinked capsules were investigated. RIN-5F is a rat insulinoma cell line that continuously produces insulin without glucose stimulation. This property makes it an excellent cell line to employ when optimizing of a novel crosslinking system to be applied in a bioartificial pancreas. The cell line can be readily grown in large numbers in the lab and function or cell health can be directly correlated to insulin production as well as cell viability.

A number of variables could affect the success of employing 'click' chemistry; namely, the concentrations of Cu^{+2}, NaAsc, and EDTA and the duration to which cells are exposed to these potentially cytotoxic chemicals. Another variable is the functional groups attached to Aln, chiefly the azide and alkyne. Determining the cytotoxic effect of these variables was the focus of Chapter 5. However, the results from chapter 5 were inconclusive in regards to the cytotoxicity of $CuSO_4$, EDTA, and NaAsc. Functionalized Aln was determined not to be directly cytotoxic to RAW264.7 cells or elicit an inflammatory response. Therefore, the focus of the experiments in this chapater was to explore the appropriate concentrations and conditions under which RIN-5F cells can be encapsulated within Aln capsules formed by 'click'

crosslinking and to compare function and viability to RIN-5F cells encapsulated in ionically crosslinked capsules.

6.2 Methods

6.2.1 Materials

Stock solutions of the different reagents and samples were prepared as follows. Complete medium (CM) was composed of RPMI 1640 medium containing 10% fetal calf serum, 2 mM glutamine, 100 U/mL penicillin, and 100 l g/mL streptomycin). Collagenase was diluted in RPMI 1640 to a concentration of 5 mg/mL, aliquoted, and frozen at -20^{o}C. Medical grade Aln (Pronova; viscosity ≤ 100 mPas, Guluronate ≥ 60%) was reconstituted in sterile, LAL water to a concentration of 2.5% w/v and stored at 4^{o}C. A 2.5% w/v Aln solution composed of a 2:1:1 ratio of Aln, Aln-Alk, and Aln-Az or Aln (Sigma; Guluronate ≥ 43%) was prepared with sterile, LAL water, passed through a 0.45 μm filter, and stored at 4^{o}C.

6.2.2 Cell Culture of RIN-5F

Aliquots of RIN-5F (ATCC CRL-2058; American Type Culture Collection, Manassas, VA), a rat insulinoma cell line, were removed from liquid nitrogen, rapidly thawed, and cultured in 5% CO_2/95% air, 70% humidity at 37ºC until the adhered monolayer reached 50% confluency (usually one to two weeks). The monolayer was harvested by washing the cells two times with PBS (w/ Ca^{+2}, Mg^{+2}), incubated in the presence of 0.05% trypsin for 5 min at 37^{o}C, gently blown up, and transferred into an equal amount of CM. The cells were centrifuged for 10 min at 1000 rpm, the

supernatant decanted off, and resuspended in CM to a concentration of $1x10^6$ cells/mL.

6.2.3 Encapsulation of RIN-5F

RIN-5F cells were encapsulated in a similar manner as described by Lyle et al[36]. Briefly, RIN-5F cells were microencapsulated in either Aln (Pronova), Aln (Simga) or functionalized Aln (2 parts Aln:1 part Aln-Az:1 part Aln-Alk). In general, 0.2 mL of RIN-5F was gently mixed with 0.8 mL of 2.5% w/v Aln to yield a homogenous mixture of 2 % w/v Aln/cells (final cell concentration $8x10^5$ cells/mL). The mixture was then passed through an electrostatic encapsulator (Nisco encapsulation unit, Zurich Switzerland) utilizing a voltage of 7.5 kV, a pump rate of 20 mL/hr, and a nozzle diameter of 1.1 mm. Gelation of capsules occurred in either a 50 mM $CaCl_2$/200 mM mannitol solution at pH =7.4 or 50 mM $CuSO_4$/200 mM mannitol solution at pH=7.4.

Capsules (2 part Aln, 1 part Aln-Az, 1 part Aln-Alk) that were dripped into a 50 mM $CuSO_4$/200 mM mannitol bath and were immediately collected and incubated in 10 mM NaAsc for 2.5 min. The NaAsc solution was replaced with 20 mM EDTA and the capsules were incubated for a total of approximately 30 min to remove any copper present. The EDTA was replaced roughly every 3 min with fresh EDTA. Encapsulated RIN-5F cells were then washed three times with CM and 4 to 5 capsules were added per well of a 96-well plate that contained 0.2 mL of CM. The capsules were uniformly round in shape and clear in appearance with an average diameter of approximately 1.8 mm.

Capsules that were fabricated utilizing Pronova were allowed to gel for 30 min in 50 mM $CaCl_2$/200 mM mannitol, washed three times with CM and 4 to 5 capsules were transferred per well of a 96-well plate that contained 0.2 mL of CM. Capsules were round and clear in appearance with a diameter of approximately 2 mm.

Capsules that were fabricated utilizing 2 parts Aln, 1 part Aln-Az, and 1 part Aln-Alk were split into two groups. The first group were allowed to gel for 30 min in 50 mM $CaCl_2$/200 mM mannitol and used as described above. The second group was allowed to gel for 15 min in the $CaCl_2$ gelation bath, incubated in the presence of 1 mM $CuSO_4$ and 5 mM NaAsc for 2.5 min, 10 mM EDTA washes for 10 min, and 50 mM $CaCl_2$/200 mM mannitol for 5 min. EDTA washes were in general kept to 3 min before being changed and the pH was monitored. When the capsules and the EDTA solution was clear in appearance and the pH had equilibrated the capsules were collected, washed thre times with CM, and 4 to 5 capsules were transferred per well of a 96-well plate that contained 0.2 mL of CM. Capsules in both groups were for the most part round in shape, with small tails, and clear in appearance.

The top 50 μL of supernatant from each well was removed and placed in another plate at 24, 48, and 72 hrs and frozen at -70^{o}C to be assessed for insulin concentration.

6.2.4 Insulin Assay

Frozen supernatant samples were thawed, equilibrated to room temperature, and analyzed for insulin release according to Mercodia High Range Rat Insulin ELISA (Alpco Diagnostics) instructions. Absorbance levels were measured at 465 nm utilizing a Tecan Plate Reader.

6.2.5 Live/Dead Cell Viability

Live/dead viability was assessed 72 hrs post-encapsulation, utilizing the Live/Dead® cell viability kit for mammalian cells following manufacture's instructions. A representative capsule from each crosslinking chemistry was used. The capsules were sandwiched between a microscope slide and cover slip to destroy the capsule. Representative pictures were taken utilizing a fluorescent microscope (Axioskop 2plus microscope, Zeiss; AttoArc 2 HBO 100 W Hg lamp) and images were processed with Image J software.

6.2.6 Statistical Analysis

Data are expressed as mean ± standard deviation of *n* independent observations. Statistical significance was calculated using the two-tailed unpaired Student's *t* test or ANOVA. A $p \leq 0.05$ was considered statistically significant.

6.3 Results

6.3.1 Experiment Parameter Optimization

Numerous experiments were performed to optimize crosslinking with 'click' chemistry. The criteria utilized to determine the optimal 'click' crosslinking conditions were insulin secretion, cell viability, and capsule stability compared to cells encapsulated in Ca^{+2}-crosslinked capsules.

The goals of the first experiment were to determine appropriate time points to measure insulin secretion and to compare RIN-5F cells encapsulated in 'click' crosslinked capsules to RIN-5F cells encapsulated in Ca^{+2}-crosslinked medical grade

Aln (Pronova). As shown in Figure 40, significant quantities of insulin can be measured over time for all four different crosslinking scenarios. In general, RIN-5F cells encapsulated in ionically crosslinked capsules secreted more insulin than capsules that utilized covalent crosslinking. RIN-5F cells encapsulated in Ca^{+2}-crosslinked functionalized Aln secreted the highest level of insulin at each time point. Interestingly, capsules that were crosslinked with only 'click' chemistry secreted more insulin than capsules that contained both ionic and covalent crosslinking (Ca^{+2}-'click') ($p \leq 0.002$). The fact that Ca^{+2}-'click' capsules secreted less insulin than 'click' capsules at each time point could be due to either the amount of Cu^{+2} present (~10 mM), the time spent in the presence of EDTA, or that after incubation in EDTA the capsules were transferred back into a Ca^{+2} -gelation bath to ensure adequate ionic crosslinking.

After 72 hrs, the CM was replaced with fresh CM as suggested by ATCC when culturing RIN-5F cells. At 96 and 144 hrs, ionically crosslinked capsules (Pronova Aln) secreted more insulin than their 24 and 72 hr counter parts ($p \leq 1x10^{-4}$). There are perhaps three possibilities for this observation. First, RIN-5F cells encapsulated in ionically crosslinked capsules were proliferating thereby increasing the total number of insulinoma cells present per capsule. Second, as the ionically crosslinked capsules swelled or degraded there was less of a physical barrier to prohibit insulin diffusion. Third, a combination of the increase in cell number per capsule and swelling of the capsule led to a significant increase in insulin production. However, after 72 hrs when the CM was changed, capsules containing RIN-5F cells that employed 'click' chemistry did not produce measurable quantities of insulin.

According to ATCC, sub-culturing RIN-5F cells requires up to 3 days for full attachment. Cell attachment of RIN-5F cells was not known to be a requirement for insulin production. Based on this information, insulin secretion was measured up to 144 hrs was chosen for the first experiment. Since RIN-5F cells produced significantly more insulin in Ca^{+2}-crosslinked capsules within the first 72 hrs post encapsulation all subsequent experiments measured insulin up to 72 hrs.

Upon examination of the capsules after 72 hrs, striking differences in physical appearance of the capsules were noted. Capsules that were composed of Prononva Aln had swelled in size and cracks or deformities were present in the capsule. Capsules that were composed of functionalized Aln had degraded to the point where individual capsules were indistinguishable from each other and fragments of capsules were present. However, capsules that contained covalent crosslinking (or 'click' crosslinks) appeared intact with no swelling or visual deformities (both Ca^{+2}-'click' and 'click' capsules).

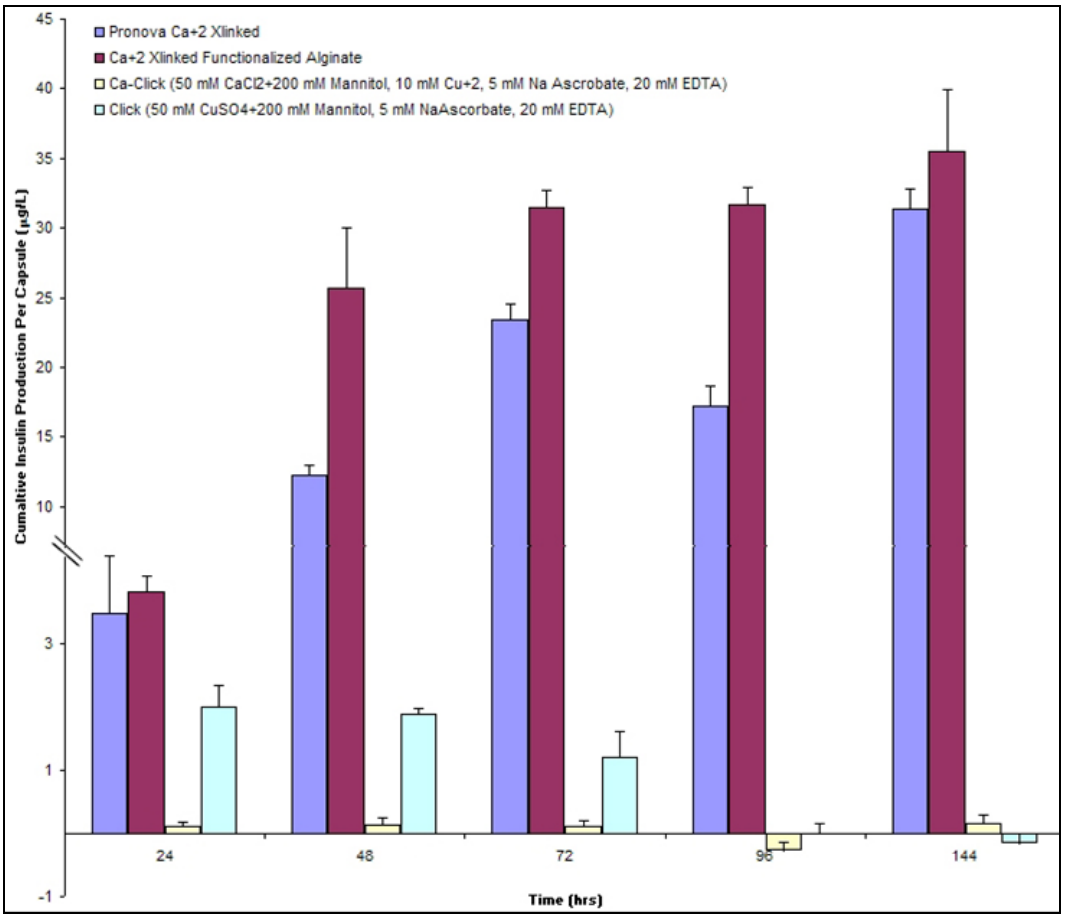

Figure 40. Comparison of insulin secretion of RIN-5F encapsulated in alginate via different crosslinking chemistries.
RIN-5F cells were encapsulated in Aln (Pronova) or functionalized Aln via ionic and/or covalent crosslinking at $8x10^5$ cells/mL. Four-five capsules were seeded in a 96-well plate per time period and insulin secretion was measured for up to 144 hrs. Data shown are mean ±1 standard deviation of 4 replicate wells per condition.

6.3.2 Effect of 'Click' Reagents on Insulinoma Function

In Chapter 5, different components of the 'click' reaction were tested in varying concentrations and combination on RAW264.7 cell viability. The second experiment expanded on these findings and studied the affect of each component of the 'click' reaction on RIN-5F insulin secretion and viability. The test conditions are summarized in Table 12.

Table 12. Summary of experimental purposes.

Test Condition	Annotated Experimental Conditions	Purpose
Ca^{+2}-crosslinked Aln (43% G-block)	• 50 mM Ca^{+2} and 200 mM mannitol for 30 min	Positive Control
Ca^{+2}-crosslinked functionalized Aln	• 50 mM Ca^{+2} and 200 mM mannitol for 30 min	Is functionalized Aln (a mixture containing azides and alkynes) itself cytotoxic for RIN-5F cells and will it affect insulin production?
Cu^{+2}-crosslinked functionalized	• 50 mM $CuSO_4$ and 200 mM mannitol for 30 min	Is Cu^{+2} in the presence of functionalized Aln cytotoxic for RIN-5F and will it affect insulin production?
Cu^{+2}-NaAsc crosslinked functionalized Aln	• 50 mM $CuSO_4$ and 200 mM mannitol for no more than 10 min, capsules collected immediately after last capsule formed • 10 mM NaAsc for 2.5 min	NaAsc reduces Cu^{+2} to $Cu^{+1/0}$ where Cu^{+1} catalyzes the 'click' reaction. Is this combination of NaAsc and $Cu^{+2+1/0}$ cytotoxic to RIN-5F and will it affect insulin production?
'Click' functionalized Aln	• 50 mM $CuSO_4$ and 200 mM mannitol for no more than 10 min • 10 mM NaAsc for 2.5 min • 20 mM EDTA 3 min washes for up to 20 min • 50 mM Ca^{+2} and 200 mM mannitol for 20 min	Is the combination of all four cytotoxic to RIN-5F and does it affect insulin production?
Ca^{+2}-'click' functionalized Aln	• Incubate in the presence of 5 mM CuSO4 and 10 mM NaAsc for 2.5 min • 20 mM EDTA 3 min washes till capsules clear in appearance	Does decreasing the concentration of some of the 'click' reactants affect insulin production?

Insulin secretion of encapsulated RIN-5F cells with different cross-linking chemistries was monitored for up to 72 hrs as shown in Figure 41. The number of capsules per well was determined 24 hrs post encapsulation. During this time, Ca^{+2}-crosslinked Aln and Cu^{+2} crosslinked functionalized Aln capsules degraded to the

point where individual capsules were indistinguishable from one of another. When seeding the plate, the goal was for each well to contain 4-5 capsules. RIN-5F cells encapsulated in Aln or functionalized Aln capsules utilizing Ca^{+2} crosslinking secreted similar amounts of insulin. This suggests that functionalized Aln is not detrimental to RIN-5F cell function. Encapsulating RIN-5F cells in capsules utilizing Cu^{+2} resulted in a significant decrease in insulin secretion. However, insulin secretion did increase overtime indicating some functioning insulinoma cells were still present. After 24 hrs, the capsules had degraded to the point of being indistinguishable and the CM was blue/purple in appearance. RIN-5F cells in capsules that employed 'click' chemistry for crosslinking exhibited decreased insulin secretion. However, these capsules were completely intact. For capsules containing RIN-5F cells that were Ca^{+2} and 'click' crosslinked, the insulin secretion was up to 10X lower than its Ca^{+2}-crosslinked counterpart. However, insulin secretion did increase over time and the capsules were still present and spherical in appearance after 72 hrs. Capsules containing RIN-5F cells that employed only 'click' chemistry as a crosslinker, exhibited the lowest amounts of insulin secretion over time compared to the other crosslinking schemes and the insulin secretion did not significantly increase over time suggesting a significant decrease in insulinoma function. Based on these combined results, further experiments used Ca^{+2}, 'click' (50 mM Cu^{+2}, 10 mM NaAsc, 20 mM EDTA), and Ca^{+2}-'click' crosslinking chemistries.

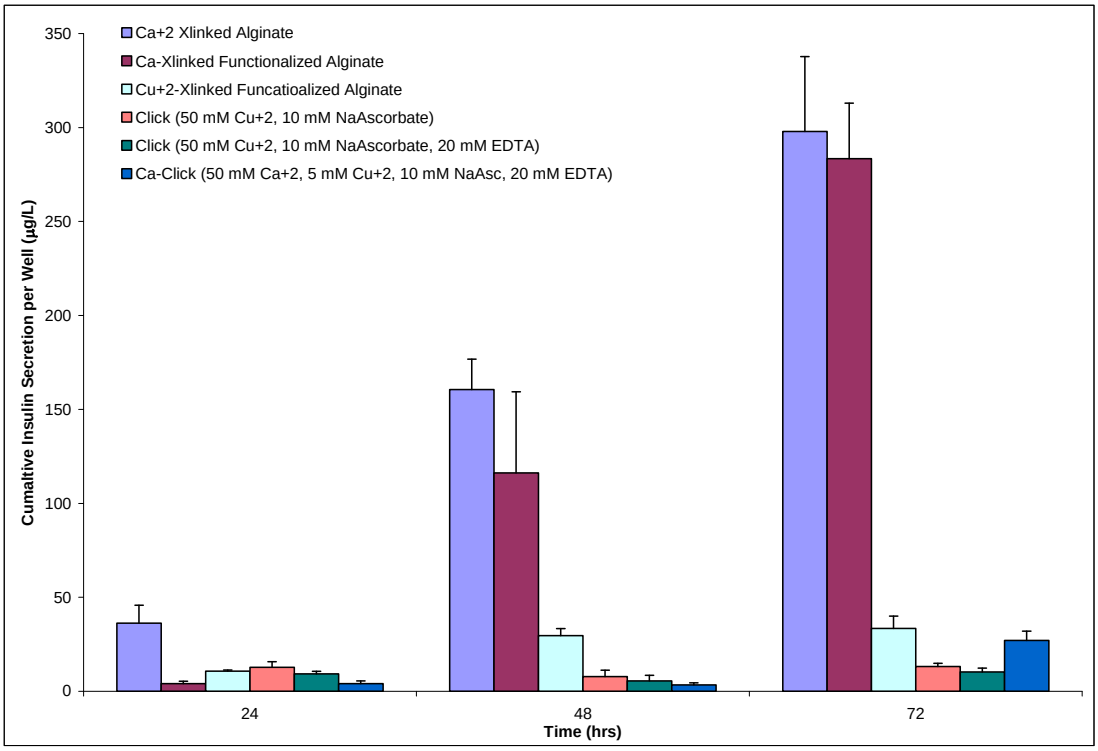

Figure 41. Effect of 'click' reactants on insulin secretion of RIN-5F alone or in combination. RIN-5F was encapsulated in Aln (Sigma) or functionalized Aln via ionic and/or covalent crosslinking at $8x10^5$ cells/mL. Four or five capsules were seeded in a 96-well plate per time period and insulin secretion was measured for up to 72 hrs. Data shown are mean ±1 standard deviation of 4 replicate wells per condition.

6.3.3 Optimization of 'Click' Chemistry for Encapsulation

The third experiment in this series focused on optimizing the concentrations of 'click' reactants and order of reagents added. Specifically, lower concentrations of $CuSO_4$ were tested and whether to add $CuSO_4$ to the gelation bath (which consists of 50 mM $CaCl_2$ and 200 mM) or to use as 'wash' meaning to collect the capsules from the Ca^{+2} -gelation bath and transfer them to a Cu^{+2} bath and then add the NaAsc. Again, traditional Ca^{+2} crosslinked medical grade Aln was employed as a positive control. Another positive control was functionalized Aln that was only crosslinked with Ca^{+2}. Similar results were obtained for ionically and covalently crosslinked encapsulated RIN-5F cells as from before. Interestingly, for both Cu^{+2} concentrations tested (1 mM and 5 mM) when $CuSO_4$ was added to the gelation bath instead of using the wash

method higher amounts of insulin secretion were produced at each time point. One explanation for this result is that the $CuSO_4$ solution had a pH= 4.7 while the Ca^{+2}-gelation solution had a pH=6.3 and the NaAsc solution had a pH=5.8. The lower pH associated with the $CuSO_4$ solution might have adversely affected the RIN-5F cell function.

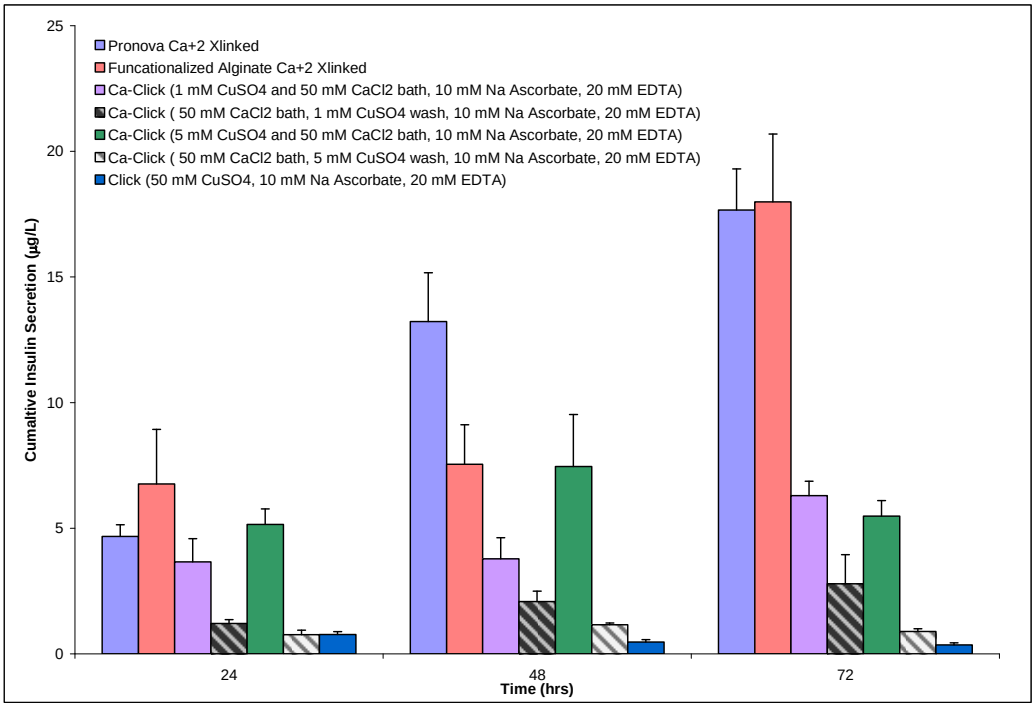

Figure 42. Comparison of insulin production from RIN-5F encapsulated in alginate with various crosslinking chemistries.
RIN-5F was encapsulated in Aln (Sigma) or functionalized Aln via ionic and/or covalent crosslinking at $8x10^5$ cells/mL. Four or five capsules were seeded in a 96-well plate per time period and insulin secretion was measured for up to 72 hrs. Data shown are mean ±1 standard deviation of 4 replicate wells per condition.

The final experiment in this series investigated if lowering the $CuSO_4$ concentration increased insulin production (Figure 43). All three encapsulation methods that employed 'click' chemistry produced measurable and significant quantities of insulin. Also, in general as the amount of $CuSO_4$ was decreased insulin production increased although never reaching the quantities of ionically crosslinked encapsulated RIN-5F cells.

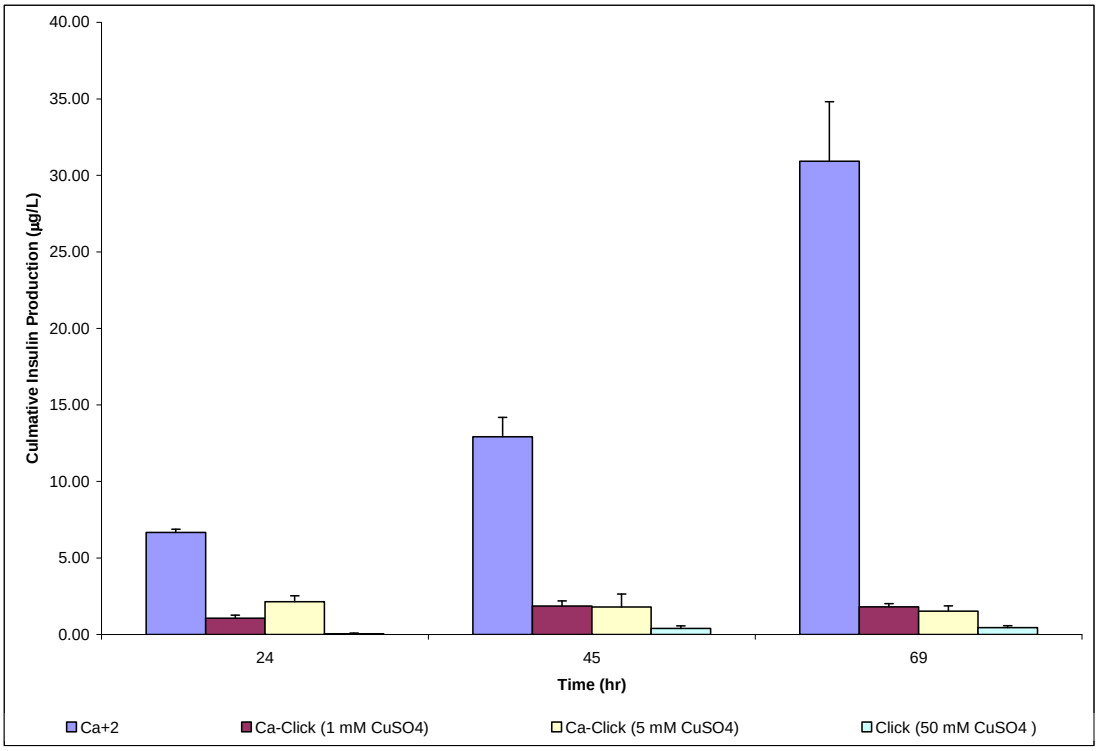

Figure 43. Comparison of insulin production from RIN-5F encapsulated in alginate with various crosslinking chemistries.
RIN-5F was encapsulated in Aln (Sigma) or functionalized Aln via ionic and/or covalent crosslinking at $8x10^5$ cells/mL. Four or five capsules were seeded in a 96-well plate per time period and insulin secretion was measured for up to 72 hrs. Data shown are mean ±1 standard deviation of 4 replicate wells per condition.

6.3.4 Capsule Stability and Appearance

Capsule appearance and stability was observed for each type of crosslinking utilized after cell encapsulation and each time point. Capsules composed of medical grade Aln (Pronova) were spherical in appearance after encapsulation (Figure 44 A).

Over the time course of the experiment, the Pronova Aln capsules swelled. These capsules increased in size over the time course of the experiment but did not rupture compared to the 'click' crosslinked capsules. Capsules that were composed of functionalized Aln but only ionically crosslinked with Ca^{+2} were almost spherical in appearance after encapsulation, some were observed with small tails (Figure 44 B). This might be due to interference of the functional groups being attached to the G-

block of Aln interfering with Ca^{+2}-crosslinking. This assumption is supported by the observation that when a 2% w/v Aln-Alk solution is dripped into a 50 mM $CaCl_2$ bath capsules are formed while a 2% w/v Aln-Az solution does not form capsules when dripped into a Ca^{+2}-gelation bath.

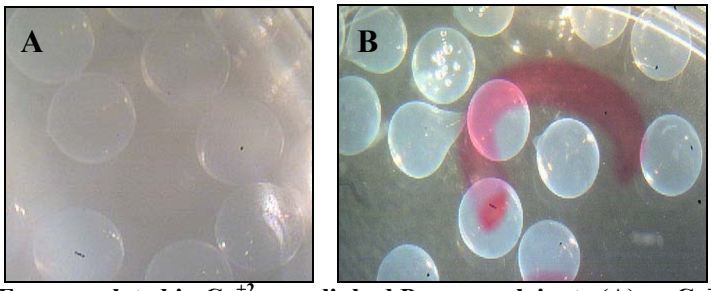

Figure 44. RIN-5F encapsulated in Ca^{+2}-crosslinked Pronova alginate (A) or Ca^{+2}-'click' alginate (B).
Ca^{+2}-crosslinked (A) capsules are spherical in appearance while Ca^{+2}-'click' (B) capsules are also spherical but with small tails are present on most of the capsules. Capsules are approximately 1.8-2 mm in appearance.

Within 24 hrs the Ca^{+2}-crosslinked capsules ruptured and continued to degrade over the course of the experiment. In addition, removal of the CM and replacement with fresh CM or PBS seemed to accelerate capsule degradation. The cell viability measurements utilizing the Live/Dead assay could not be assessed for ionically crosslinked Aln (43% G-block) or functionalized Aln due to capsule degradation. Ca^{+2}-'click' crosslinked capsules were also spherical in appearance after encapsulation, remained intact, and appeared stable over the course of the experiment.

Capsules containing only covalent crosslinks or 'click' crosslinks were spherical in appearance after encapsulation. After exposure to EDTA, an inner, concentric sphere inside the capsule appeared which persisted throughout the remainder of the experiments. 'Click' capsules seemed to be the most stable. Their appearance did not change throughout the experiment (up to 72 hrs) nor did the capsules swell, crack, or rupture compared to ionically crosslinked capsules.

6.3.5 Live/Dead Viability of Encapsulated Cells

At the end of 72 hrs, the cell viability of encapsulated RIN-5F cells was assessed utilizing the Live/Dead® assay. As mentioned earlier, capsules composed of Aln (43% G-monomer) or functionalized Aln that were just ionically crosslinked, with Cu^{+2} or Ca^{+2}, ruptured or degraded over time. While after 72 hrs, Ca^{+2}-crosslinked capsules (either composed of functionalized Aln or Aln (43% G monomer) were still present, the act of washing the capsules with PBS to remove CM for the live/dead® assay completely degraded the remaining capsules. This capsule dissolution made it impossible to assess the encapsulated cell viability in ionically crosslinked capsules. Representative pictures of encapsulated RIN-5F cells encapsulated with various crosslinking chemistries are shown in Figure 45. The capsules were sandwiched in between two microscope slides to destroy the capsule such that more cells could be visualized at the plane of focus for the microscope. The 'click' capsules were noticeably more difficult to sandwich between glass slides than Ca^{+2}-crosslinked Pronova crosslinked capsules.

Cell viability of encapsulated RIN-5F cells was attempted utilizing a live/dead assay. After 72 hrs, encapsulated RIN-5F cells were labeled with EthD-1 and/or CalAM. The live/dead values were compared with the encapsulation method that gave the highest fluorescence numbers (either live or dead controls) in an attempt to normalize the values across crosslinking chemistries (Figure 46). Regardless of the crosslinking chemistry method, the percentage of insulinoma cells (RIN-5F) labeled as 'dead' was approximately the same. Whereas, the percentage of insulinoma cells labeled as 'live' was the lowest in capsules that employed only 'click' crosslinking.

Live cells in capsules that contained both Ca^{+2} and 'click' crosslinking were approximately the same. According to the manufacturer's instructions, intracellular esterase activity and an intact plasma membrane are distinguishing characteristics of live cells. CalAM stains green to indicate intracellular esterase activity while EthD-1 stains DNA red to indicating the loss of integrity in the plasma membrane. When staining with just CalAM, 'live' cells are present in capsules regardless of the crosslinking chemistry utilized. When both stains are combined, cell populations are labeled as both 'live' and 'dead' and some damaged cells might still be functioning. While staining is useful in visualizing encapsulated cells it does not correlate with insulin production. In other words, while insulinoma cells encapsulated in capsules that employed 'click' chemistry produce less insulin than in ionically crosslinked capsules they might still be alive but not producing insulin.

Ca^{+2}-'Click' (1 mM $CuSO_4$, 10 mM NaAsc, 20 mM EDTA and 50 mM $CaCl_2$)

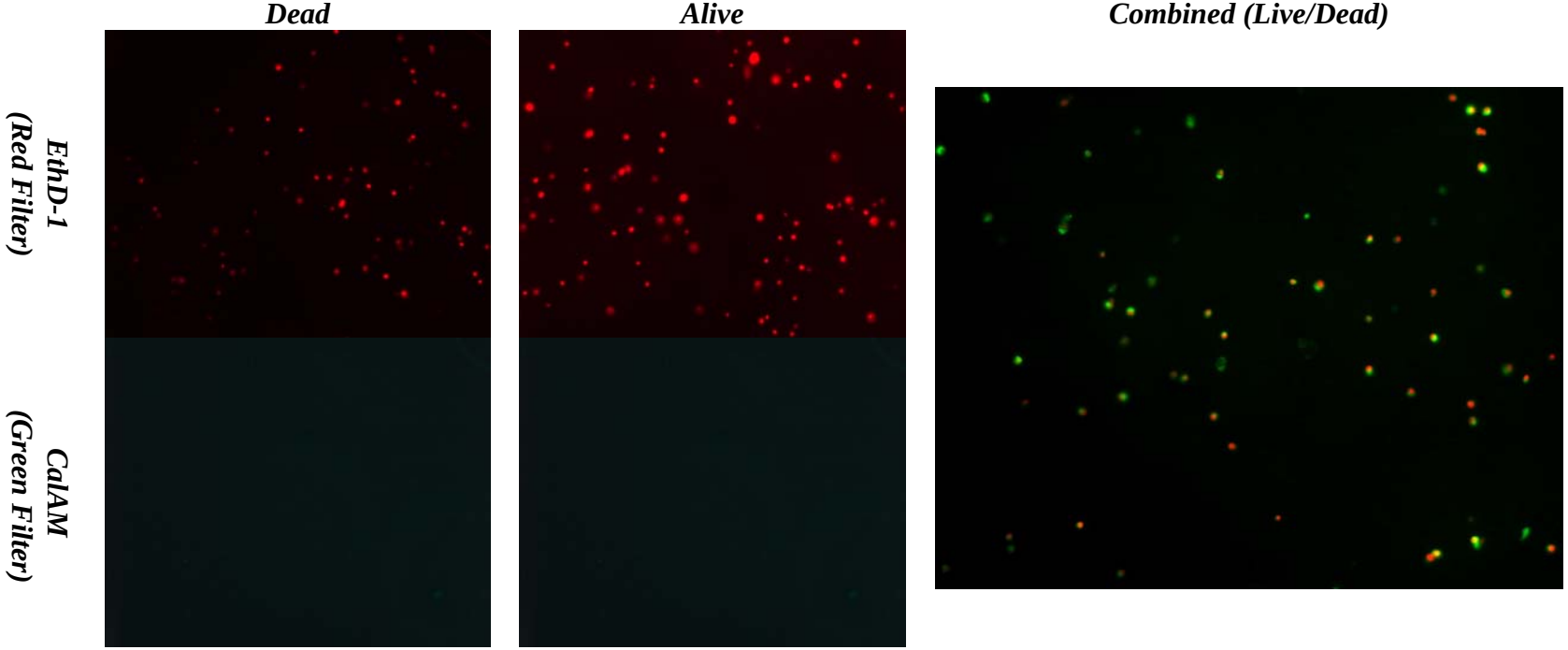

Ca^{+2}-'Click' (5 mM $CuSO_4$, 10 mM NaAsc, 20 mM EDTA and 50 mM $CaCl_2$)

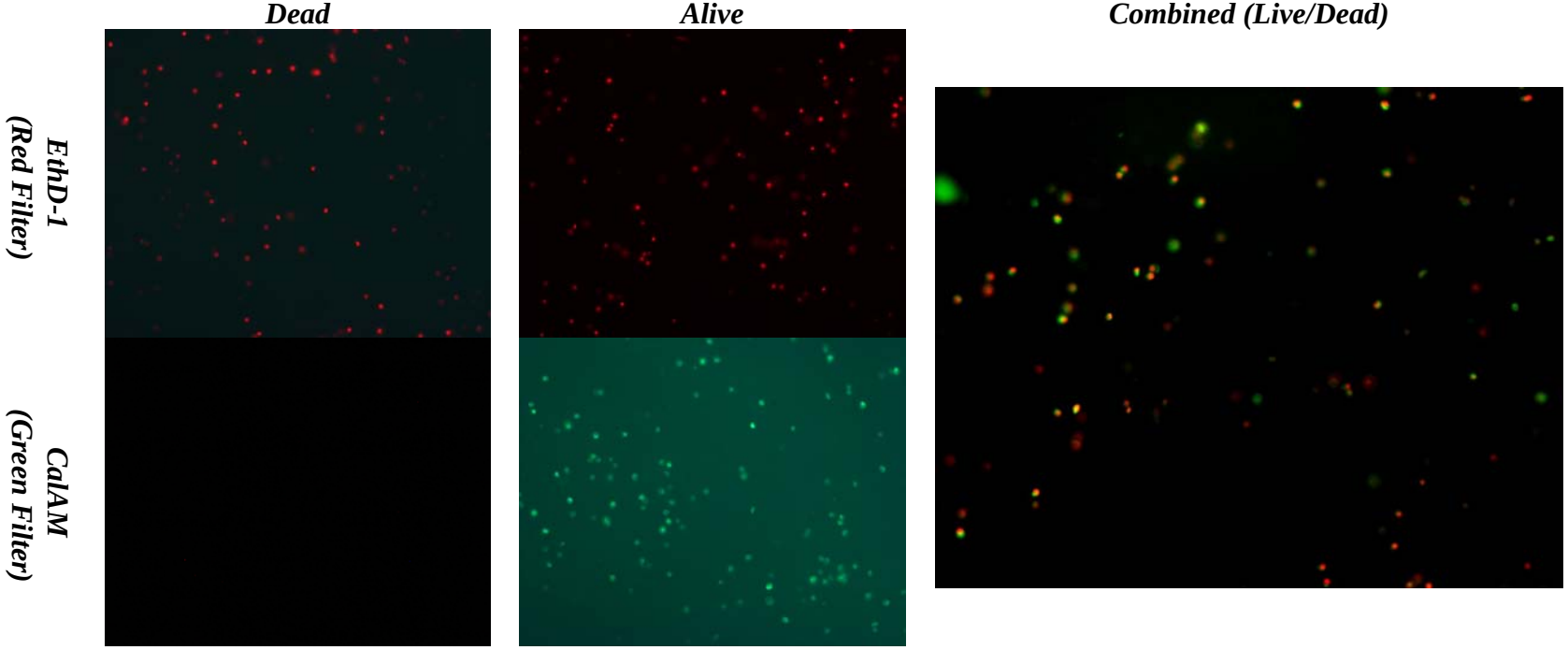

'Click' (50 mM $CuSO_4$, 10 mM NaAscorbate, 20 mM EDTA)

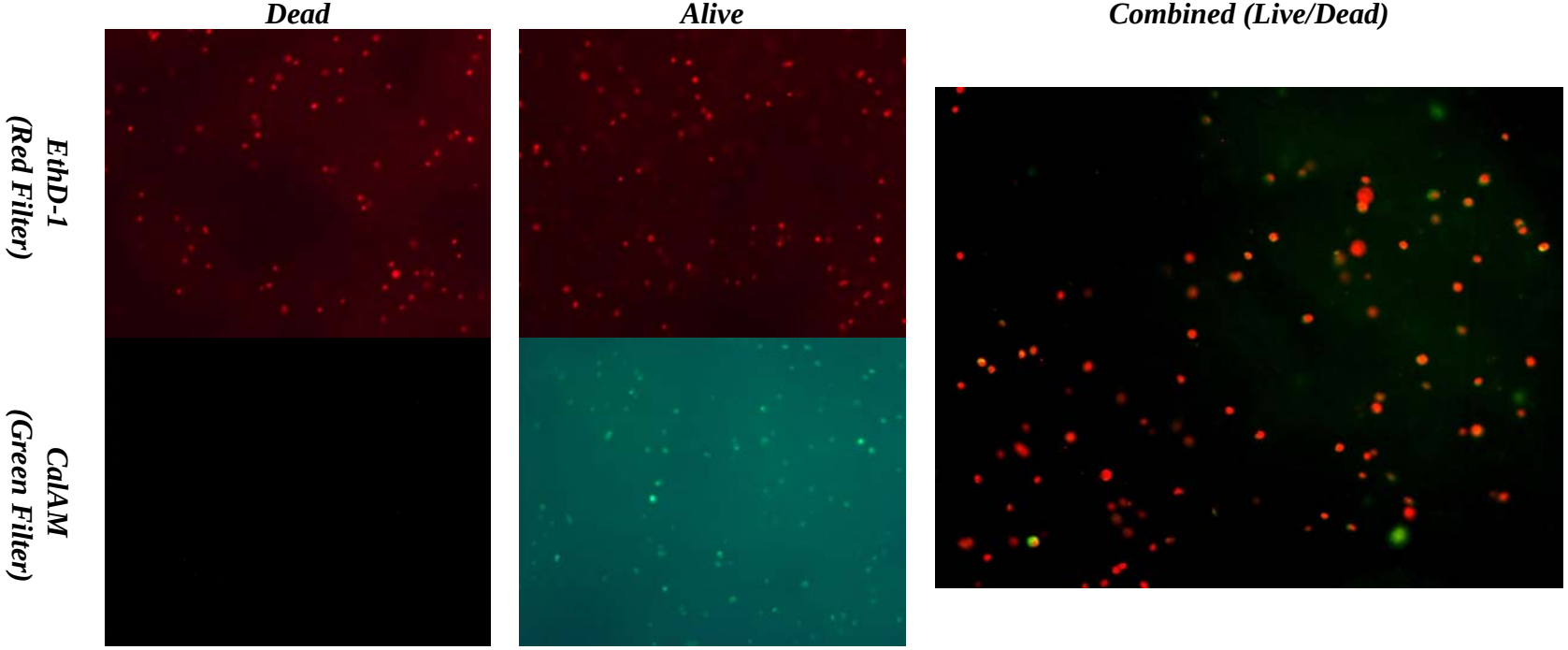

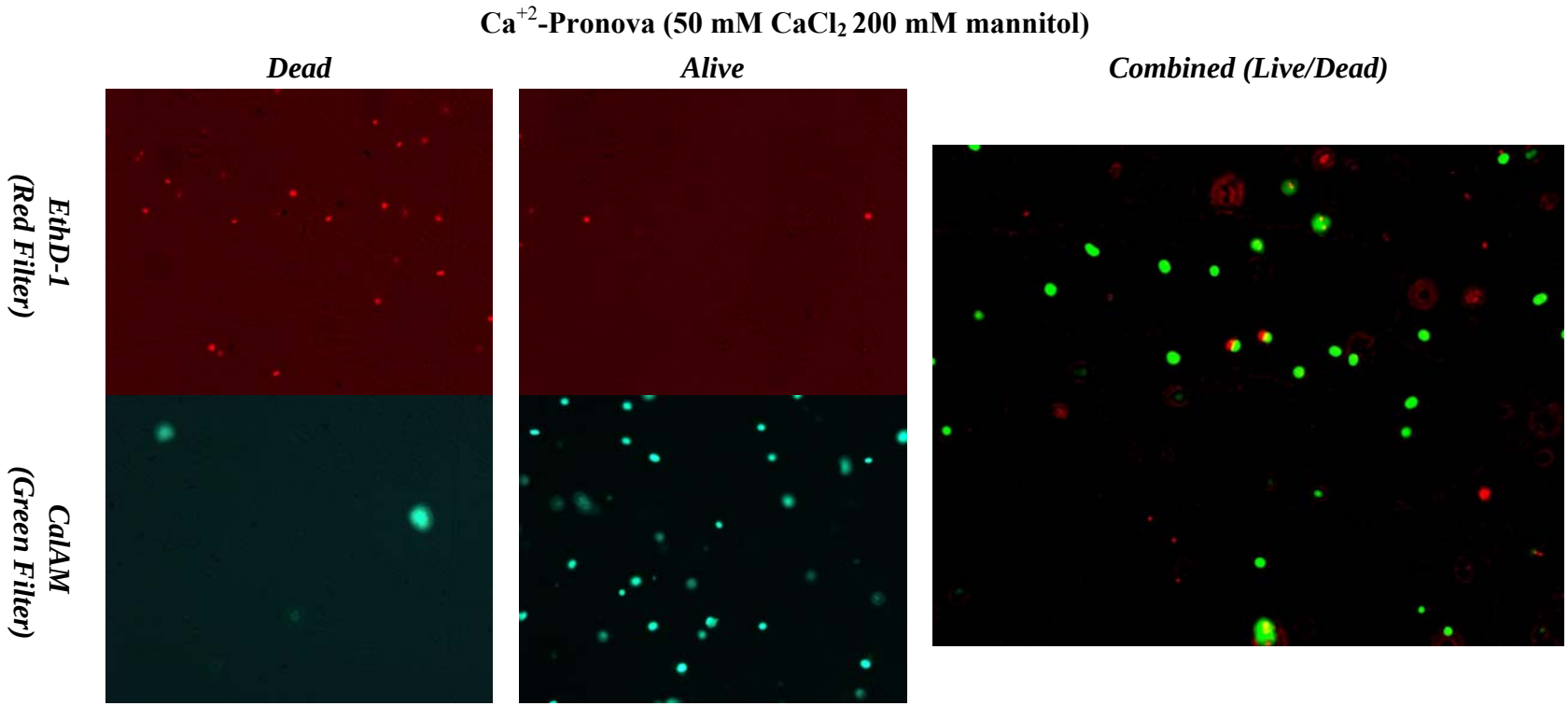

Figure 45. Representative pictures of RIN-5F encapsulated in either ionic and/or covalent crosslinked capsules.
The capsules were sandwiched in between two microscope slides to destroy the capsule such that more cells could be visualized at the plane of focus for the microscope. The 'click' capsules were noticeably more difficult to sandwich between glass slides than Ca^{+2}-crosslinked Pronova crosslinked capsules.

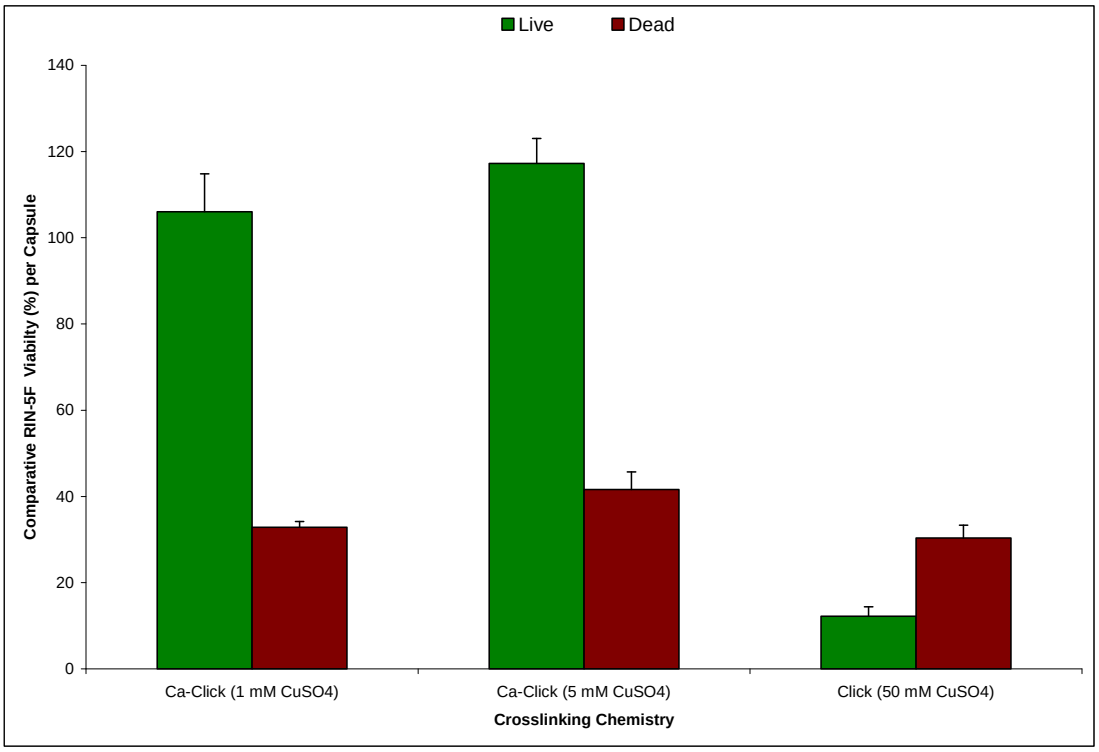

Figure 46. Comparative live/dead viability of encapsulated RIN-5F.
RIN-5F was encapsulated in functionalized Aln via ionic and/or covalent crosslinking at $8x10^5$ cells/mL. The relative viability was determined utilizing the Live/Dead ® Assay. Four-five capsules per well were seeded in a 96-well plate. Data shown are mean ±1 standard deviation of 4 replicate wells per condition.

6.4 Conclusions

In conclusion, a number of observations can be made from attempting to optimize the experimental conditions for producing stable and biocompatible encapsulating constructs. First, RIN-5F cells are an excellent and applicable cell line for determining appropriate experimental conditions for creating a matrix for a potential bioartificial pancreas. These cells produce a robust and continuous amount of insulin whereas islets of Langerhans need to be externally stimulated into producing insulin. Second, significant and quantifiable amounts of insulin can be measured up to 72 hrs post encapsulation. Therefore, for these experiments 72 hrs was the chosen time point

for determining the affect of 'click' crosslinking conditions on insulinoma function compared to ionic crosslinking conditions. Third, decreasing the amount of Cu^{+2} and limiting the exposure of RIN-5F cells to EDTA lead to increased insulin production compared to capsules containing only 'click' crosslinking. Finally, the viability of encapsulated RIN-5F cells can not only be quantified utilizing the Live/Dead® assay and the viability results should be used in conjunction with the insulin results when assessing the overall health and function of encapsulated RIN-5F.

6.5 Future Work

There are a number of experiments that can be done in the future to optimize the utilization of 'click' chemistry of Aln for the encapsulation of cells. For example, an experiment designed to use even lower concentrations of Cu^{+2} to determine if the 'click' reaction can be catalyzed and provided adequate covalent crosslinking while minimizing Cu^{+2}-associated toxicity could be performed. Another experiment could explore the utilization of different chelating agents like citrate. EDTA itself is toxic towards cells as it chelates divalent metal ions besides Cu^{+2} that are necessary for cell function. As EDTA chelates divalent cations, protons are released lowering the overall pH of the solution. An overtly acidic environment is also potentially harmful to cells. Other classified 'click' reactions could be employed to minimize cell toxicity. For example, Bertozzi et al. [57, 58] produced a nontoxic 'click' reaction without copper to label developing fish embryos. Currently, the reagents require a lengthy synthesis and are not yet commercially available. But in the future this technique might be useful for the encapsulation of other cell types. Finally, other assays can be employed to assess viability and proliferation of encapsulated cells.

Such assays, like those based on nontoxic Alamar Blue, might be used to assess whether cells have enough energy to proliferate. The Live/Dead® assay was able to distinguish between cells that were 'dead' based on an intact nuclear membrane and 'live' cells based on esterase activity. However, in these experiments the insulinoma cells should still be proliferating and this could not be addressed by the Live/Dead assay.

Chapter 7: Encapsulation of Islets of Langerhans

7.1 Introduction

Optimization of 'click' reagents for cellular encapsulation was determined utilizing RIN-5F cells in Chapter 6. RIN-5F is an insulinoma cell line composed of immortal rat β-cells. The islet cluster is composed of three main different cell types, each responsible for producing a different endocrine byproduct: β-cells (insulin), α-cells (glucagon), and δ-cells (somatostatin). Since RIN-5F cells continuously produce insulin without glucose stimulation, cell survival and function in the presence of potentially toxic 'click' reagents could be studied and maximized. In these experiments, the results from Chapter 6 were utilized for encapsulation of primary porcine islet-like clusters in covalently crosslinked capsules employing 'click' chemistry. Islets encapsulated in 'click' capsules were subjected to a glucose challenge and the amount of insulin produced over a 24 hr period was compared to non-encapsulated islets and islets encapsulated in the traditional Ca^{2+}-crosslinked Aln capsules. Viability and capsule integrity was assessed after the 24 hr glucose challenge and compared between ionically and/or covalently crosslinked encapsulated islets.

7.2 Methods

7.2.1 Materials

Islet isolation grade collagenase, purchased from Fisher Bioreagents, was diluted with RPMI to a concentration of 5 mg/mL, aliquoted, and stored at -20^{o}C. Nicotinamide and D-glucose were purchased from Sigma. A 1.0 M stock solution of nicotinamide was prepared with RPMI, passed through a 0.22 μm sterile filter system, and stored at 4^{o}C. A stock solution of glucose was made by dissolving D-glucose in RPMI to a final concentration of 0.310 M. Complete culture medium was made with RPMI containing 10 % fetal calf serum, 2 mM glutamine, 100 U/mL penicillin, and 100 μg/mL streptomycin (CM). "Low" glucose culture medium was composed of RPMI-1640 with out glucose, 10 % fetal calf serum, 2 mM glutamine, 25 mM HEPES, and 2.22 mM glucose (40 mg %). "High" glucose culture medium was composed of RPMI-1640 without glucose, 10 % fetal calf serum, 2 mM glutamine, 25 mM HEPES, and 22.2 mM glucose (400 mg %). Medical grade Aln was purchased from Pronova (viscosity ≤ 100 mPas, Guluronate ≥ 60%) and reconstituted in sterile, LAL water to a concentration of 2.5% w/v and stored at 4^{o}C. A 2.5% w/v Aln solution composed of a 2:1:1 ratio of Aln, Aln-Alk, and Aln-Az was made with sterile, LAL water, passed through a 0.45 μm filter, and stored at 4^{o}C.

7.2.2 Isolation and Culture of Porcine Islets

Digestion of porcine pancreata is described in detail elsewhere[36]. Briefly, porcine pancreata harvested from euthanized Gottingen Minipigs were purchased from Marshall BioResources and shipped overnight in CM packaged on ice/ice packs.

Upon arrival, the tissue was cold but not frozen. The tissue was washed three times with aliquots of ice-cold PBS w/ Ca^{+2}, Mg^{+2} and 25 mM HEPES and then sliced into 1-2 mm pieces under aseptic conditions. This was followed by digestion for 30 min in 20 mL of 0.5 mg/mL collagenase under gentle agitation in a 37 ^{o}C water bath. The solution was then put to ice for 15 min to allow partially digested tissue to settle to the bottom of the tube. The supernatant was removed leaving behind approximately 2 mL of partially digested tissue and solution. To this pellet, 4 mL of 5 mg/mL stock collagenase was added and the solution was vigorously shaken for 10 min in a 37 ^{o}C water bath. Ice cold CM was added giving a final volume of 40 mL and the solution was allowed to settle for 15 min on ice. After this settling period, the supernatant was discarded and the settled islet-like clusters were resuspended in CM containing 10 mM nicotinamide. The solution was placed in a non-stick Petri dish and incubated overnight at 37^{o}C (5%CO_2/95% air at 70% humidity). Following this recovery period, islet-like clusters were blown up and transferred to a 50 mL tube were they were allowed to settle for 15 min. The supernatant was discarded and replaced with fresh CM containing 10 mM nicotinamide. The resulting solution was dispersed to non-stick Petri dishes and placed back into the incubator for another overnight incubation at 37^{o}C.

7.2.3 Dithizone Staining of Islet-like Clusters

A stock solution of DTZ (10mg/mL) was prepared as described in pervious studies[88, 89], aliquoted, and stored at -20^{o}C. Islets were added to a 96-well plate at ~$1.53x10^2$ cells/well and allowed to adhere overnight at 37^{o}C in 5%CO_2/95% air, at 70% humidity. The next day DTZ was added to each well at a final concentration of 100

μg/mL and the islets were allowed to incubate in the dark for 15 min. Following this incubation period, the wells were washed 3 times with PBS w/Ca^{+2}, Mg^{+2} and 25 mM HEPES to remove excess DTZ. Islet like clusters were observed under an inverted phase microscope and diameter of islets was measured by employing a calibrated eye piece.

7.2.4 Encapsulation of Porcine Islets

After approximately 48 hrs post digestion, porcine islets were passed through a 600 μm screen to remove any large, undigested tissue debris and combined. The solution was allowed to settle for 15 min where upon the supernatant was removed and put aside, leaving behind 5 mL of solution and settled islets. The cells were resuspended into solution. An aliquot was removed and the cell count was determined to be $1.02x10^3$ cells/mL. The cell solution was split into three equal batches, allowed to settle for another 15 min, and the supernatant was discarded leaving behind approximately 0.2 mL of settled islets in solution. The first batch of settled cells was resuspended in CM to total volume of 1.0 mL. Aliquots of 100 μL of islets were transferred to each well of a 24 well plate with a final cell concentration of $1.53x10^2$ cells/well.

For the second batch of settled islets, 0.8 mL of 2.5 % w/v Aln was added and carefully mixed yielding a homogenous 2% w/v Aln/cells (~$1.53x10^3$ cells/mL) mixture. This mixture was than passed through an electrostatic encapsulator as described in Chapter 6. After incubating in the gelation mixture for 30 min, the capsules were collected, washed 3X with CM, and immediately seeded to 24 well

plate yielding 11 islet containing capsules per well. The capsules were approximately 1.8-2.0 mm in diameter, spherical, and clear in appearance.

The third batch of settle islets (0.2 mL) was added to 0.8 mL of 2.5% w/v functionalized Aln (2:1:1 Aln, Aln-Alk, Aln-Az) yielding a homogenous 2% w/v Aln/cell solution. This was passed through an electrostatic encapsulator, as described previously, into a gelation bath composed of 50 mM $CaCl_2$, 200 mM mannitol, and 1 mM $CuSO_4$. The capsules were allowed to ionically gel for 20 min after which time they were collected, allowed to settle, and the gelation solution discarded. To the capsules, 10 mM NaAsc was added and the 'click' reaction was allowed to proceed for 2.5 min. The NaAsc solution was subsequently discarded and replaced with 3 aliquots of 20 mM EDTA until the capsules were clear in appearance. The entire gelation and 'click' reaction time was kept to 30-35 min. The capsules were washed with 3X CM and immediately seeded to a 24-well plate yielding 16 capsules per well.

7.2.5 Glucose Challenge Assay

Following overnight incubation at 37^{o}C, CM was removed and islets or encapsulated islets were washed twice with low glucose media. The plate containing islets, encapsulated islets, and low glucose media was incubated for 1 hr at 37^{o}C in 5%CO_2/95% air, at 70% humidity. After incubation for 1 hr, the low glucose media was removed from all the wells and replaced with either fresh 40 mg % glucose (low) or 400 mg % glucose (high) media. After the addition of glucose media to each well, the plate was incubated at 37^{o}C in 5%CO_2/95% air, at 70% humidity for up to 24 h. At 1, 3, 6 and 24 hr, 100 μL of supernatant was removed from each well and transferred to a clean, 96-well plate. The plate was centrifuged at 4^{o}C for 10 min and

the top 50 μL of supernatant from each well was transferred to another 96-well plate. These samples were frozen at -70^{o}C and later analyzed for insulin content utilizing an insulin EILSA. Following the glucose challenge, encapsulated islets (either ionically or covalently crosslinked) underwent Live/Dead staining to determine viability.

7.2.6 Insulin Assay

Frozen glucose challenge samples from encapsulated (either ionically or covalently crosslinked) and unencapsulated islets were thawed, equilibrated to room temperature, and assayed for insulin content. Samples were assayed according to Porcine/Canine Insulin ELISA (Alpco Diagnostics) instructions. Absorbance levels were measured at 465 nm utilizing a Tecan plate reader.

7.2.7 Encapsulated Porcine Viability

Viability of encapsulated islets was determined utilizing a Live/Dead ® Cell Viability kit as described in section 6.2.5 with some modifications. The final concentrations of CalAM and EthD-1 were 4 μM and 8 μM, respectively. Also, the incubation time was increased to 1 hr since islet-like clusters are composed of multiple cell types packed closely together. Capsules were not broken by sandwiching between a cover slip and microscope slide as this broke apart the islet.

7.2.8 Statistical Analysis

Data are expressed as mean ± standard deviation of *n* independent observations. Statistical significance was calculated using the two-tailed unpaired Student's *t*-test or ANOVA. A $p \leq 0.1$ was considered statistically significant.

7.3 Results

7.3.1 Dithizone Staining of Islet-like Clusters

DTZ is a commonly employed stain to identify pancreatic islets, staining them red in comparison to surrounding tissue. Zinc, which islets of Langerhans have in higher amounts of as compared to surrounding tissue, chelates with DTZ. The β-cells of islets employ zinc when packaging insulin. There are conflicting reports to what degree DTZ is toxic towards islets so representative islet-like clusters were utilized for staining[88]. As seen in Figure 47, islet-like clusters that had been isolated from the neonatal porcine pancreas 72 hrs after digestion were stained red by DTZ indicating the presence of a large quantity of β-cells. β-cells make up to 80% of the cell distribution of an islet of Langerhans. Therefore, these islet-like clusters will be referred to as islets of Langerhans.

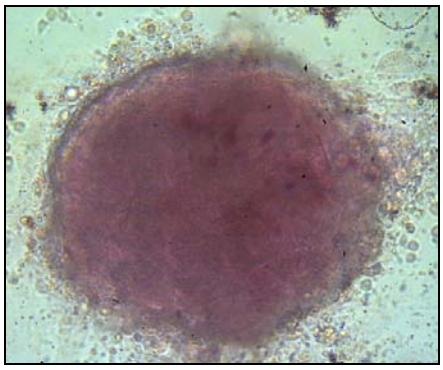

Figure 47. Islet-like cluster stained with dithizone.
Dithizone chelates with the Zinc present in β-cells turning the islet red. This makes DTZ a useful stain for identifying islets of Langerhans and assessing islet purity.

7.3.2 Glucose Challenge

Insulin secretion of free islets and encapsulated islets was measured for up to 24 hrs. The insulin content was adjusted per capsule for each measurement (Figure 48). This was done for a number of reasons. First, ionically crosslinked capsules swell as they

crosslink and continuing swelling when in an ionic medium such as CM. They also degrade or burst when in cell culture. Therefore, if the volume of an ionically crosslinked capsule was employed to determine absolute cell number present the count would be artificially high. Second, not all of the Aln/cell mixture is passed through the microencapsulator; some of the mixture remains behind in the syringe. Therefore, not all the Aln/cell mixture is made into a capsule. The number of capsules per well can be absolutely determined while adjusting for the number of cells per well would be an estimate. An estimate for the number of capsules that could be formed from 0.1 mL was utilized for adjusting the insulin content of free islets. The diameter of ionically or covalently crosslinked capsules typically ranges from 1.8 to 2.2 mm in diameter which corresponds to 17-32 capsules per 0.1 mL volume. A conservative estimate of 17 "capsules" could be made from 0.1 mL of islets given that the entire volume would not be made into capsules. Unencapsulated islets, free in solution, produced significantly more insulin after 24 hrs than either Ca^{+2}- or Ca^{+2}-'click' crosslinked encapsulated islets when assuming that the volume of free islets is equivalent to 17 capsules ($p \leq 0.05$).

Unencapsulated islets or free islets were incubated for 1 hr in low glucose media (40 mg%) and then exposed to either low glucose media (40 mg %) or high glucose media (400 mg%) for up to 24 hrs (Figure 48). For free islets in either low or high glucose media, there was no significant difference in insulin production at 1, 3, and 6 hr ($p \leq 0.05$). Only after 6 hr of exposure to either low glucose media or high glucose media could a significant difference in insulin production of free islets be discerned ($p \leq 0.1$).

Islets encapsulated in Ca^{+2}-crosslinked Aln also underwent a glucose challenge as described above. No difference in insulin production could be determined until 24 hrs between encapsulate islets in high glucose media compared to low glucose media ($p \leq 0.05$). Ca^{+2}-crosslinked encapsulated islets exposed to low glucose media (40 mg%) did not produce a significant amount of insulin over the entire time course of the experiment compared to the first time point (1 hr) (Figure 48). However, Ca^{+2}-crosslinked encapsulated islets did produce significant amounts of insulin over time when exposed to high glucose media (400 mg%) ($p \leq 0.05$). In general, Ca^{+2}-crosslinked encapsulated islets produced increasing amounts of insulin over time in either low or high glucose media.

Finally, islets encapsulated with ionic and covalent (Ca^{+2} and 'click') crosslinking underwent a glucose challenge (Figure 48). There was no significant difference between the amounts of insulin produced by the encapsulated islets in high glucose media as compared to encapsulated islets in low glucose media until after 24 hrs of exposure ($p \leq 0.1$). Ca^{+2}-'click' encapsulated islets produced significant amounts of insulin after 24 hrs when in low glucose media. In high glucose media, Ca^{+2}-'click' encapsulated islets produced significant amounts of insulin over the time course of the experiment with significant increases ($p \leq 0.1$) in insulin production after 3 hrs. After adjusting for the number of capsules per well, there was no significant difference in insulin production from Ca^{+2}-'click' capsules as compared to Ca^{+2}-crosslinked capsules in low glucose media. In high glucose media, Ca^{+2}-'click' encapsulated islets produced a comparable amount of insulin as compared to Ca^{+2} - crosslinked capsules.

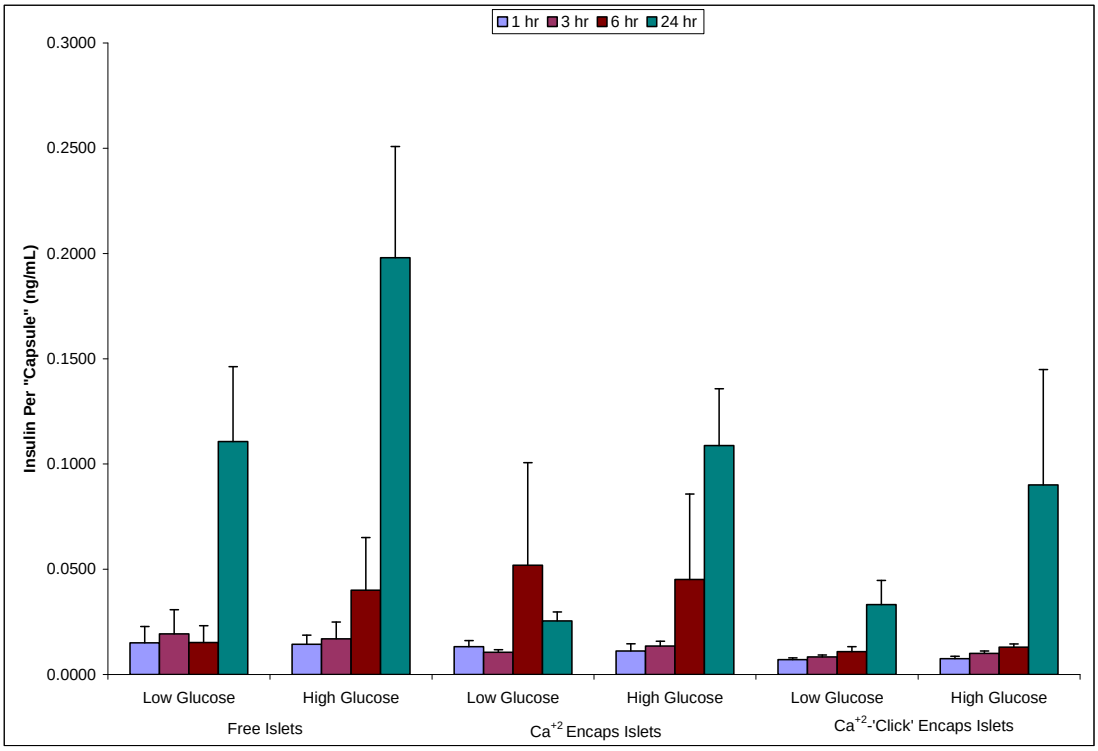

Figure 48. Insulin secretion of free and encapsulated islets for up to 24 hrs.
Porcine islets of Langerhans were seeded into a 24-well plate as either free in solution or encapsulated in Ca^{+2} or Ca^{+2}-'click'- crosslinked Aln. The free islets were allowed to adhere overnight and then all the islet conditions were exposed to either low (40 mg%) or high (400 mg%) glucose media for up to 24 hrs. Supernatant samples were taken at 1, 3, 6 and 24 hr to be measured for insulin content. Data shown are mean ± 1 standard deviation of 4 replicate wells per condition.

7.3.3 Porcine Viability

The viability of porcine islets was determined 72 hrs post digestion and then again 24 hrs later. A representative sample of unencapsulated and encapsulated islets was employed to determine the starting viability 72 hrs post digestion and 24 hrs post encapsulation or seeding (Figure 49). Both types of crosslinked capsules contained live and dead cells however it did appear that the Ca^{+2}-'click' capsules contained a higher amount of dead islets as compared to Ca^{+2}-crosslinked capsules (Figure 49).

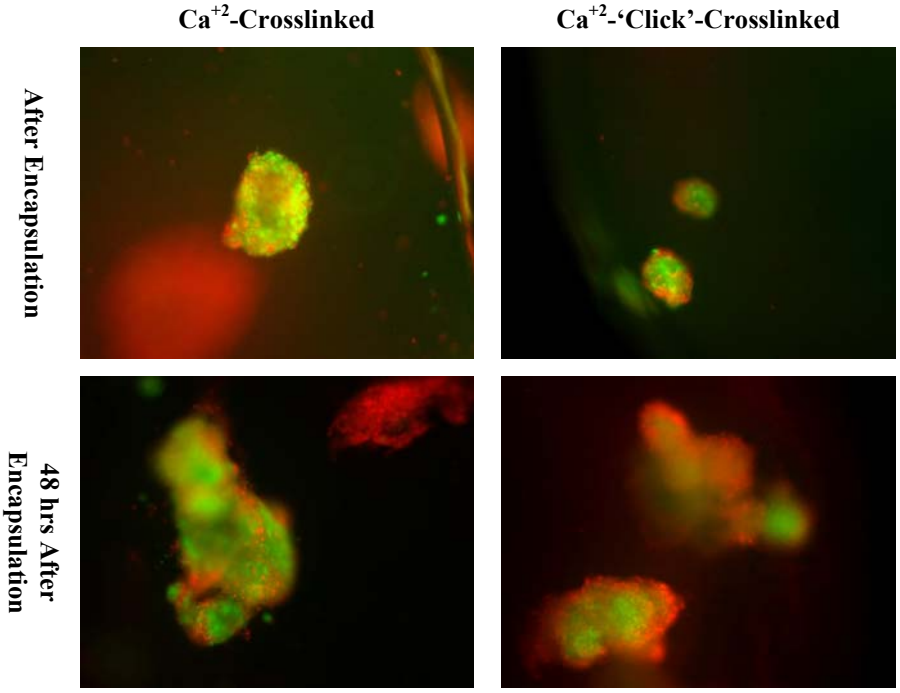

Figure 49. Representative images of encapsulated porcine islets in ionic (Ca^{+2}) and/ or covalently (Ca^{+2}-'click') crosslinked alginate capsules labeled with EthD-1 and CalAM.
To obtain the images of encapsulated islets, the capsules were sandwiched in between a cover slip and microscope slide. Capsules were not physically broken as this would also destroy the majority of encapsulated islets present. Islet cells were labeled with either CalAM which stains live cells green or EthD-1 which stains dead cells red. Both types of crosslinked Aln capsules contain live and dead stained cells after encapsulation and 48 hrs after that. Ca^{+2}-'click' capsules seem to have a qualitatively higher number of dead cells present after 48 hrs as compared to islets encapsulated in Ca^{+2}-crosslinked Aln.

7.3.4 Capsule Stability and Appearance

Ionically (Ca^{+2}) crosslinked capsules were clear and spherical in appearance after encapsulation of islets of Langerhans. The glucose challenge of encapsulated and unencapsulated islets was performed 24 hrs post encapsulation and/or seeding of islets into a 96-well plate. After 24 hrs, capsules containing islets composed of Ca^{+2}-crosslinked Aln had begun to burst with visible cracks and deformations observed in the majority of the capsules. After 48 hrs post encapsulation capsules of either crosslinking chemistry method were still present in all the wells. Ca^{+2}-crosslinked capsules had an average non-broken capsule diameter of 2.64 ±0.08 mm (left side of Or[pFigure 50). On the other hand, covalently crosslinked capsules containing islets

(right side of Or[pFigure 50) were much smaller in appearance (diameter = 1.80±0.05 mm) as compared to ionically crosslinked capsules and remained intact. No deformations in the capsule were present indicating a lesser degree of swelling and a much more structurally stable capsule. However, small tails were present on Ca^{+2}-'click' capsules as compared to Ca^{+2}-crosslinked capsules. Upon close inspection, individual islets can be distinguished with the naked eye in capsules of both crosslinking chemistries.

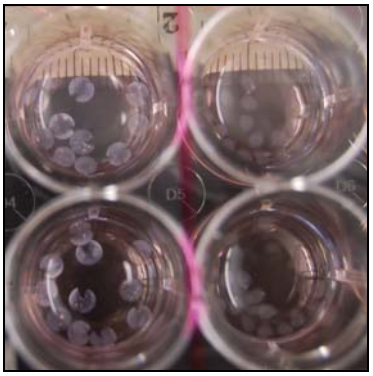

Or[pFigure 50. Capsule stability 48 hrs post encapsulation.
Ca^{+2}-crosslinked capsules have burst and the majority appears broken (left side of the figure) with an average diameter of 2.64±0.08 mm. Ca^{+2}-'click' capsules (right side of the figure) remained intact and exhibit a lesser degree on swelling as compared to Ca^{+2}-crosslinked capsules (1.80±0.05 mm) n =4 $p=1.9x10^{-6}$.

7.4 Conclusions

Islets encapsulated in Ca^{+2}-'click' capsules produced insulin over the time course of the experiment in response to a glucose challenge. These capsules are much more structurally stable compared to Ca^{+2}-crosslinked capsules over the time course of the experiment. Ca^{+2}-crosslinked capsules immediately started to swell to the point where the majority of the capsules were broken 48 hrs post encapsulation; exposing primary porcine islets to the surrounding media. Neither type of encapsulated islets produced as much insulin as free, unencapsulated islets. This may be due to impediment of the diffusion by the Aln structure. Islets were alive 1 hr and also at 48 hrs post

encapsulation in Ca^{+2}-'click' capsules. The islets were much more resilient to the 'click' reaction compared to the RIN-5F insulinoma cell line (Chapter 6). There are a number of possibilities for this. First, while Cu^{+2} is cytotoxic towards cells, the chelation with EDTA causes a sharp decrease in the solution pH. EDTA will also chelate other divalent cations, some of which might be necessary for cell function and survival. The sharp decrease in solution pH and the absence of vital ions might be more detrimental to cell survival and function than limited exposure to Cu^{+2}. EDTA washes were kept to 1.5 min instead of 3 min for Ca^{+2}-'click' encapsulated islets to minimize the amount of time islets were in a low pH solution. Second, islets are composed of a cluster of different cell types with β-cells composing of 60-80% of the population. All these cells are tightly packed together to form a single islet. This close packing of cells might infer protection for cells in the center of the islet. When observing islets encapsulated in Ca^{+2}-'click' capsules, the edges of the islet are bright red (indicating cell death) while the islet core is bright green (indicating live cells). Employing 'click' chemistry to covalently crosslink Aln increases the stability of capsules and does not destroy therapeutic cell function of cells encapsulated in these capsules.

7.5 Future Work

There are many avenues that can be explored in continuing this project. One necessary avenue would be to encapsulate islets in much smaller Aln capsules. Typically, capsule sizes range from 350-550 μm in diameter. This is done to increase the diffusion characteristics nutrients, hormone signal, and waste products into and out of the capsules for maintaining islet health. By encapsulating islets in much

smaller capsules that employ 'click' chemistry, the possible diffusion limitations associated with the reaction are also minimized. This could increase the 'click' reaction efficiency while limiting the exposure time of islets to 'click' reactants, specifically EDTA and Cu^{+2}. With such large capsules that were utilized in this dissertation, the EDTA chelation reaction could be monitored with the naked eye. As EDTA chelates $Cu^{+2/+1}$ the Aln capsule becomes clear with the middle still faintly blue in appearance. As the chelation reaction proceeds, this inner concentric sphere becomes smaller and smaller. By decreasing capsule size, the efficiency of this chelation reaction could possibly be increased and this could affect islet cell viability and function.

Another avenue that could increase cell survival might be to utilize different reactants or concentrations associated with the 'click' reaction. One example would be to utilize a different chelation reactant such as citrate. The reactant conditions were roughly optimized with RIN-5F cells but islets were surprisingly more resilient to the 'click' reaction. A series of more rigorous experiments should be performed that optimize the minimum reactant concentrations of EDTA, Cu^{+2}, and NaAsc while maintaining sufficient 'click' crosslinking.

Other experiments could be designed to test other types of 'click' reactions most notably the copperless 'click' reaction described by Bertozzi et al[57, 58]. Currently, the copperless 'click' reactants are not commercially available or are prohibitively expensive which is why they were not utilized in this dissertation. Also, employing other reagents that increase the efficiency of the 'click' reaction such as the accelerating ligand tris((1-benzyl-1H-1,2,3-triazol-4-yl)methyl)amine (TBTA) [90]

Other future research could explore improving the glucose challenge methodology for encapsulated islets. Given the limited number of islets that were harvested from the neonatal porcine pancreas all of them were employed for encapsulation. Typical experiments employ islets around 150 μm in diameter which are usually referred to as the islet equivalent (IEQ). Large islets secret less insulin per IEQ than small islets. By digesting more than one neonatal porcine pancreas and pooling samples, more islets could be recovered and islets based on size could be isolated. By employing smaller islets, the insulin production in response to a glucose challenge might be optimized. Insulin results need to be normalized to a standard number of islets. If the size of islets is relatively constant or has a narrow size distribution than insulin results should be normalized against islet number. For the large capsules that were employed in this dissertation, more than one islet was encapsulated per capsule. The exact number of islets varied from capsule to capsule. To achieve an absolute cell count would be extremely labor intensive. When decreasing the capsule size, it is easier to achieve one islet per capsule but the Aln/cell solution needs to be sufficiently dilute and some capsules will contain no islets. Future experiments should involve seeding plates by hand to ensure the same numbers of islets are present in each well.

Finally, other types of therapeutic cells could be encapsulated in Aln crosslinked via divalent cations and ‘click’ chemistry. The reactions conditions would have to be optimized for the cell type employed but the possibilities are substantial.

Chapter 8: Overall Conclusions and Discussion

The focus of this dissertation was to investigate the possibility of employing 'click' chemistry as a means to covalently crosslink Aln and/or HA to increase the stability and biocompatibility of novel biomaterials for the encapsulation of therapeutic cells. Employing covalent crosslinking techniques would increase the durability of Aln by increasing the stability to the hydrogel structure. Even a minimal amount of covalent crosslinking in addition to traditional ionic crosslinking would be beneficial to maintaining the hydrogel structure by maintaining a critical concentration of ionic crosslinking.

Functionalization of Aln or HA was confirmed by FTIR, NMR, and/or GPC techniques. The DPn of the functionalized polysaccharides could not be resolved with NMR due to the complex spectra of both HA and Aln. Functionalization of Aln with Az functional groups resulted in an increase in the overall branching which was determined by GPC and observationally in the lab due to Aln-Az's inability to form stable hydrogel structures in the presence of Ca^{+2}. Functionalization of Aln with Alk end groups did not greatly influence the overall branching or affect Aln-Alk's ability to form stable hydrogel structures in the presence of Ca^{+2}. If the MW of the functionalized polysaccharides was low, the effect of branching or confirmation of functionalization could not be determined via GPC.

In this work, alginate capsules that were covalently crosslinked via 'click' chemistry exhibited superior stability and diffusion properties as compared to ionically crosslinked capsules. The diffusion properties of these 'click' capsules exhibited characteristic 'Fickian' diffusion while ionically crosslinked capsules did

not. The value of the D for ionically crosslinked capsules was dependent on the ionic strength of the solvent and approached the Do as the ionic strength of the solvent increased indicating rapid capsule degradation. 'Click' crosslinked capsules had a similar MWCO as compared to ionically crosslinked capsules. This demonstrates the 'click' crosslinking could be utilized in fabricating an immune barrier from a biomaterial such as Aln. Small components of the immune system such as NO, oxygen radicals, or small polypeptides could still easily diffuse through 'click' crosslinked Aln capsules but they would also diffuse through ionically crosslinked Aln capsules. However, 'click' capsules are also impermeable to larger components of the immune system such as immunoglobulins or cytokines just like ionically crosslinked capsules. 'Click' capsules have the same permeability characteristics as ionically crosslinked capsules. Capsules that utilize 'click' crosslinking allowed the diffusion of nutrients and cell products while maintaining hydrogel structure.

The inflammatory potential of functionalized polysaccharides was determined as a function of MW (HA) and functional group (Az or Alk). Modest increases in inflammatory potential were found for functionalized polysaccharides and LMW HA under simulated high inflammatory states (RAW264.7 cells in the presence of γ-IFN and/or LPS). Further studies need to be conducted to determine if these increases are the result of the biomaterial MW (as in the case of HA) due to the degree of functionalization, or due to contamination.

The cytotoxicity of all the reagents involved in the 'click' reaction was also studied with relevant concentrations and time points to establish conditions that provided adequate 'click' catalyzation while maximizing biocompatibility. In general,

at the concentrations tested none of the reactants were found to be overtly toxic. However, Cu^{+2} was found to interfere with the fluorescence of the live/dead assay giving false results. Another cytotoxic assay should be considered to confirm that the 'click' reactants are not cytotoxic under defined time points and concentrations.

Primary porcine islets of Langerhans were encapsulated in ionically crosslinked and/or covalently crosslinked Aln capsules. Islets encapsulated in capsules that utilized 'click' crosslinking were responsive to glucose stimulation and secreted insulin in comparable amounts to ionically encapsulated islets. Encapsulated islets were confirmed to contain live, functioning islets. However, islets in capsules that employed 'click' crosslinking were found to have higher number of dead cells. Further research should be conducted to better optimize the 'click' reaction conditions for islet cell encapsulation. However, the results from the glucose stimulation of encapsulated islets in ionically and covalently crosslinked capsules were promising.

Although this dissertation focused on employing 'click' crosslinking of Aln for a bioartificial pancreas many of the general conclusions found here could be applied to other diverse applications that utilize biopolymer capsules, such as drug delivery vehicles, or other cell encapsulation/scaffold therapies. The results from this research project have demonstrated that long term stability of these biopolymer capsules can be increased by utilizing 'click' chemistry.

References

1. de Vos,P., Hamel,A.F., & Tatarkiewicz,K. Considerations for Successful Transplantation of Encapsulated Pancreatic Islets. *Diabetologia* **25**, 159-173 (2002).

2. Orive,G. *et al.* History, challenges and perspectives of cell microencapsulation. *Trends in Biotechnology* **22**, 87-92 (2004).

3. Kuo,C. & Ma,P.X. Ionically crosslinked alginate hydrogels as scaffolds for tissue engineering: part 1. structure, gelation rate, and mechanical properties. *Biomaterials* **22**, 511-521 (2001).

4. Kulseng,B. *et al.* Transplantation of alginate microcapsules: generation of antibodies against alginate and encapsulated porcine islet-like cell clusters. *Transplantation* **67**, 978-984 (1999).

5. Zimmermann,U. *et al.* Production of mitogen-contamination free alginates with variable ratios of mannuronic acid to guluronic acid by free flow electrophoresis. *Electrophoresis* **13**, 269-274 (1992).

6. [Anon] Economic costs of diabetes in the U.S. In 2007. *Diabetes Care* **31**, 596-615 (2008).

7. Thanos,C.G. & Elliott,R.B. Encapsulated porcine islet transplantation: an evolving therapy for the treatment of Type I diabetes. *Expert Opinion on Biological Therapy* **9**, 29-44 (2009).

8. Thu,B. Alginate polycation microcapsules: a study of some molecular and functional properties relevant to their use as a bioartifical pancreas. 1996. Trondehim, Norges tekniski-naturvitenskapelige universitet, Institutt for Bioteknologi.
Ref Type: Thesis/Dissertation

9. Morch,Y.A., Donati,I., Strand,B.L., & Skjak-Braek,G. Effect of Ca+2, Ba+2, and Sr+2 on alginate microbeads. *Biomacromolecules* **7**, 1471-1480 (2006).

10. Thanos,C.G. *et al.* Formulating the alginate-polyornithine biocapsule for prolonged stability: Evaluation of composition and manufacturing technique. *Journal of Biomedical Materials Research Part A* **83A**, 216-224 (2007).

11. van Hoogmoed,C.G., Busscher,H.J., & de Vos,P. Fourier transform infrared spectroscopy studies of alginate-PLL capsules with varying

compositions. *Journal of Biomedical Materials Research Part A* **67A**, 172-178 (2003).

12. Chandy,T., Mooradian,D.L., & Rao,G.H.R. Evaluation of modified alginate-chitosan-polyethylene glycol microcapsules for cell encapsulation. *Artificial Organs* **23**, 894-903 (1999).

13. Huguet,M.L. & Dellacherie,E. Calcium alginate beads coated with chitosan: Effect of the structure of encapsulated materials on their release. *Process Biochemistry* **31**, 745-751 (1996).

14. ASTM,F. Standard guide for characterization and testing of hyaluronan as starting materials intended for use in biomedical and tissue engineered medical product application. *Annual Book of ASTM Standards* **13.01**, 1377-1385 (2006).

15. Balazs,E.A. Hyaluronan as an ophthalmic viscoelastic device. *Current Pharmaceutical Biotechnology* **9**, 236-238 (2008).

16. Turner,W.S. *et al.* Human hepatoblast phenotype maintained by hyaluronan hydrogels. *Journal of Biomedical Materials Research Part B-Applied Biomaterials* **82B**, 156-168 (2007).

17. Zavan,B. *et al.* Extracellular matrix-enriched polymeric scaffolds as a substrate for hepatocyte cultures: in vitro and in vivo studies. *Biomaterials* **26**, 7038-7045 (2005).

18. Yoon,D.M., Curtiss,S., Reddi,A.H., & Fisher,J.P. Addition of Hyaluronic Acid to Alginate Embedded Chondrocytes Interferes with Insulin-like Growth Factor-1 Signaling In Vitro and In Vivo. *Tissue Engineering Part A* **15**, 3449-3459 (2009).

19. Aigner,J. *et al.* Cartilage tissue engineering with novel nonwoven structured biomaterial based on hyaluronic acid benzyl ester. *Journal of Biomedical Materials Research* **42**, 172-181 (1998).

20. Oerther,S. *et al.* Hyaluronate-alginate gel as a novel biomaterial: Mechanical properties and formation mechanism. *Biotechnology and Bioengineering* **63**, 206-215 (1999).

21. Lindenhayn,K. *et al.* Retention of hyaluronic acid in alginate beads: aspects for in vitro cartilage engineering. *Journal of Biomedical Materials Research* **44**, 149-155 (1999).

22. Kelly,M.A., Moskowitz,R.W., & Lieberman,J.R. Hyaluronan therapy: looking toward the future. *Am J Orthop* **33**, 23-28 (2004).

23. Bae,K.H., Yoon,J.J., & Park,T.G. Fabrication of hyaluronic acid hydrogel beads for cell encapsulation. *Biotechnology Progress*(2006).

24. Burdick,J.A., Chung,C., Jia,X., Randolph,M.A., & Langer,R. Controlled degradation and mechanical behavior of photopolymerized hyaluronic acid networks. *Biomacromolecules* **6**, 386-391 (2005).

25. Khademhosseini,A. *et al.* Micromolding of photocrosslinkable hyaluronic acid for cell encapsulation and entrapment. *Journal of Biomedical Materials Research Part A* **79A**, 522-532 (2006).

26. Jeon,O., Bouhadir,K.H., Mansour,J.M., & Alsberg,E. Photocrosslinked alginate hydrogels with tunable biodegradation rates and mechanical properties. *Biomaterials* **30**, 2724-2734 (2009).

27. Dusseault,J. *et al.* Microencapsulation of living cells in semi-permeable membranes with covalently cross-linked layers. *Biomaterials* **26**, 1515-1522 (2005).

28. Cho,S.H., Oh,S.H., & Lee,J.H. Fabrication and characterization of porous alginate/polyvinyl alcohol hybrid scaffolds for 3D cell culture. *Journal of Biomaterials Science-Polymer Edition* **16**, 933-947 (2005).

29. Gattas-Asfura,K.M. & Stabler,C.L. Chemoselective Cross-Linking and Functionalization of Alginate via Staudinger Ligation. *Biomacromolecules* **10**, 3122-3129 (2009).

30. Crescenzi,V., Cornelio,L., Di Meo,C., Nardecchia,S., & Lamanna,R. Novel hydrogels via click chemistry: Synthesis and potential biomedical applications. *Biomacromolecules* **8**, 1844-1850 (2007).

31. Di Meo,C. *et al.* Novel types of carborane-carrier hyaluronan derivatives via "Click Chemistry". *Macromolecular Bioscience* **8**, 670-681 (2008).

32. Lutz,J.F. & Zarafshani,Z. Efficient construction of therapeutics, bioconjugates, biomaterials and bioactive surfaces using azide-alkyne "click" chemistry. *Advanced Drug Delivery Reviews* **60**, 958-970 (2008).

33. Shi,Q., Chen,X.S., Lu,T.C., & Jing,X.B. The immobilization of proteins on biodegradable polymer fibers via click chemistry. *Biomaterials* **29**, 1118-1126 (2008).

34. Coleman,J.W. Nitric Oxide in Immunity and Inflammation. *International Immunopharmacology* **1**, 1397-1406 (2001).

35. Lyle,D.B. *et al.* Screening biomaterials for stimulation of nitric oxide-mediated inflammation. *Journal of Biomedical Materials Research Part A* **90A**, 82-93 (2009).

36. Lyle,D.B., Shallcross,J.C., & Langone,J.J. Sensitivity of insulin production from encapsulated islets to endotoxin-stimulated macrophage inflammatory mediators. *Journal of Biomedical Materials Research Part A* **91A**, 1221-1238 (2009).

37. Ryrfeldt,A. Drug-induced inflammatory responses to the lung. *Toxicology Letters* **112-113**, 171-176 (2000).

38. Swindle,E.J. & Metcalfe,D.D. The Role of Reactive Oxygen Species and Nitric Oxide in Mast Cell-dependent Inflammatory Processes. *Immunological Reviews* **217**, 186-205 (2007).

39. Tang,L., Liu,L., & Elwing,H.B. Complement activation and inflammation triggered by biomaterial surfaces. *Journal of Biomedical Materials Research* **41**, 333-340 (1998).

40. Kroncke,K.D., Brenner,H.H., Rodriguez,M.L., & Etzkorn,K. Pancreatic islet cells are highly susceptible towards the cytotoxic effects of chemically generated nitric oxide. *Biochimica et Biophysica Acta* **1182**, 221-229 (1993).

41. Wiegand,F., Kroncke,K.D., & Kolb-Bachofen,V. Macrophage-Generated Nitric Oxide As Cytotoxic Factor in destruction of Alginate-Encapsulated Islets. *Transplantation* **56**, 1206-1212 (1993).

42. Breger,J.C., Lyle,D.B., Shallcross,J.C., Langone,J.J., & Wang,N.S. Defining Critical Inflammatory Parameters for Endotoxin Impurity in Manufactured Alginate Microcapsules. *Journal of Biomedical Materials Research Part B-Applied Biomaterials* **91B**, 755-765 (2009).

43. Kim,Y.M. & Son,K. A nitric oxide production bioassy for interferon-g. *Journal of Immunological Methods* **198**, 203-209 (1996).

44. Lowenstein,C.J. *et al.* Macrophage nitric oxide synthase gene: two upstream regions mediate induction by interferon g and lipopolysaccharide. *Proc. Natl. Acad. Sci. USA* **90**, 9730-9734 (1993).

45. Tsikas,D. Methods of Quantitative Analysis of the Nitric Oxide Metabolites Nitrite and Nitrate in Human Biological Fluids. *Free Radical Research* **39**, 797-815 (2005).

46. Kroncke,K.D., Rodriguez,M.L., Kolb,H., & Kolb-Bachofen,V. Cytotoxicity of activated rat macrophages against synfeneic islet cells is arginine-dependent, correlates with citrulline and nitrite concentration and is identical to lysis by the nitric oxide donor nitroprusside. *Diabetologia* **36**, 17-24 (1993).

47. Matsuura,M., Saito,S., Okamura,H., & Hirai,Y. A pathway through interferon-g is the main pathway for induction of nitric oxide upon with bacterial lipoploysaccharide in mouse peritoneal cells. *European Journal of Biochemistry* **270**, 4016-4025 (2003).

48. Zhuang,J.C. & Wogan,G.N. Growth and viability of macrophages continuously stimulated to produce nitric oxide. *Proc. Natl. Acad. Sci. USA* **94**, 11875-11880 (1997).

49. Chae,S.Y., Lee,M., Kim,S.W., & Bae,Y.H. Protection of insulin secreting cells from nitric oxide induced cellular damage by crosslinked hemoglobin. *Biomaterials* **25**, 843-850 (2004).

50. Kaneto,H., Fujii,H., Seo,H.G., Suzuki,K., & Matsuoka,T. Apoptotic cell death triggered by nitric oxide in pancreatic beta-cells. *Diabetes* **44**, 733-739 (1995).

51. van Schifgaarde,R. & de Vos,P. Factors influencing the properties and perfomance of microcapsules for immunoprotection of pancreatic islets. *Journal of Molecular Methods* **77**, 199-205 (1999).

52. Kolb,H.C., Finn,M.G., & Sharpless,K.B. Click chemistry: Diverse chemical function from a few good reactions. *Angewandte Chemie-International Edition* **40**, 2004-+ (2001).

53. Kolb,H.C. & Sharpless,K.B. The growing impact of click chemistry on drug discovery. *Drug Discovery Today* **8**, 1128-1137 (2003).

54. Simon,C.G., Stephens,J.S., Dorsey,S.M., & Becker,M.L. Fabrication of combinatorial polymer scaffold libraries. *Review of Scientific Instruments* **78**, (2007).

55. Binder,W.H. & Sachsenhofer,R. 'Click' chemistry in polymer and materials science. *Macromolecular Rapid Communications* **28**, 15-54 (2007).

56. Wu,P. *et al.* Multivalent, bifunctional dendrimers prepared by click chemistry. *Chemical Communications*5775-5777 (2005).

57. Baskin,J.M. & Bertozzi,C.R. Bioorthogonal click chemistry: Covalent labeling in living systems. *QSAR & Combinatorial Science* **2007**, 1211-1219 (2007).

58. Baskin,J.M. *et al.* Copper-free click chemistry for dynamic in vivo imaging. *Proceedings of the National Academy of Sciences of the United States of America* **104**, 16793-16797 (2007).

59. Scrafton,D.K., Taylor,J.E., Mahon,M.F., Fossey,J.S., & James,T.D. "Click-fluors": Modular fluorescent saccharide sensors based on a 1,2,3-triazole ring. *Journal of Organic Chemistry* **73**, 2871-2874 (2008).

60. Speers,A.E. & Cravatt,B.F. Profiling enzyme activities in vivo using click chemistry methods. *Chemistry & Biology* **11**, 535-546 (2004).

61. von Maltzahn,G. *et al.* In vivo tumor cell targeting with "Click" nanoparticles. *Bioconjugate Chemistry* **19**, 1570-1578 (2008).

62. Morales-Sanfrutos,J., Ortega-Munoz,M., Lopez-Jaramillo,J., Hernandez-Mateo,F., & Santoyo-Gonzalez,F. Synthesis of molecular nanocages by click chemistry. *Journal of Organic Chemistry* **73**, 7772-7774 (2008).

63. ASTM,F. Standard guide for characterization and testing of alginates as starting materials intended for use in biomedical and tissue-engineered medical products application. *Annual Book of ASTM Standards* **13.01**, 1074-1081 (2006).

64. Gottlieb,H.E., Kotlyar,V., & Nudelman,A. NMR chemical shifts of common laboratory solvents as trace impurities. *Journal of Organic Chemistry* **62**, 7512-7515 (1997).

65. Toffanin,R. *et al.* Nmr-Studies of Oligosaccharides Derived from Hyaluronate - Complete Assignment of H-1 and C-13 Nmr-Spectra of Aqueous Disaccharides and Tetra-Saccharides, and Comparison of Chemical-Shifts for Oligosaccharides of Increasing Degree of Polymerization. *Carbohydrate Research* **245**, 113-128 (1993).

66. Alkrad,J.A., Mrestani,Y., Stroehl,D., Wartewig,S., & Neubert,R. Characterization of enzymatically digested hyaluronic acid using NMR, Raman, IR, and UV-Vis spectroscopies. *Journal of Pharmaceutical and Biomedical Analysis* **31**, 545-550 (2003).

67. F 2259-03 Standard Test Method for Determining the Chemical Composition and Sequence In Alginate by Proton Nuclear Magnetic Resonance (1H NMR) Spectroscopy. ASTM International , 1-5. 2008.
Ref Type: Generic

68. Clementi,F., Mancini,M., & Moresi,M. Rheology of alginate from Azotobacter vinelandii in aqueous dispersions. *Journal of Food Engineering* **36**, 51-62 (1998).

69. Holme,H.K., Davidsen,L., Kristiansen,A., & Smidsrod,O. Kinetics and mechanisms of depolymerization of alginate and chitosan in aqueous solution. *Carbohydrate Polymers* **73**, 656-664 (2008).

70. Zimm,B.H. & Stockmayer,W.H. The Dimensions of Chain Molecules Containing Branches and Rings. *Journal of Chemical Physics* **17**, 1301-1314 (1949).

71. Garcia-Franco,C.A., Lohse,D.J., Robertson,C.G., & Georjon,O. Relative quantification of long chain branching in essentially linear polyethylenes. *European Polymer Journal* **44**, 376-391 (2008).

72. Miller,M.L. Branched Molecules in *The structure of polymers* 105-139 (Reinhold Publishing Corporation, New York, 1966).

73. Armstrong,J.K., Wenby,R.B., Meiselman,H.J., & Fisher,T.C. The hydrodynamic radii of macromolecules and their effect on red blood cell aggregation. *Biophysical Journal* **87**, 4259-4270 (2004).

74. Crank,J. *The Mathematics of Diffusion*(Oxford University Press, Oxford, 1975).

75. Lebrun,L. & Junter,G.A. Diffusion of Dextran Through Microporous Membrane Filters. *Journal of Membrane Science* **88**, 253-261 (1994).

76. Brissova,M., Lacik,I., Powers,A.C., Anilkumar,A.V., & Wang,T. Control and measurement of permeability for design of microcapsule cell delivery system. *Journal of Biomedical Materials Research* **39**, 61-70 (1998).

77. Nishinari,K. *et al.* Solution Properties of Pullulan. *Macromolecules* **24**, 5590-5593 (1991).

78. Amsden,B. Solute diffusion in hydrogels. An examination of the retardation effect. *Polymer Gels and Networks* **6**, 13-43 (1998).

79. Amsden,B. Solute diffusion within hydrogels. Mechanisms and models. *Macromolecules* **31**, 8382-8395 (1998).

80. Gombotz,W.R. & Wee,S. Protein release from alginate matrices. *Advanced Drug Delivery Reviews* **31**, 267-285 (1998).

81. Chretien,C. & Chaumeil,J.C. Release of a macromolecular drug from alginate-impregnated microspheres. *International Journal of Pharmaceutics* **304**, 18-28 (2005).

82. Dembczynski,R. & Jankowski,T. Determination of pore diameter and molecular weight cut-off of hydrogel-membrane liquid-core capsules for immunoisolation. *Journal of Biomaterials Science-Polymer Edition* **12**, 1051-1058 (2001).

83. Amsden,B. & Turner,N. Diffusion characteristics of calcium alginate gels. *Biotechnology and Bioengineering* **65**, 605-610 (1999).

84. Kulseng,B., Thu,B., Espevik,T., & Skjak-Braek,G. Alginate polylysine of cytokines and immunoglobulins over the capsule membrance. *Cell Transplantation* **6**, 387-394 (1997).

85. Lyle,D.B. *et al.* Low molecular weight hyaluronic acid effects on murine macrophage nitric oxide production. *Journal of Biomedical Materials Research Part A* **94A**, 893-904 (2010).

86. Lyle,D.B., Bushar,G.S., & Langone,J.J. Screening biomaterials for functional complement activation in serum. *Journal of Biomedical Materials Research Part A* **92A**, 205-213 (2010).

87. Misko,T.P., Schilling,R.J., Salvemini,D., Moore,W.M., & Currie,M.G. A Fluorometric Assay for the Measurement of Nitrite in Biological Samples. *Analytical Biochemistry* **214**, 11-16 (1993).

88. Kuo,C., Burghen,G., Myracle,A., & Herrod,H. Isolation of islets from neonatal pig pancreatic tissue. *Journal of Tissue Culture Methods* **16**, 73-79 (1994).

89. Rayat,G.R., Rajotte,R.V., Ao,Z.L., & Korbutt,G.S. Microencapsulation of neonatal porcine islets: Protection from human antibody/complement-mediated cytolysis in vitro and long-term reversal of diabetes in nude mice. *Transplantation* **69**, 1084-1090 (2000).

90. Rodionov,V.O., Presolski,S.I., Gardinier,S., Lim,Y.H., & Finn,M.G. Benzimidazole and related Ligands for Cu-catalyzed azide-alkyne cycloaddition. *Journal of the American Chemical Society* **129**, 12696-12704 (2007).